Epidermis and Re-epithelialization in *Schmidtea mediterranea*

Thesis

Epidermis and re-epithelialization in *Schmidtea mediterranea*

Aurimas Gumbrys, B.Sc., M.Sc.

A thesis submitted in fulfillment of the

requirements of the Open University

for the Degree of Doctor of Philosophy

The Stowers Institute for Medical Research

Kansas City, USA

an Affiliated Research Center of the

Open University, UK

31 Decemer 2016

Abstract

Epidermal layer is crucial for organism's survival as its ability to close the wound is essential for tissue recovery. Planarian epidermis enables animal recovery and survival after virtually any body part amputation. Nevertheless, neither the epidermis nor the mechanisms endowing such a remarkable wound healing capacity is described in detail in planarians. Our work introduces live imaging methodology, which allows following epidermal cells and their response to tissue damage or tissue loss for extended time (hours) and in high resolution. Using our methods, we followed planarian cells live for the first time and in conjunction with electron microscopy analysis we described epidermal cell behaviors during tissue maintenance, response to tissue damage and tissue loss. Our data provides comprehensive description of cellular wound response, wound closure as well as preexisting tissue contribution to tissue restoration. In addition, we performed epidermal expression profile analysis to identify the candidate list of epidermally expressed genes to depict the machinery endowing these epidermal cell behaviors. In the pilot functional (RNAi) screen an array of transcription factors with a tissue maintenance phenotypes were identified. Our work established tools for subsequent functional studies of other epidermal expressed genes and paved the way to dissect the mechanisms of the epidermis' maintenance and efficient wound healing in planarians.

Joriui ir Agnei, Brangiausiem mano

Acknowledgements

It is ten years since I first entered into a research lab. Five laboratories, four countries and two continents later I am getting ready to finish my studies. It has been a journey through which I was privileged to meet countless inspiring people. Although I will not be able to mention them all, I want to express my gratitude to those who made the most profound influence to my recent personal and professional development. I want to start by thanking my mentor Alejandro Sánchez Alvarado. Meeting him allowed me to discover what is the most important in science – the great joy of exploration. I am thankful to Alejandro for opportunity to join the lab I loved as well as for helping me to find courage to overcome challenges I did not think I was capable to solve.

I am grateful to my wife, Agne, with whom I shared this journey from the very beginning. No achievement would mean much if I could not share it with her. She is the best partner and friend and no journey is too long if we travel together. I thank my son Joris for all the beautiful emotions he brought to my life.

I am thankful to Sarah Elliott, Kim Tu, Erin Davies, Alessandro Rossi, Li-Chun Chen, Kai Lei and Carrie Adler for all the emotional support they provided. I also want to thank my parents, family and friends I left back in Lithuania. Not being able to see each other was a sacrifice, but they supported me throughout the way. I also want to thank all of my new friends in Kansas City. They made this city feel like home and I cherish moments we shared together.

I want to thank my thesis committee members Robb Krumlauf, Matt Gibson and Tatjana Piotrowski, who guided me throughout the project. I want to thank all past and current colleagues for opportunity to learn from them. Thank you, Sarah Elliott, An Zeng, Hanh Vu, Christopher Arnold, Alessandro Rossi, Longhua Guo, Li-Chun Cheng, Carrie Adler, Stephanie Nowotarski, Beth Duncan, Kim Tu, Erin Davies, Kai Lei, Shasha Zhang, Carlos Guerrero, Eric Ross, Wei Wang and others for their insight at my lab meetings.

I am thanking Leanne Wiedemann for organizing my graduate studies, Stephanie Nowotarski, Sarah Elliott, Kim Tu, Erin Davies, Hugo Parker, Nishal Patel and Mark Mattingly for helping me to improve my writing skills. I want to thank Melainia McClain and Rhonda Ross for assisting electron microscopy work, Chris Seidel and Stowers molecular biology core for genomic analysis, Jeff Lange for PDMS device fabrication, library staff as well as all the other Stowers Institute members whose work and expertise contributed to this project.

Table of Contents

Table of Figures

Table of Tables

Chapter 1

Introduction

1.1 Epidermis – ectodermal epithelia

Epithelia are polarized sheet-like arrangements of cells interconnected with each other by belt-like junctions and connected to an underlining basal membrane by focal adhesions (Van Lommel, 2003). The ability to establish epithelia was fundamental for multicellular life forms to evolve. Although the beginning of epithelial evolution can be traced back to sponges, which form polarized monolayers, these organisms do not have basal membrane and do not form belt junctions. Therefore, it is believed that sponge tissues are not true epithelia. The first true epithelia arose in Cnidarians and its form and function have subsequently evolved throughout Metazoan evolution (Tyler, 2003). Epithelia can have ectodermal, mesodermal or endodermal origins. Ectodermal epithelia, e.g., the epidermis, covers the surface of the animal. In contrast, the endoderm gives rise to epithelia lining the majority of the internal organs, and the mesoderm gives rise to the circulatory system endothelium, the kidney and lining of the reproductive organs (Van Lommel, 2003).

Variations of epithelial architecture and physiology are apparent. Epithelia range from columnar or cuboidal single cell layers to more complex pseudo-stratified or stratified multi-layered epithelia in vertebrates (Van Lommel, 2003). Although the primary function of epithelia is to support and protect underlining tissues from environmental insults, epithelia can also mediate the exchange of substances between underlying tissues and the body cavity. Mucosal epithelia lining internal organs or aquatic animal body surfaces facilitate absorption of food or oxygen, as well as secretion of biologically active substances or waste products. The apical surface of these tissues in organisms other than Nematodes and Arthropods may also be covered with cilia. Cilia move fluids along stationary mucociliar epithelia surfaces to aid feeding, digestion, respiration, transportation or cleansing of the respiratory tract. Epithelia can be also covered by micro-villi, apical membrane extensions which increase the absorptive surface in a tissues like the vertebrate gastrointestinal tract. Moreover, epithelia cells exposed to external fluxes evolved to detect and respond to specific stimuli and are called sensory epithelia (Van Lommel, 2003).

Despite differences in epithelial architecture among phyla or organs, the mechanisms determining epithelial structure are conserved between animals. Studies of epithelial cell differentiation in Cnidarians, Arthropods, Nematodes and mammals show that epithelia are

established using a similar set of proteins (Knust and Bossinger, 2002; Krämer, 2000; Tyler, 2003). Epithelial integrity is maintained by the cytoskeleton and cellular junctions. The vertebrate epithelial cells are joined by desmosomes as well as belt-like junctions, including the apical-most tight junctions and adherens junctions arrayed just proximal to them. Although tight junction-like structures are also seen in certain invertebrate groups, invertebrate Chordates and Ctenophores (Harrison and Jane, 1991; Tyler, 2003), most invertebrates lack these structures and do not form typical desmosomes. Instead of tight junctions, invertebrates form the functionally equivalent septate junctions, which lay basal to the most apically situated adherens junctions (Bereiter-Hahn et al., 1984; Tyler, 2003).

The epidermis is a highly-specialized epithelium of ectodermal origin which comprises the surface of an organism. Adult vertebrate skin is composed of a stratified epidermis and an underlying mesodermally-derived mesenchymal dermis. The majority of invertebrates, on the other hand, possess single cell layer epidermis. It can contain single cell or multiple cell types (Van Lommel, 2003), some of which, like those nematocysts in Cnidarians, are highly specific to particular clade (David et al., 2008). However, a cellular epidermis is not universal for all invertebrates: parasitic flatworms and certain Nematodes have a syncytial epidermis (Bereiter-Hahn et al., 1984).

The epidermis has evolved to provide a protective barrier, however it can also act as a secreting surface (Bereiter-Hahn et al., 1984). Keratinized epidermis of terrestrial vertebrates and the cuticle covered epidermis of Ecdysozoa (Arthropods and Nematodes) are primary barriers, while the mucosal epidermis of Cnidarians and Lophotrochozoans is also secretory. The mucociliary epidermis in Turbellaria and Nemertea was adapted for locomotion. Not dissimilar to vertebrate airway epithelia, the epidermis in these animals is covered with cilia and contains gland cells. Gland cells secrete mucus to coat the adjacent substrate, whereas cilia act upon this mucus to generate a gliding form of motility (Bereiter-Hahn et al., 1984).

The epidermal sheet is far from simply being a static barrier. Ectodermal sheet movements and interactions with the underlining mesenchyme are especially important during early embryonic development (Gilbert, 2014). Epithelial roles in animal body morphogenesis are conserved across Metazoa, suggesting their ancestral origin. Arguably, as critical and ancient is the ability of epithelia to respond to injury. Occasional damage is an inevitable and potentially fatal challenge to any organism. An inherent property of epithelial sheets is their ability to respond and reseal themselves.

1.2 Wound healing across Metazoa

Re-establishing homeostasis after injury is essential for the survival of all known animal species. A key step in this process is wound healing. Although the relative complexity of wound responses increases with evolutionary inventions such as multicellularity or immune systems, the principal mechanisms of damage repair appear to be conserved among eukaryotes. For example, cellular membrane disruption in yeast or amoeba, as well as cutaneous wounds in vertebrates are closed by calcium influx, Rho family small GTPases, and mitogen activated protein kinase (MAPK) mediated responses (Levin, 2011; Sonnemann and Bement, 2011). Intra-cellular membrane compartment fusion, cytoskeleton re-arrangement and subsequent actomyosin contraction drive wound closure in these distinct phylogenetic groups suggesting that at least initial steps of wound healing are governed by an evolutionarily ancient damage repair mechanism.

Mechanisms of damage repair have likely been elaborated upon evolution, and phylogenic group-specific gain or loss of certain wound responses must have occurred. However, our current knowledge of wound repair is based on studies of a handful of model systems in which some, and perhaps important, wound responses may be under-represented and, thus, their roles have yet to be fully appreciated. Distinct model systems offer different methodological, anatomical, and biological advantages for their investigation. For instance, cutaneous wound healing in mammals is a traditional example of Metazoan damage repair; however, it was only after visualization of wound closure in the *Drosophila* (Millard and Martin, 2008) that the dynamic interaction between opposing wound edges became apparent. Similarly, the mechanism of cellular damage repair is primarily followed in sea urchin eggs/early embryos and *Xenopus* oocytes (Mandato and Bement, 2001; Terasaki et al., 1997). Therefore, it is reasonable to assume that a multiphyletic approach that combines the strengths of well-established model systems with the study of wound response in both understudied and unexplored organisms is likely to prove very informative.

Injury is one of the most drastic stimuli cells can encounter. Yet, a complete understanding of how cells sense and coordinate a response to tissue damage remains elusive. The beginning of wound closure often precedes a transcriptional response by many hours, indicating that *de novo* protein synthesis is not necessary for the initial re-epithelialization stages (Clark et al., 2009; Lacy and Ito, 1984; Wood et al., 2002). As such, preexisting proteins can accommodate early cellular wound responses. Transcription independent signals (Cordeiro and Jacinto, 2013) and exposure of normally sequestered

cues are the most likely candidates to induce wound repair programs. For instance, while roles of exocytosis in membrane damage repair are well established, the contribution of intracellular membrane transport to wound closure still has to be explored.

Cellular wound healing – miniature model for damage repair

The plasma membrane encapsulates and protects vital biochemical reactions of the cell from deleterious environmental effects. Traumatic stress and environmental insults damage membrane integrity requiring immediate repair. Notably, the mechanisms of cellular damage repair are deeply evolutionarily conserved. Membrane disruptions in plants, yeast, amoeba, and animals are repaired by two calcium-mediated responses at the damage site: exocytosis and cytoskeleton reorganization.

Visualization of membrane repair in amoeba (Szubinska, 1971) and Echinoderm eggs (Steinhardt et al., 1994; Terasaki et al., 1997) demonstrated cellular membrane disruptions are immediately resealed by intracellular membrane deposition at the damage site. In sea urchin eggs, exocytosis and fusion of abundant yoke granules patch membrane disruption and prevent deleterious cytoplasm loss. Since yolk granules have only been identified in sea urchin and amphibian eggs thus far, the intracellular compartment responsible for patch formation in other animal cells remains unknown. Calcium mediated fusion of lysosomes is implicated in damage repair in mammalian cells (Bement et al., 2007), whereas peroxisome related Woronin bodies clog septate of damaged hyphae in fungi (Jedd and Chua, 2000).

Studies in sea urchin eggs/embryos and cultured fibroblast suggest that the molecular machinery responsible for membrane resealing recapitulates neurotransmitter release: calcium/calmodulin-mediated CaM kinase and kynesin motors target intracellular vesicles to the damage site where they are fused by calcium dependent SNARE proteins (Steinhardt et al., 1994). SNARE proteins are also necessary for freeze damage repair in *Arabidopsis*, indicating that a similar wound response is also present in plants (Schapire et al., 2008). Studies in mammalian cells complement the mechanism of cellular wound response by suggesting that cytoskeleton remodeling at the damage site by calpains (calcium dependent actin severing proteins) is also necessary for membrane fusion and wound patch formation (Godell et al., 1997).

Exocytosis-mediated membrane resealing is followed by cytoskeleton contraction-driven cellular wound closure, another calcium dependent wound response most

extensively studied in frog oocytes (Bement et al., 1999; Benink and Bement, 2005). Concentric Rho-family GTPase Cdc42 and RhoA activity zones at the damage site mediate closure of cellular membrane disruption. Cdc42 acts to assemble an F-actin and myosin2 array at the wound periphery, after which small GTPases mediate its contraction and brings membrane edges together.

In yeast, cellular damage is detected and transmitted to Rho GTPase by cell-surface integrity sensors (Jendretzki et al., 2011). Rho and its effector Protein kinase C (PKC) activate the cell wall integrity (CWI) pathway (Levin, 2011), which governs various processes necessary for damage repair. The CWI pathway regulates cell wall biogenesis via enzyme function control and MAPK cascade mediated induction of necessary gene transcription. The CWI pathway also governs membrane repair by targeting cytoskeletal and exocytic wound responses to the damage site (Kono et al., 2012). In intact cells, the machinery responsible for this response is deployed at the bud region, thus it has to be re-polarized upon damage. This reorganization is mediated by CWI induced proteolysis at the bud. Since re-polarization is a hallmark of epithelial wound closure, it is possible that analogous or even homologous proteolytic responses could also be present in higher eukaryotes.

Mechanisms of cellular membrane repair are also integrated into the multi-cellular wound response. Studies in the early frog epithelium have demonstrated that when cellular damage is close to cell-cell junctions it is transmitted into neighboring cells (Clark et al., 2009). These surrounding cells activate Rho and assemble F-actin bundles along the edge of the wound of the damaged cells, providing a cyto-architectural scaffold upon which to execute a multi-cellular wound response. This observation may suggest that along the evolution of multi-cellularity, the mechanism of cellular damage response may have been co-opted and redeployed to reseal damaged epithelium.

Tissue damage repair across phylogeny: model systems and their adaptations

Damage in tissues often cannot be repaired by membrane damage repair mechanisms alone. Severely damaged cells, for instance, die and tissue integrity has to be reestablished by undamaged neighboring cells. These cells detect the wound/damage in surrounding cells and proceed to reorganize their cytoskeleton, repolarize and migrate to reseal the wound. Although superficially this process seems different from the previously described

membrane damage repair, it is also driven by calcium and small GTPase-mediated cytoskeleton remodeling and contraction. Nevertheless, the pattern of cellular wound response substantially varies between taxa, tissues, and developmental stages of the same organism. The following sections will provide an overview of examples of wound closure in different taxa and provide a comprehensive representation of this response in Metazoan phylogeny.

Wound healing in Cnidarians

Although Cnidarians are not a conventional system to study wounds, some of the most remarkable examples of wound response are evident in this phylum. Cnidarians are pre-bilaterian animals composed of primarily two single-cell-layer epithelial sheets: ectodermal myo-epithelium, and endodermal gastro-epithelium. The life cycle of Cnidarians varies from species to species, but after spawning, most if not all known species go through the formation of planulas, primary polyps and swimming hydrozoans (Technau and Steele, 2011). Several studies have described the cellular responses to wound in polyps (Bibb and Campbell, 1973; DuBuc et al., 2014) and swimming hydrozoa (Lin et al., 2000) indicating that wound-healing mechanisms are in place throughout the ontogenitc phases of development of these organisms.

In *Hydra*, for example, healing of cut-through body wall transplant starts by filopodial interactions and re-adhesion within the gastro-epithelium. Subsequently, and within minutes, the ectodermal cells extend long flattened processes along the gastro-epithelia, contact each other, and then reestablish cellular junctions between ectodermal sheets (Bibb and Campbell, 1973). Ectodermal cell contribution to wound closure could also be observed after amputation (Shimizu et al., 2002). After anterior amputation, ectodermal cells along the cut edges elongate, contact, and fuse with each other to close the anterior pole. It was proposed that this ectodermal cell shape change could also be mediated by the under-lying mesoglea, the extracellular matrix (ECM) between ecto- and endo-epithelia, contraction in response to wounding. As epithelia reestablish mesoglea within days after injury, epithelial cells regain their initial cuboidal shape. The remarkable healing potential of *Hydra* epithelial cells is best illustrated by their ability to reassemble polyps from a pellet of dissociated cells (Gierer et al., 1972; Technau et al., 2000). In this process, epithelial cells re-aggregate, adopt new spatial identity, synthesize mesoglea, proliferate, and coordinate axial patterning of the polyp. The plasticity of *Hydra* epithelial cells is also evident during lost tissue restoration. These animals can heal their wounds and

reestablish missing tissues without proliferation (Cummings and Bode, 1984; Hicklin and Wolpert, 1973), indicating that a high degree of tissue reorganization potential exists in *Hydra*.

Wound response to tissue damage was also studied in *Nematostella*. Shortly after through-body wall puncture, the resulting wound is plugged by ejected sticky mucus-like material and mesentery structures. Subsequently, wound closure proceeds as the wound edge epidermis extends into the wound surface. These wound epithelia extensions can be quite long. In a small set of animals they did not join the opposite wound edge but rather transversed the entire body cavity and reached into the damaged site on the opposite side body wall. It was demonstrated that the wound closure in *Nematostella* requires extracellular signal–regulated kinase (ERK) pathway activation at the wound edge epidermis, pharmacological inhibition of this signaling cascade perturbs wound closure as well as lost tissue regeneration (DuBuc et al., 2014).

Ectodermal wounds in another hydrozoan, the jellyfish *Polyorchis penicillatus*, are healed by remarkable phenotypic and functional transformations in their myo-epithelium (Lin et al., 2000). When damaged, myo-epithelium at the wound vicinity undergoes a phenotypic and functional transformation from a highly polarized "swimming muscle" to flat, migratory epithelial sheet cells. Along this transformation myo-epithelial cells reabsorb muscle myosin bundles, lose contractility, extend lamellipodia, and crawl to re-epithelialize the wound. Strikingly, this conversion is achieved by re-arrangement of existing proteins rather than *de novo* protein synthesis. Within 18hr ectodermal wounds are re-epithelialized and flattened myo-epithelial cells slowly begin to reestablish their polarity and contractibility.

Wound healing in Ecdysozoa

The Nematode roundworm *Caenorhabditis elegans*

Studies in *C. elegans* have shown that calcium also triggers wound response in the epidermis of this roundworm. Interestingly, it has been demonstrated that wound-associated calcium wave is dependent on GTL2, a cytoplasmic membrane-associated, TRPM family ion channel (Xu and Chisholm, 2011). This is an intriguing observation since the TRPM family of ion channels is involved in mechano-sensation, and thus provides an intriguing possibility to explain how wound induced changes in membrane tension are translated into molecular signals inside the epidermis. It was also demonstrated

that initial calcium influx is accompanied by internal calcium flux. Phospholipase C (PLC) acts downstream or parallel of GTL-2 to induce calcium release from internal stores by Inositol 1,4,5 trisphosphate (IP_3) production and its subsequent binding to IP_3 receptor ITR-1 (Baylis et al., 1999; Xu and Chisholm, 2011).

Epidermal wounds in the adult *C. elegans* epidermis are closed by calcium dependent cytoskeleton re-organization. Minutes after injury F-actin bundles are assembled along the wound edge. GTL2 mutants as well as animals treated with calcium chelators exhibit severely compromised F-actin ring formation and wound healing. Analysis of F-actin bundle function revealed that actin polymerization, rather than actomyosin contraction, is responsible for wound closure in the *C. elegans* epidermis. Loss of function of Rho-family GTPases, conserved regulators of actin organization, demonstrated that Cdc42 is necessary for wound closure, whereas knockdown of other Rho-family GTPases did not impair healing. In fact, reduction of Rho or its target non-muscle myosin accelerated wound closure (Xu and Chisholm, 2011).

The fruitfly Drosophila melanogaster

Established genetic and live imaging methodologies in *Drosophil*a have allowed for real-time observation and quantification of cellular behaviors associated with wound closure (Galko and Krasnow, 2004; Wood et al., 2002). *Drosophila* wounds are closed by two main behaviors within the epidermal cells at the wound perimeter: contraction of continuous actomyosin cables, and activity of cellular protrusions.

Wounds in embryonic epithelia are predominantly closed by formation and subsequent contraction of a continuous actomyosin cable along the wound periphery, the wound closure mechanism known as “purse string” (Wood et al., 2002). As wound closure proceeds and the wound circumference gradually becomes smaller, some epidermal cells are withdrawn from the front row or edge of the wound. During re-epithelialization, cells at opposite wound edges extend filopodia, which interact with each other, as well as with the wound surface (Millard and Martin, 2008). This behavior ultimately is modulated into a spatially coordinated wound closure process. At the final stage of re-epithelialization, an array of filopodial interactions bring wound edges together, to finally mediate their resealing.

Lamellipodial crawling drives re-epithelialization in post-embryonic *Drosophila* epidermis. Wound closure starts by rapid plug formation at the wound site. At the same

time, epidermal cells at the wound edge polarize towards damage. Within hours after injury, epithelial cells extend lamellipodia and start crawling along the plug. Along this process, migrating epithelial cells fuse their lateral membranes and form large syncytia, which in the adult fly is also accompanied by chromosome duplication leading to polyploid cell formation (Galko and Krasnow, 2004; Losick et al., 2013). This process is likely regulated by signaling events since down regulation of the Hippo pathway has been shown to increase syncytium size and decrease polyploid nuclei number (Losick et al., 2013).

Mechanistic analyses have demonstrated that Stitcher and Platelet-derived growth factor/Vascular endothelial growth factor tyrosine kinase receptors (Stit and Pvr), calcium influx, Rho-family small GTPases, and MAPK cascades are required for cytoskeleton reorganization and cell migration in response to wounding (Galko and Krasnow, 2004; Razzell et al., 2013; Wang et al., 2009; Wood et al., 2002; Wu et al., 2009). Tyrosine kinase receptors Stit and Pvr are necessary for re-epithelialization of embryonic and post-embryonic wounds respectively (Wang et al., 2009; Wu et al., 2009). Stit mutants fail to assemble an actomyosin ring, suggesting that signaling through tyrosine kinase receptors plays a role in the initial wound response (Wang et al., 2009). In larvae wound healing, Pvr and its ligand Platelet-derived growth factor/Vascular endothelial growth factor 1 (Pvf1) have been shown to be necessary for lamellipodia formation and subsequent wound closure (Wu et al., 2009). It is proposed that in intact epidermis Pvf1 is sequestered underneath the basal membrane and remains inaccessible to Pvr at the lateral membranes of epidermal cells. When epidermis and basal membrane are damaged, Pvf1 is released making it possible for it to bind and activate Pvr at the wound edge.

Stit dependent ERK activation at the wound vicinity is observed in the embryonic epidermis (Wang et al., 2009), whereas another MAPK, JNK (c-Jun N-terminal kinase) is activated at wound edges in larval wounds (Galko and Krasnow, 2004). JNK perturbation impairs cytoskeleton reorganization, decreases the number of cellular protrusions and halts re-epithelialization, suggesting that MAPK has a crucial function in wound closure (Baek et al., 2010; Galko and Krasnow, 2004; Kwon et al., 2010; Lesch et al., 2010). MAPK role in transcriptional wound response was successfully demonstrated (Wang et al., 2009), yet its contribution to immediate, transcription independent cellular responses has not been extensively explored. Defective assembly of wound edge F-actin bundles after non-functional JNK expression (Kwon et al., 2010) suggest transcription independent MAPK function in the epidermal wound response. Moreover, mechanistic studies revealed that

JNK activation causes membrane fusion and syncytial wound epithelia formation by disassembling focal adhesion complexes shortly after injury(Wang et al., 2015).

Cytoskeletal response to the wound is coordinated through Rho-family small GTPases. In larvae, Rac1, Rho or Cdc42 loss of function disrupts the cellular wound response and wound edge epidermis fails to re-polarize and assemble actin bundles (Baek et al., 2010). Distinct Rho-family member contributions to cellular wound response are easier to segregate in embryonic wounds. Rho deletion impairs continuous actin ring assembly and efficient migration of wound epithelia, whereas Cdc42 function is necessary for filopodia formation and final resealing of wound edges (Wood et al., 2002). Unlike Rho and Cdc42, Rac1 does not seem to be necessary in embryonic re-epithelialization, but is critical in post-embryonic wound closure. Interestingly, it was proposed that Rac, Cdc42 and Rho act upstream of JNK cascade in a partially redundant manner (Baek et al., 2010). Thus, Rho-family GTPase deletion phenocopies tyrosine kinase receptor mutations; however, the functional interaction between them remains to be explored. Studies also revealed an essential role for Toll receptor signaling at wound induced cytoskeletal remodeling and wound closure. Toll and NF-κB transcription factor mutants fail to remodel their adherens junctions and do not form actin-cables at the wound edge epidermis (Carvalho et al., 2014), suggesting that the Rho-family GTPase mediated wound response is either regulated by Toll signals or is tightly linked to cellular junction reorganization at the wound margin.

Wound healing in vertebrates

The complexity of the wound response has greatly increased in vertebrates (Clark, 2013; Martin, 1997; Singer and Clark, 1999; Sonnemann and Bement, 2011). Along evolution, these animals have elaborated a sophisticated immune response and developed stratified epithelia, both of which provide better protection from environmental insults and infection. However, and for still unclear reasons, the re-epithelialization and tissue restoration efficiency has decreased in these animals when compared to other phyla. For example, the lag phase prior to epidermal cell migration to cover the wound has dramatically increased in vertebrates (Galko and Krasnow, 2004; Martin, 1997; Sonnemann and Bement, 2011; Wood et al., 2002), suggesting the requirement of activation of immune system components, or dependence on *de novo* protein synthesis. Due to its clinical significance, wound healing is traditionally studied in mammalian models. In fact, wound healing in adult mammalian epidermis is commonly used to

generally represent the process of wound repair (Martin, 1997; Singer and Clark, 1999). In vertebrates, this process encompasses multiple responses, which are generalized into hemostasis, immune system response, wound closure by epidermal cell migration, and wound tissue resolution. As in fly, wounds in adult vertebrate epidermis are primarily closed by lamellipodial crawling, whereas actomyosin cable contraction drives embryonic tissue resealing. However, such apparent and distinct developmental segregation is not definitive, because wounds in adult cornea or small wounds in the adult intestine are also closed by a purse string (Danjo and Gipson, 1998; Russo et al., 2005).

It takes days to weeks to repair mammalian wounds, however hemostasis and the resulting clot formation provides a quick way to seal the wound (Clark, 2013; Martin, 1997; Singer and Clark, 1999; Sonnemann and Bement, 2011). This process starts by blood-derived platelet activation at the wound. Once activated, these cells aggregate along the wound surface and degranulate – release an array of crucial enzymes and signaling cues from their abundant intracellular compartment. A release of proteases activates an enzymatic cascade that generates a fibrin clot to plug the wound. Upon degranulation platelets also release multiple chemokine and growth factors that initiate the next phases of wound healing. Consequently, immune system cells, neutrophils and monocytes, are recruited to the wound. Neutrophils arrive at the wound where they clear the invading pathogens minutes after injury. Monocytes differentiate into macrophages which surveille and phagocytose pathogens, remove cell or extracellular matrix debris and release an additional battery of growth factors and chemokines into the wound.

Immune cell infiltration is simultaneous with the epidermal wound response. The mechanism of wound response induction in the epidermis is not completely understood, but is likely complex (Clark, 2013; Cordeiro and Jacinto, 2013; Sonnemann and Bement, 2011). The content of damaged cells, growth factors secreted by immune or connective tissue cells, changes in composition or properties of the extracellular matrix and even changes in potential difference are all thought to coordinate cellular migration through the re-epithelialization phase. Before the epidermis can migrate, it has to reorganize existing junctions as well as express the proteins needed for new ones. Epidermal cells at the wound margin lose desmosomal junctions (cell-cell) and focal adhesions (cell-substrate) and start to express a wound-specific set of adhesion molecules (Grinnell, 1992; Martin, 1997; Singer and Clark, 1999). Consequently, these cells repolarize toward the tear, flatten, and start migrating forward by lamellipodia extension driven crawling. Migrating cells secrete proteolytic enzymes ahead of them and cut their way through the fibrin clot

(Grondahl-Hansen et al., 1988). Although it is accepted that wounds within multilayered mammalian epidermis are closed by migration of basal epidermal layer cells (Clark, 2013; Martin, 1997; Odland and Ross, 1968), the mechanism of re-epithelialization is somewhat controversial. Two adult cutaneous wound re-epithelialization models were proposed: sliding and leapfrog. The sliding model assumes that although epithelial cells may occasionally change their neighbors and thus break and reestablish cellular junctions, the order of the cell layers is fairly well established and retained throughout wound closure (Stenn and Depalma, 1988; Woodley, 1988). Contrary to sliding model, the leapfrog (or rolling) model postulates that wounds are re-epithelialized by repetitive supra-basal cell roll over the basal keratinocytes (Krawczyk, 1971; Paladini et al., 1996; Stenn and Depalma, 1988).

Growth factors are the key chemotactic cues, and the pivotal roles of keratinocyte growth factor (KGF), epidermal growth factor (EGF), transforming growth factor–alpha (TGF-alpha) and beta (TGF-beta), and heparin binding epidermal growth factor (HB-EGF) are well established in mammalian models. Growth factor mediated epidermal wound responses are induced by several mechanisms. After the injury, immune and connective tissue cells secrete growth factors, which diffuse to the wound periphery and activate receptor tyrosine kinases at the wound margin epithelia (Clark, 2013; Martin, 1997; Singer and Clark, 1999; Sonnemann and Bement, 2011). Alternatively, epidermal tissue damage can expose receptors, which are normally sequestrated within or separated by epidermal sheets (Carraway and Carraway, 2007; Vermeer et al., 2003; Vermeer et al., 2006). This mechanism is *de novo* protein synthesis independent and therefore proposed to be present in organs where rapid healing is crucial. Studies of tracheal re-epithelialization demonstrated that TGF- or EGF- family proteins and their receptors reside at different sides of intact tracheal epithelia, and thus come into contact only after epithelial sheet damage (Vermeer et al., 2003; Vermeer et al., 2006). Receptor tyrosine kinase activation subsequently act through the MAPK signaling cascade to activate transcriptional wound responses (Deng et al., 2006; Martin, 1997; Singer and Clark, 1999; Sonnemann and Bement, 2011).

Although *in vitro* systems do not represent the native complexity of the wound healing process, studies in cultured mammalian cells defined the machinery responsible for cellular migration (Ridley et al., 2003). Cultured cells crawl by continuously extending lamellipodia at the leading edge and repeatedly retracting the trailing edge. Cellular movement is regulated by local activation of Rho-family GTPases. Cdc42 establishes

polarity and defines the leading edge of the cell. Cdc42 recruits Rac GTPase, which subsequently activates Wiskott-Aldrich syndrome family protein complex and therefore induces lamellipodial extension by Arp2/3-mediated polymerization of branched actin filament network (Welch and Mullins, 2002). Extended lamellipodia bind to ECM via integrin family receptors to provide a strong traction point for migration. Subsequently, Rho GTPase mediated myosin contraction at the trailing edge pulls the cellular body along the protrusion, and therefore the cell translocates (Riento and Ridley, 2003). As the cell body is finally pulled to the leading edge, integrin adhesions are disassembled. Subsequently, the cell initiates formation of new lamellipodia and repeats the locomotory cycle.

Contrary to actin polymerization and myosin contribution to cellular migration, the role of the secretory machinery and microtubules (MT) in repolarization is less understood. In migrating cells Cdc42 polarizes Golgi and vesicle trafficking MT cables towards the protruding edge (Rodriguez et al., 2003). Although the MT cytoskeleton likely contributes to F-actin by providing mechanical support in lamellipodia, the pivotal function of MT re-organization may be redirection of vesicle secretion. Directed secretion of proteases is necessary to cut through ECM ahead of migrating wound edge epithelia (Grondahl-Hansen et al., 1988); however other, more fundamental, functions of vesicle trafficking were also proposed. It is suggested that the cellular membrane surface is constantly internalized and recycled. Therefore, polarized exocytosis kinetically traps receptors on the leading edge of the migrating cell (Bretscher, 1983; Bretscher, 2008; Thompson and Bretscher, 2002) Directed exocytosis is likely responsible for constant delivery of the ECM binding molecules or chemotactic receptors to protruding lamellipodia. Thus, it is also likely acts to supply membrane to the surface of extending lamellipodia .

Onset of vertebrate wound re-epithelialization is followed by proliferation at the base of wound margin epidermis (Grinnell, 1992; Poleo et al., 2001; Singer and Clark, 1999). This response can be observed several hours after onset of epidermal cell migration at the base of the wound margin, but not at migrating leading edge cells (Garlick and Taichman, 1994). As closure of mammalian wounds continues, the cellular pool wound edge cells are expanded by stem cell activation at skin appendages. Stem cells residing in hair follicles and sweat glands provide the progeny, which migrate to the wound site and assist in re-epithelialization (Ito et al., 2005; Langton et al., 2008; Levy et al., 2007; Rittie et al., 2013; Taylor et al., 2000). At late stages of wound closure, invading fibroblasts replace the fibrin clot with collagen rich matrix (Clark, 2013; Martin, 1997). At the same

time a subset of fibroblasts responds to TGF-1 (Desmouliere et al., 1993) as well as mechanical forces (Grinnell, 1994) in the wound and transform into myofibroblasts. These cells express smooth muscle actin and consequently support re-epithelization by bringing wound edges closer together.

While it takes weeks to heal deep cutaneous or mucosal tissue wounds in vertebrates, the re-epithelization is remarkably fast if the integrity of basal membrane is retained and thus no inflammatory response occurs (Donaldson and Dunlap, 1981; Lacy and Ito, 1984; Radice, 1980; Rees, 1988). After the chemical ablation of the entire gastric epithelia surface, the denuded basal membrane is rapidly repopulated by gastric pit epithelia cells. Within 7 minutes after damage, these columnar cells flatten and start migrating along the damage site by extending wide lamellipodia. These cells maintain their contacts within the epithelia and almost complete recovery of gastric surface lining occurs within 15 minutes after damage, suggesting that neither *de novo* protein synthesis nor proliferative response is required for this process (Lacy and Ito, 1984; Rees, 1988). A cellular wound response can be as fast in a *Xenopus* tadpole (Radice, 1980) or newt (Donaldson and Dunlap, 1981) mucosal epidermis. If basal membrane has remained intact, tadpole wound re-epithelization begins within seconds after wounding. Interestingly, these wounds are closed by individual cell migration, not a collective epidermal sheet migration. As cells extend lamellipodia and crawl forward, their epidermal neighbors respond to the recently vacated space in front of them and thus join the migratory behavior. Once the basal membrane is repopulated and advancing epidermal cells contact each other, they do not extend further suggesting that space/mechanical cues might play a role in closure of these wounds.

These observations indicate that delayed re-epithelialization in mammals is likely a result of reorganization of machinery required for migration on non-native ECM and/or negative effect of the inflammatory response, underscoring the critical importance of basal membrane integrity. Upon basal membrane damage the native substrate on which epithelial cells adhere is removed and thus new, wound specific, matrix has to be laid at the wound bed. Consequently, in order to bind and migrate on the new substratum, cells have to re-express the appropriate receptors (Grinnell, 1992; Martin, 1997; Sonnemann and Bement, 2011). Rodent models depleted of neutrophil and macrophage lineages show accelerated re-epithelialization (Dovi et al., 2003; Martin and Parkhurst, 2004) suggesting an inhibitory effect for the immune system in this process. Indeed, wounding in oral mucosa, a tissue possessing high re-epithelialization and tissue restoration potential, leads to a much

reduced influx of neutrophils and macrophages, and consequently lower levels of several inflammatory cytokines and of TGFb1 at the wound site (Szpaderska et al., 2003).

Discussion

Studies in various model systems have contributed to our understanding of wound healing. Sea urchin embryos and *Xenopus* oocytes, *Drosophila* and cultured mammalian cells have provided venues to explore membrane damage responses, to follow and manipulate wound closure and has helped explain the mechanics of cellular migration. Comprehensive analysis in these and other systems have revealed a conserved core of molecules mediating damage repair in distinct phylogenetic groups suggesting the existence of ancient damage repair machinery. Injury triggers a battery of signaling cascades, which orchestrate wound repair. In general, wounds are closed by an array of cellular damage responses (Fig. 1.1): cytoskeleton re-organization and phenotypic transformation; cell migration by continuous F-actin ring formation and contraction or lamellipodilal crawling; and polarized exocytosis.

Although the major effectors of wound responses are becoming clear, the mechanisms activating and coordinating the wound repair program is far less understood. Environmental calcium influx through damage sites is believed to induce cellular damage repair (Clark et al., 2009; Steinhardt et al., 1994; Szubinska, 1971; Terasaki et al., 1997). However, dissolved calcium ion influx from the aquatic environment cannot explain wound response initiation in terrestrial animals, thus other signals must function in such species. Moreover, it is unclear how the tissue damage response is so rapidly initiated in cells not immediately adjacent to the damage site. Transcription independent signals, such us as oxidation, electro- or mechano-sensation, represent putative candidates (Cordeiro and Jacinto, 2013); however, their contribution still has to be explored.

Intact epidermis is a highly polarized tissue consisting of tightly connected cells – this structure provides an impermeable barrier, which in turn protects the organism. Upon injury, epithelial cells undergo drastic morphologic changes. These cells rapidly activate cytoskeleton regulatory machinery and re-polarize towards the tear. Cytoskeleton re-organization is also part of the cellular membrane damage response. The mechanism of membrane repair seems to be conserved from yeast to vertebrates (Bement et al., 1999; Benink and Bement, 2005; Clark et al., 2009; Kono et al., 2012; Levin, 2011). However, the phenotypic plasticity is greater in the lower Metazoan wound response. Cnidarian epidermis responds to injury by drastic phenotypic and functional transformation (Lin et

al., 2000) (Fig. 1.1). Most remarkable is that re-epithelialization in Cnidarians can be achieved by existing proteins rather than *de novo* protein synthesis (Lin et al., 2000), indicating that all the machinery necessary for this response is already present in the cell prior to wounding. The remarkably fast epithelial restitution in mammalian mucosal epithelia suggests that a similar molecular mechanism might also function during vertebrate tissue healing (Donaldson and Dunlap, 1981; Lacy and Ito, 1984; Radice, 1980; Rees, 1988).

For yet not understood reasons, two re-epithelialization mechanisms are evident across district phylogenic groups or developmental stages: purse-string and lamellipodial crawling (Sonnemann and Bement, 2011) (Fig. 1.1). Embryonic wounds are closed by a purse string mechanism driven by continuous actomyosin ring assembly along the wound edge and its gradual contraction, which creates force bringing epithelial edges together. At the final stages of wound closure actin polymerization mediated filopodila formation reseal opposite epidermal edges (Wood et al., 2002). Although purse string is commonly associated with embryonic wound healing, actin cable formation was also described in adult *C. elegans* wound healing. Nevertheless, the mechanism of adult nematode wound closure seems to differ from embryonic context – it driven by actin cable polymerization rather that its contraction (Xu and Chisholm, 2011). Post-embryonic wounds are usually closed by lamellipodial crawling (Galko and Krasnow, 2004; Sonnemann and Bement, 2011). Cells crawl by actin polymerization driven lamellipodial extension at the front (leading edge) and subsequent cellular body translocation by actomyosin contraction at the trailing edge (Kwon et al., 2010; Ridley et al., 2003). Contrary to purse string-mediated re-epithelialization, the force for crawling is generated by grasping the wound bed surface, which is an extracellular matrix different from one epidermal cells encounter in intact tissue. Since a set of wound specific adhesion molecules must be produced before cells can engage into lamellipodial crawling (Grinnell, 1992; Martin, 1997) it might explain why epidermal resealing by a purse string appears to be faster wound closure mechanism.

Live imaging studies in *Drosophila* have demonstrated that wound closure in embryonic tissues follows a well-defined pattern. In developing tissues, where reestablishment of tissue patterning is crucial for development, filopodia interactions guide wound closure and ensure the wound will be repopulated by epidermis of corresponding spatial identity (Millard and Martin, 2008). Analogous interactions control correct animal axis establishment during morphogenesis. When fusing epidermal sheets are misaligned during dorsal closure, filopodial interactions identify correct longitudinal patterning and

pull tissue back into alignment (Millard and Martin, 2008). Filopodia abolishment lead to an increase of animal plan pattering abnormalities (Gates et al., 2007). Although filopodia mediated spatial recognition has not yet been described in adult tissue context, it has been proposed that positional identity incompatability within wound epithelia have a role in regenerative response initiation (Carlson, 1974).

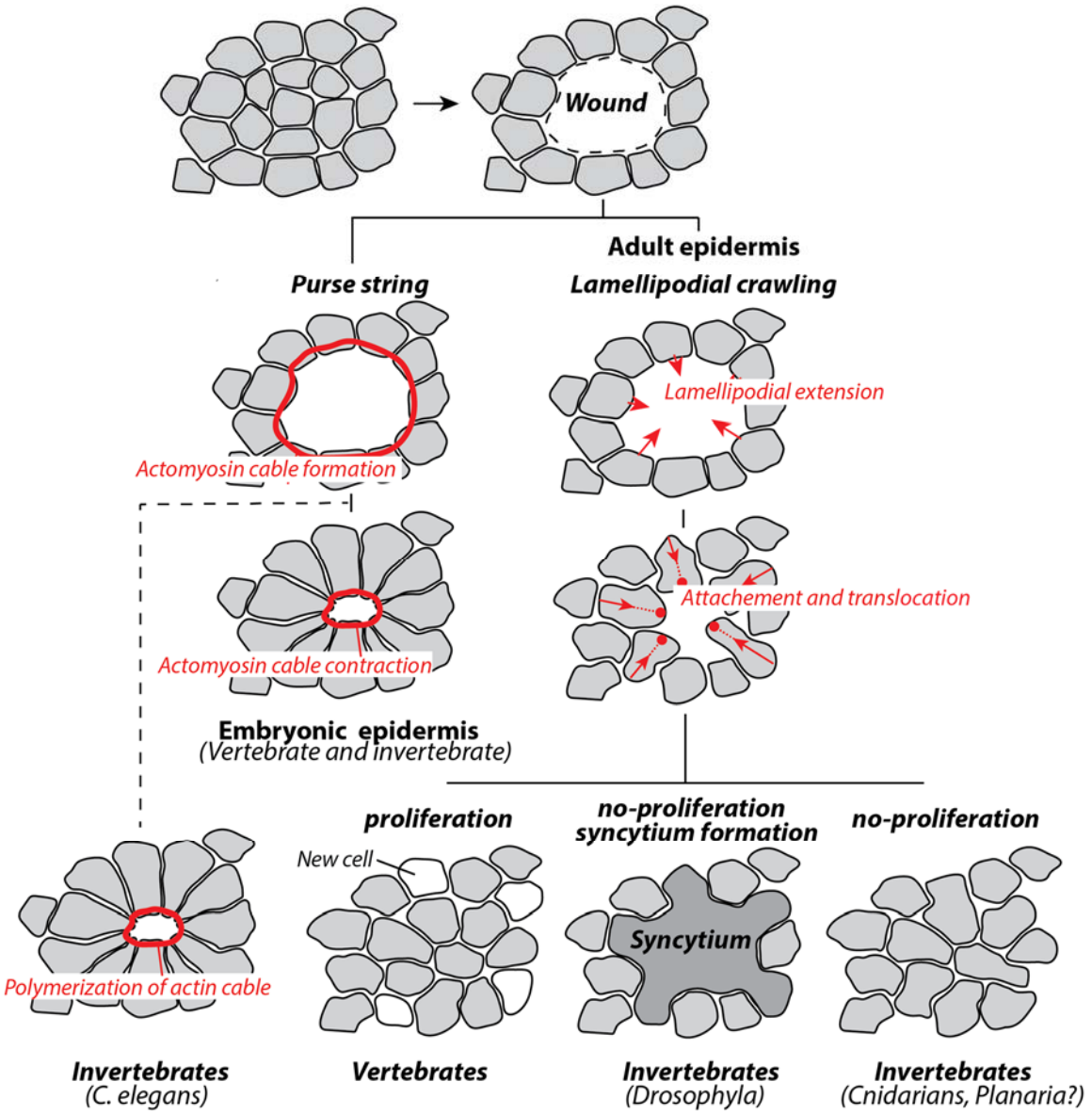

Figure 1-1. Diversity of wound closure mechanisms in Metazoa.
Adult wounds are usually closed via lamellipodial crawling of wound edge epidermis. In vertebrates, this process is followed by epidermal proliferation and new cell incorporation. In *Drosophila*, advancing wound edge epidermis expands its surface by cell fusion and syncytium formation. Cnidarians and Planarians are able to close their wounds solely by morphological transformation of their epidermal cells. Embryonic wounds as well as adult *C. elegans* wounds are closed by actomyosin cable formation at the wound edge epidermis. Actin cable contraction drives wound closure in embryos, whereas nematode wounds are closed by actin polymerization.

In vertebrate skin, on the other hand, the covering of the wound surface is likely achieved by a proliferative response at the wound edge, as well as *de novo* molecule synthesis. These are time demanding processes, which likely contributes to relatively slow wound closure. This response does not seem to be abundant in lower Metazoan epidermis; however, chromosome duplication and polyploid epidermal cell formation at *Drosophila*

wounds (Losick et al., 2013) (Fig. 1.1) could represent an interesting transition towards more vertebrate-like wound closure. Moreover, observed cell fusion and syncytium formation at post-embryonic fly wounds (Galko and Krasnow, 2004; Losick et al., 2013) suggest that different systems possess diverse adaptations of the wound healing mechanism. Lateral membrane fusion could provide a way to increase available membrane surface, whereas genome duplication at the wound edge epithelial could enhance the *de novo* synthesis of the molecules necessary for wound healing.

Wounding represents one of the most drastic stimuli animals can experience throughout their lifetime. In order to survive, animals devote vital cellular machineries to repair damage. Therefore, by studying wound responses, we are exploring fundamental cell biology. Cellular migration and morphogenesis are also involved in various developmental processes such as cancer, and cytokinesis. Thus, knowledge gained from wound response studies should help inform a wide array of physiological and pathological contexts. Although it is apparent that mechanisms of wound closure as well as wound healing capacity varies among metazoans, the detailed wound healing studies so far were only done in few ecdysozoans and vertebrates. It is likely that certain aspects of metazoan wound healing were not well represented in these models. Exploring wound responses in diverse animal groups holds a potential to expand our understanding of wound healing. It can help to uncover wound healing strategies or behaviors which were not pronounced in available models and thus can provide the comprehensive representation of metazoan wound healing.

1.3 Regeneration

All animals heal wounds, however, the outcome of this process varies across Metazoans. In some animals wound closure is followed by the activation of a regenerative program, which restores damaged or missing body parts. Other animals, like mammals, fail to activate this program, thus scaring occurs and damaged tissue fails to re-establish its original form and function. The hallmark of regenerative response initiation is blastema tissue formation - accumulation of undifferentiated cells underneath the closed wound epithelia (Nacu and Tanaka, 2011). Although undifferentiated, blastema cells are lineage restricted. Cell tracing after murine distal digit-tip or axolotl limb amputation established that blastema is composed, and thus regeneration driven, by a heterogeneous collection of progenitor cells (Kragl et al., 2009; Rinkevich et al., 2011). It has been long debated

whether the blastema cells arise from the resident adult stem cells or differentiated cells (Nacu and Tanaka, 2011). Recently, the contributions of both cellular compartments were demonstrated: the blastema can be established by progeny derived from adult stem cells, which reverted into more embryonic or less committed state, as well as by cell dedifferentiation and subsequent propagation (Kragl et al., 2009; Rinkevich et al., 2011; Sandoval-Guzman et al., 2014). The degree to which both mechanisms contribute varies among metazoans, for example amputated limb muscle regeneration in the axolotl is driven by muscle stem cells activity, while new limb muscle restoration is driven by myofiber dedifferentiation (Sandoval-Guzman et al., 2014). Dedifferentiation examples were also reported during damaged epithelia tissue restoration. After murine intestinal epithelium injury, undifferentiated secretory progenitors that are the immediate villin-negative progeny of stem cells can revert to a stem cell state after injury (van Es et al., 2012). After severe airway epithelia injury differentiated secretory cells occasionally give rise to cells that express basal stem cell markers after severe injury (Rawlins et al., 2009). Dedifferentiation is more prominent when damage ablates residing stem cells, Such injury not only induces fully committed secretory cell proliferation but also converts them into stable and functional epithelial stem cells (Tata et al., 2013).

1.4 Epidermal role in regeneration

It has been known for decades that the interaction between the wound epithelium and the underlying wound mesenchyme is essential for successful regeneration. The first indication of the epidermal role in this process was demonstrated by various surgical manipulations in vertebrates that prevented wound epithelium formation. For example, newt limb regeneration capacity is lost if wound re-epithelialization is prevented by inserting the stump of an amputated newt limb into the body wall (Goss, 1956) or by grafting a full-thickness skin flap over the stump (Mescher, 1976; Tassava and Garling, 1979). The importance of wound epithelia formation for tissue restoration has also been reported in humans, children lose their ability to regenerate lost fingertips if surgeons suture wound edges together after the injury (Illingworth, 1974). Intriguingly, it was also demonstrated that spatial identity of the cells within wound epithelia is crucial for regenerative response. Urodele limbs do not regenerate if the stump is covered by wound epithelia composed of only cells with a single positional identity (i.e. dorsal) (Carlson, 1974). The role of spatial identity in regenerative response onset is even more prominent in

invertebrates, where juxtaposition of opposite identity tissue is sufficient to induce regenerative response even without tissue loss in flatworms (Kato et al., 2001).

The molecular mechanism by which the wound epithelia contributes to regeneration has been described in vertebrate models. After limb amputation, wound epithelia transforms into a crucial regenerative response signaling center called the Apical Ectodermal Cap (AEC). AEC cells, which are in direct contact with underlying wound tissue, acquire cuboidal morphology and polarize their secretory machinery towards the wound mesenchyme (Nye et al., 2003; Thornton, 1960). Analogous basal wound epithelia transformation into secretory epithelia also takes place during zebrafish caudal fin regeneration (Poss et al., 2003). Wound epithelia interact with underlying wound tissues and secrete regenerative response crucial signals such as fibroblast growth factors (Fgfs), Sonic hedgehog (Shh), Bone morphogenetic proteins (Bmps), newt anterior gradient (nAG) factor, MARCKS-like protein and Wnts (Beck et al., 2006; Kumar et al., 2007; Lee et al., 2009; Lin and Slack, 2008; Poss et al., 2000a; Poss et al., 2000b; Quint et al., 2002; Schnapp et al., 2005; Smith et al., 2006; Stoick-Cooper et al., 2007; Sugiura et al., 2016; Whitehead et al., 2005; Yokoyama et al., 2007). Exposure to AEC secreted factor Fgf8 is sufficient to induce partial regenerative response in developmental stages which normally do not possess regenerative capacity (Yokoyama et al., 2001). AEC formation and function is regulated by underlying wound tissues. Perturbation of blastema derived signals results deficient AEC (Beck et al., 2006; Kawakami et al., 2006), whereas their activation or exposure to the blastemal tissue secreted Fgf10 induce AEC formation, *fgf8* expression and consequently endow regenerative capacity (Kawakami et al., 2006; Yokoyama et al., 2001; Yokoyama et al., 2000). The importance of nervous tissue derived signal for epidermal function in regeneration has also been demonstrated. Nerves are necessary for nAG, a crucial regeneration factor, which is expressed at the wound epithelia (Kumar et al., 2007). Nerve tissue is able to transform wound epithelia into AEC, presumably via Kgf (Keratinocyte growth factor) secretion (Satoh et al., 2008). Thus, nerve deviation into the lateral wound site can induce ectopic limb formation if a contralateral skin transplant is grafted next to deviated nerve (Endo et al., 2004). The ability of nervous tissue to induce tissue formation is also reported in invertebrates, where deviation of ventral nervous cord to the lateral epidermis results in ectopic anterior and posterior structure formation in Annelids (Kiortsis et al., 1965).

1.5 Planarians as a model for Lophotrochozoan wound healing

The intact planarian epidermis

The planarian epidermis (Fig. 1.2) is composed of a single layer of entirely post-mitotic cells. There are obvious morphological differences between the dorsal and ventral epidermis. Cells within the dorsal epidermis are tall and columnar, whereas cells of the ventral epidermis are shorter and cuboidal. The apical surface of the dorsal epidermis appears irregular and rough (Hori, 1989), whereas the ventral surface is smoother. Various types of ciliated cells, and in some species even cells with microvilli, are found throughout the epidermis. Ciliated cells are most abundant on the ventral surface of the animal, where most cells project multiple long motile cilia required for locomotion. The dorsal epidermis, on the other hand, contains both non-ciliated and ciliated cell domains. (Hori, 1989; Morita and Best, 1974; Pedersen, 1976; Spiegelman and Dudley, 1973). Distinct and less abundant types of ciliated cells also been described in the epidermal layer. Short straight cilia containing cells are scattered along the epidermal surface (Pedersen, 1976), and ciliated sensory cells reside at the anterior body edge of the animal (Macrae, 1967). Thus, the planarian epidermis provides a rich cellular palette for studies of wound healing and regeneration.

As in other invertebrates, cells within the planarian epidermis closely adhere to each other by septate junctions at their apical edge (Hori, 1989; Macrae, 1967). On the basal surface, epidermal cells attach to the underlying basal membrane by focal adhesions. However, contrary to epidermis of other organisms, planarian epidermis attach to basal membrane only by specific basal processes and not through the entire basal surface of the cell (Fig. 1.2). Thus, it appears that epidermal cells attach to the basal membrane by intermediate filament-rich cytoplasmic “feet” (Hori, 1978, 1989). These basal processes are well pronounced and the gaps between them and the basal membrane are filled with electron-lucent extracellular material (Hori, 1989). Another defining feature of planarian epidermis sections is the presence of irregular and variable size empty spaces (Hori, 1978, 1989; Morita and Best, 1974; Spiegelman and Dudley, 1973). These structures seem to spread throughout the epidermal layer, however since the cellular boundaries of planarian epidermis is hard to discern in the histological sections it is not clear whether they are intra- or extra-cellular.

The planarian epidermis is highly secretory, and various intracellular vesicles are present in the cytoplasm of both dorsal and ventral epidermal cells. In fact, one defining

characteristic of the planarian epidermis is the presence of rhabdites. Rhabdites are abundant rod-shape vesicles surrounded by a double membrane and filled with colorless, electron-dense, gelatinous material (Caira and Littlewood, 2001; Skaer, 1961). In *Dugesia tigrina*, *Dusesia japonica*, and *Policelis nigra,* rhabdites are present in virtually every epidermal cell (Hori, 1978, 1989; Pedersen, 1976; Skaer, 1961; Spiegelman and Dudley, 1973), whereas in *Dugesia dorotocephala* these organelles are only observed in non-ciliated cells (Morita and Best, 1974) (Fig. 1.2). Regardless of the species, rhabdites appear larger and more numerous in the dorsal epidermis (Skaer, 1961).

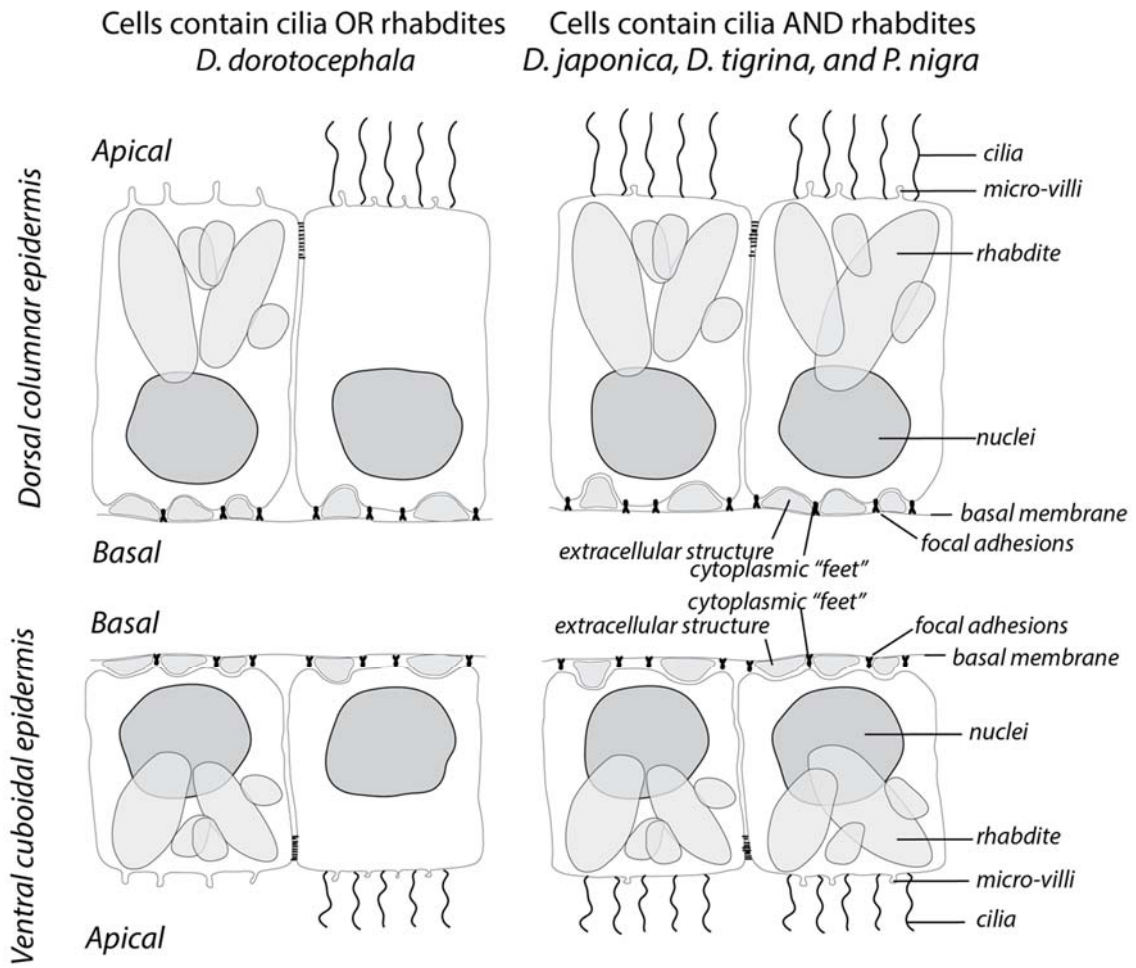

Figure 1-2. Schematic representation of major structures in planarian epidermis. Planarian epidermis is single cell layer. Dorsal epidermis is columnar and ventral epidermis is cuboidal. Apical surface of epidermis is covered with cilia and some microvilli. Apically, epidermal cells are interconnected by septate junctions. The basal surface of epidermis appears irregular. The distinct extracellular structures are situated along the epidermal and basal membrane interface. To establish focal adhesions with basal membrane, epidermal cells project the cytoplasmic feet in-between these extracellular structures. The cytoplasm of epidermal cells contains multiple rhabdites, large intra-cellular vesicles. In most planarian species examined, rhabdites are present in virtually all epidermal cells. In *D. dorotocephala*, rhabdites are only present in non-ciliated cells.

Rhabdite contents are readily ejected from epidermal cells as rod-shaped granules. Upon contact with the aquatic environment, these particles swell and coalesce to form a thin matrix on the animal's epidermal surface (Pedersen, 1976; Skaer, 1961). Despite their abundance within the epidermis of different planarian species, rhabdite function is not understood. Traditionally, rhabdites have been thought to be involved in mucus production

(Hyman, 1951; Skaer, 1961). It was suggested that rhabdite secretion might provide the amount of mucus necessary to make ciliary gliding possible. They have also been suggested to have roles in reproductive cocoon formation, prey capture, and predator repulsion (Caira and Littlewood, 2001; Hyman, 1951; Martin, 1978). However, definitive experimental evidence for any of these functions is still lacking. Histochemical rhabdite content analysis indicates that these organelles are strongly acidophilic (Pedersen, 1959; Skaer, 1961). They stain positive with polysaccharide stain Lugol's iodine. However, since this staining is not affected by diastase treatment, rhabdites are not thought to contain an abundance of starches like polysaccharides. The most thorough chemical analysis of rhabdites performed to date merely indicated that these vesicles likely contain arginine, purine, and adenine (Skaer, 1961).

Epidermal homeostasis

While the planarian epidermis displays a rapid turnover rate, cellular divisions are never observed in this tissue (Hori, 1978; Tu et al., 2015). The only dividing cells within the planarian body are neoblasts, abundant stem cells found in the mesenchyme (Báguna et al., 1989; Newmark and Sánchez Alvarado, 2000). Therefore, the epidermis, as well as other planarian tissues, are maintained by neoblast progeny incorporation (Reddien and Sánchez Alvarado, 2004; Tu et al., 2015; van Wolfswinkel et al., 2014; Wagner et al., 2012). The basal membrane separates neoblast progeny migrating out of the mesenchyme from the epidermis, creating a barrier through which these replacement cells must pass (Hori, 1978; Skaer, 1965). From a cellular biology prospective, this is a truly fascinating process. Progenitors must squeeze through an extremely tight basal membrane and integrate into the ectodermal sheet while simultaneously differentiating and establishing appropriate cellular polarity—all without disrupting the integrity of the epidermis.

This remarkable process of epidermal cell incorporation was documented in *D. japonica* (Hori, 1978). By electron microscopy, presumed progenitors were "caught" in the process of traversing the basal membrane, displaying signs of partial integration into the epidermis. Interestingly, these progenitors appeared to extrude cellular regions containing nuclei first through the basal membrane, while the non-nucleated portion of the cell with the Golgi, endoplasmic reticulum (ER), and mitochondria trailed behind in the mesenchyme. Once cells penetrated enough into the epidermal layer, they began to make contacts with their neighbors through apical intermediate junctions. Meanwhile, newly formed focal adhesions attached the cells to the basal membrane.

Once fully incorporated into the epidermal layer, epidermal cells were observed to complete differentiation. At least in *D. japonica*, differentiation stages could be identified based upon discrete cytological characteristics (Hori, 1978). Recently incorporated cells were narrower at the apical surface. They also displayed a large nucleus containing one prominent nucleolus, a pronounced ER and Golgi bodies, a non-polarized distribution of rhabdites, few microvilli, and no obvious glycogen granules or cilia. Although the basal surface of these cells appeared rough, prominent cytoplasmic feet were not present. In contrast, more mature cells were distinguished by their irregularly shaped nucleus lacking a nucleolus, the absence of prominent synthetic organelles like the ER and Golgi, apically localized rhabdites, the presence of glycogen granules, and an abundance of microvilli and cilia. The basal surface of these cells appeared remarkably smooth, and their basal processes were well-defined.

Recently, transcription-based approaches have been used to describe epidermal lineage progression in *S. mediterranea*. A subset of stem cells, called zeta-class neoblasts, were found to give rise to the epidermal lineage (Eisenhoffer et al., 2008; van Wolfswinkel et al., 2014). Zeta-class neoblast progeny expressing *Smed-prog-1* represent early differentiating epidermal cells, while zeta-class neoblasts expressing *Smed-agat* represent late differentiating epidermal cells (Eisenhoffer et al., 2008; Tu et al., 2015). Several transcription factors regulate epidermal cell differentiation (Tu et al., 2015; van Wolfswinkel et al., 2014; Wagner et al., 2012). The zinc finger transcription factor *Smed-zfp-1* is responsible for the initial allocation of neoblast into the zeta-class (van Wolfswinkel et al., 2014; Wagner et al., 2012). Another Zn-finger transcription factor, *Smed-egr-5,* functions later in the lineage where it is required to initiate the final stages of terminal differentiation (Tu et al., 2015). *Smed-zpuf-6* (zeta-class protein with unknown function-6) expression marks the cells undergoing this final process of maturation. Specifically, *zpuf-6* is enriched in late epidermal progenitors underneath the basal membrane, as well as in a subset of epidermal cells. This epidermal *zpuf-6* expression seems to be limited to recently incorporated, juvenile cells. It is believed that as cells complete their differentiation program within the epidermal layer, e.g., sprout cilia, they downregulate *zpuf-6* expression. Two anatomically distinct ciliated cell domains can be distinguished in dorsal epidermis: the lateral multicilated cell domain and the “racing stripe”, two stripes of ciliated cells along the medial part of the animal. Ciliated cells on both sides of the animal can be depicted by *Smed-FoxJ1-4* as well as intraflagellar transport protein gene expression, perturbation of these gene expression causes motility

defects and edema formation (Rink et al., 2009; Vij et al., 2012). Although the molecular complexity of planarian epidermis has not been extensively explored, it can be further subdivided into at least two cell populations: *Smed-Fox J1-1* expression is specific to ciliated racing stripe cells (Vij et al., 2012), whereas the *Smed-laminin B* and *NB.21.11e* mark the sensory cells at the animal body edge epidermis (van Wolfswinkel et al., 2014).

Wound closure

Immediately after amputation, the body wall musculature around the wound forcefully contracts, bringing the dorsal and ventral epidermis close together. At about the same time, a dramatic morphological transformation of terminally differentiated epidermal cells at the wound boundary can be observed: normally columnar epithelial cells eject cilia, secrete rhabdites, lose their apical-basal polarity to become flattened, and extend 100 μm along the wound surface (Hori, 1978, 1989; Morita and Best, 1974). These extending cells maintain their attachments to the basal membrane and to their epidermal neighbors. Therefore, as the epidermis closes the wound, multiple rows of epidermal cells stretch over the damaged basal membrane. The epidermis, now an extremely thin single-cell layer, successfully covers the wound. Some cilia and a few microvilli can be seen along its surface (Hori, 1989). Shortly after wound closure, the body wall muscle relaxes, which helps pull additional epidermal cells at the wound margin across the wound surface (Hori, 1989; Pedersen, 1976). Consequently, the cells of the most distal wound epithelia lose their attachments to the basal membrane, but still maintain overall epithelial integrity through irregularly spaced septate junctions (Hori, 1978).

The time required for wound closure has been observed to vary amongst different planarian species. For example, *D. tigrina* and *D. japonica* were found to close wounds within a few hours after decapitation (Hori, 1989; Spiegelman and Dudley, 1973). Meanwhile, *D. lugubris* and *D. dorotocephala* required 10 and 16 hours, respectively (Morita and Best, 1974; Pascolini et al., 1984). It is currently unclear whether these variations in epidermal closure dynamics represent real biological species differences or simply experimental artifacts resulting from different preparation methods for these delicate tissues (Hori, 1989; Pascolini et al., 1979; Pedersen, 1976).

Although all investigators recognize the importance of muscle and epidermal cells during wound closure, the extent of their contribution to planarian wound healing is disputed. According to the more accepted view, active migration of epidermal cells at the wound edges is the primary mechanism of planarian wound closure, whereas muscle

contraction only aids this process by bringing the wound edges closer together. This view is supported by the examination of fixed wound tissue. The presence of thinly stretched epidermal cell extensions over the wound surface has been interpreted as evidence of cellular migration. This migratory behavior was only associated with cells directly facing the wound surface, and it was postulated that loss of basal membrane integrity provides migratory cues (Hori, 1989). It was reported that the wound epithelia closely associates with cells of the wound parenchyma. Thus, it was suggested that the parenchyma provides a substrate for epidermal cell migration (Hori, 1989; Morita and Best, 1974). Other authors suggested that migrating epidermal cells might be supported by rhabdite-derived materials (Pascolini et al., 1984; Pedersen, 1976). Shortly after injury, rhabdites are ejected from cells and their contents disperse along the wound, forming a meshwork of randomly oriented filaments that closely associate with the surface of the migrating epidermis.

Chandebois, on the other hand, argued against the notion of active cell migration mediating wound closure in planarians, and instead proposed that wounds are closed because the opposing tissue edges are brought together by muscle contraction (Chandebois, 1980b). Likewise, another researcher suggested that, upon fixation, wounds burst open and any tear apart any reestablished epidermal layer. As a result, an extensively elongated wound surface is observed by EM, producing a false impression that these epidermal cells are migratory. In support of this, filopodia and ruffles are not seen in the wound epithelia, which would be expected from migratory cells (Pedersen, 1976). Furthermore, epidermal cells at the wound edge were not observed to establish obvious cellular contacts with each other or with the basal membrane.

According to Chandebois' model, shortly after the muscle contraction brings the opposing wound edges close together, "spurs" (distinct multicellular extensions from the wound edge epidermis) link the opposing epidermal edges. Once the muscles relax and the wound edges begin shifting away from each other, the attached epidermal cells are pulled over the wound surface. Thus, a continuous thin sheet of wound epithelia is stretched over the wound. Interestingly, Chandebois also suggested that the mechanism of wound closure is different at anterior- versus posterior-facing amputations. Anterior wounds were suggested to be closed by dorsal epidermal extension, whereas the ventral epidermis was proposed to cover over the posterior wound surface. Therefore, Chandebois argued that the orientation of wound closure might provide axials cues that specify anterior- versus posterior-specific regenerative programs (Chandebois, 1980b).

Immuno-electron microscopy suggested the existence of a heterogeneous wound response in the planarian epidermis. Only distinct cells within the wound epithelia were observed to respond to damage by flattening and migrating over the wound surface. Contrary to non-responding neighbors, flattened cells displayed close contact with the basal membrane and had an extensive microfilament network. Their cytoplasm and cellular junctions were rich with actin. As cells stretched further into the wound, actin became enriched in the cortical cytoplasm and cellular processes. Adenylate cyclase became enriched in the membranes of advancing cells, and their surface stained intensively with Concanavalin A (Pascolini et al., 1988a; Pascolini et al., 1988b).

Numerous lines of evidence indicate that planarian wound healing is independent of cell proliferation. Planarians that have been lethally irradiated, which eliminates all dividing cells, are still able to close wounds in a manner indistinguishable from un-irradiated animals (Hori, 1979). Furthermore, the fact that wound healing is not affected by colchicine-induced disruption of mitotic spindles (Hori, 1978) not only indicates that wound healing is independent of proliferation, but also that microtubule dynamics is not required for wound closure. Actin polymerization, on the other hand, is crucial. When actin is perturbed by cytochalasin A treatment, wounds fail to close (Pascolini et al., 1984).

If the predominant classical view is true and planarian wounds are closed by epidermal cell migration, it is unlikely to be driven by conventional lamellipodial crawling. Most ultrastructural studies suggest that the wound epithelia does not establish prominent contacts with the wound mesenchyme. In addition, wound closure defects have not been reported after *de novo* protein synthesis inhibition with cycloheximide (Wenemoser et al., 2012), suggesting that neither integrin reorganization nor wound-specific ECM synthesis are required for wound closure in this organism.

Epidermal regeneration

Wound closure in planarians is followed by a robust regenerative response. In response to injury neoblasts proliferate and their progeny accumulate underneath the wound epithelia to form blastema tissue (Morita and Best, 1974; Spiegelman and Dudley, 1973). Blastema formation marks the beginning of regenerative response, blastema cells differentiate into all the cell types lost in the injury and subsequently their progeny reestablishes missing tissues.

Epidermal regeneration is evident by the second day after amputation (Hori, 1978). Epidermal progenitors must migrate from the mesenchymal blastema and incorporate into

the flattened wound epithelia. These progenitors can be distinguished by the presence of rhabdites, and they exhibit an elongated amoeboid morphology with cytoplasmic extensions oriented towards the body surface (Morita and Best, 1974; Spiegelman and Dudley, 1973). As new cells integrate into the epidermal layer at 2 days post amputation (dpa), the cellular density and thickness of the epidermis increases significantly (Hori, 1978; Morita and Best, 1974). Incorporating cells establish cellular junctions within the epidermis, acquire apical-basal polarity, and assume a columnar morphology. These early-integrating cells do not possess cilia; however, the basal bodies are already present (Morita and Best, 1974). Cytologically, most cells within the regenerating epidermis at this timepoint closely resemble newly differentiated cells of the intact epidermis (Hori, 1978). They have a small number of microvilli, a large nucleus, and variable sizes of cytoplasmic rhabdites. At this stage, the basal membrane and focal adhesions are still not fully restored (Hori, 1978).

The timing of basal membrane restoration—the last step in epidermal regeneration—seems to vary amongst planarian species. In *D. dorotocephala,* it is reestablished by 3 dpa (Morita and Best, 1974), whereas it takes 7 and 9 days in *D. japonica* and *D. tigrina,* respectively (Hori, 1978; Spiegelman and Dudley, 1973). Interestingly, in *D. japonica,* basal membrane restoration requires the presence of neoblasts and, thus, irradiated animals cannot reestablish this structure (Hori, 1979). Shortly after basal membrane restoration, specialized sensory cells are reestablished within the regenerating epidermis (Spiegelman and Dudley, 1973), and the new epidermis becomes indistinguishable from the old tissue.

Discussion

Several properties of planarian epidermis distinguish it from adult epidermal layer in other metazoan models. Unlike adult epidermis in other invertebrate models, planarian tissue has constant cell turnover, contrary to cuticulized ecdysozoan epidermis or keratinized vertebrate skin, planarian epidermis is highly secretory ciliated epithelia. Nevertheless, the most distinguishable feature of planarian epidermis is its remarkable wound closure capacity. Planaria is a classical regeneration model organism that is capable to recover after the most extensive tissue loss. The epidermal ability to rapidly reseal itself after severe damage is fundamental for this process. After tissue loss, the vast wound surface is closed efficiently within several hours by the mechanism independent neither of

proliferation or *de novo* protein synthesis. Yet the mechanism underpinning such a remarkable epidermal wound response or its contribution to tissue restoration are unknown.

Since planaria is an organism with high regenerative capacity, comparative studies of its wound response to tissue loss and damage provides an opportunity to identify the cellular behaviours associated with the regenerative response. The comprehensive representation of epidermal wound response in *S. mediterranea* requires cyto-structural analysis as well as live studies of epidermal cell behaviours. Electron microscopy analysis of its epidermis will have to revisit the findings made in other planarian species as well as will provide description of epidermal structures which might endow the efficient wound healing in this organism. Whereas introduction of live cellular biology studies in planarian, will allow to follow wound closure mechanism and assess cellular wound response contribution to tissue restoration.

The comprehensive study of planarian wound response requires the description of cellular and molecular composition of planarian epidermis as well as its functional analysis. Due to small number of available markers, the heterogeneity of this tissue were not yet extensively explored. Thus, since no wound closure phenotypes were described in planaria, neither the mechanism of efficient wound closure nor cellular wound response contribution to tissue restoration were investigated. Performing transcription profile analysis of planarian epidermis will allow to explore its composition as well as provide the candidates for subsequent mechanistic studies. Planaria is amenable for high throughput (RNAi) gene function studies and thus the knock-down screen of epidermal candidate genes could identify proteins required for epidermal wound response. Subsequent analysis of their phenotypes will depict the mechanism of wound closure and cellular wound response role in regenerative response.

Chapter 2

Characterization of *S. mediterranea* epidermis

2.1 General morphology of S. mediterranea epidermis

S. mediterranea is most common planarian model, however neither its epidermis nor epidermal wound response was previously described in detail. To characterize this tissue, we analyzed its structure by Transmitted Electron Microscopy (TEM) as well as immunostaining. The body of this animal is covered with a single cell layer mucociliary epidermis. The epidermis is highly secretory, and rhabdites (large rod-shaped intracellular vesicles) are abundant in the tissue. In contrast to other planarian species previously

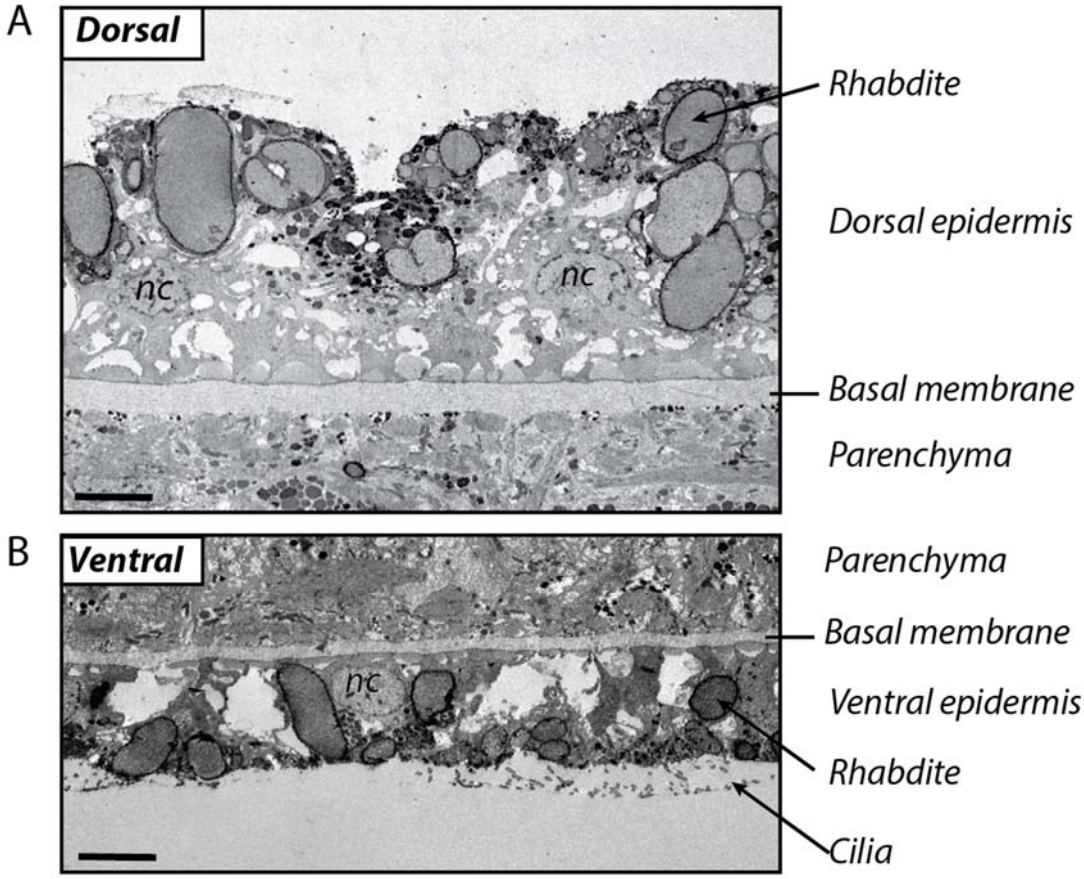

Figure 2-1. General structure of *S. mediterranea* epidermis.
Sagittal section through dorsal columnar (A) and ventral multi-ciliated cuboidal epidermis (B). Nucleus (nc). 5 μm scale bar.

studied, such as the *D. dorotocephala* epidermis (Morita and Best, 1974), no microvilli are found along the apical surface of the *S. mediterranea* epidermis. Instead, this tissue appears much more homogeneous. Very similar structures are seen throughout most of the epidermal layer, and there is no obvious specialization into exclusively ciliated or rhabdite-

forming cells. Nevertheless, epidermal cell morphology is different on the dorsal versus the ventral side of the animal. Dorsal epidermis is made of taller columnar cells, whereas cuboidal multiciliated cells make up the ventral epidermis (Fig 2.1, A and B; Fig 2.2, A). Consistent with previous depiction of planarian epidermis (Hori, 1978, 1989; Morita and Best, 1974; Spiegelman and Dudley, 1973), the irregular, various size empty spaces were also observed by TEM in *S. mediterranea* epidermis. These structures were scattered through-out the epidermal sections (Fig 2.1, A and B), however since individual cell boundaries were hard to distinguish, we could not determine whether these empty spaces represent intracellular vesicles or extracellular space between individual cells.

Although cilia are less abundant on the dorsal side, two distinct ciliated cell domains are also present at the dorsal surface (Fig 2.2, A). The so-called racing stripe is a ciliated domain highly enriched for acetylated tubulin, consisting of two rows of ciliated cells running along the body midline from anterior to posterior. A separate domain of ciliated epidermal cells expressing lower levels of acetylated tubulin are situated at the dorsal-lateral body margin. The racing stripe and dorsal-lateral domain is separated by sparsely ciliated/non-ciliated epidermis. Structurally, the cilia of dorsal domains, as well as the ventral epidermis, is similar. A typical 9+2 microtubule arrangement is visible in all of these cilia in cross-sections (Fig 2.2, B).

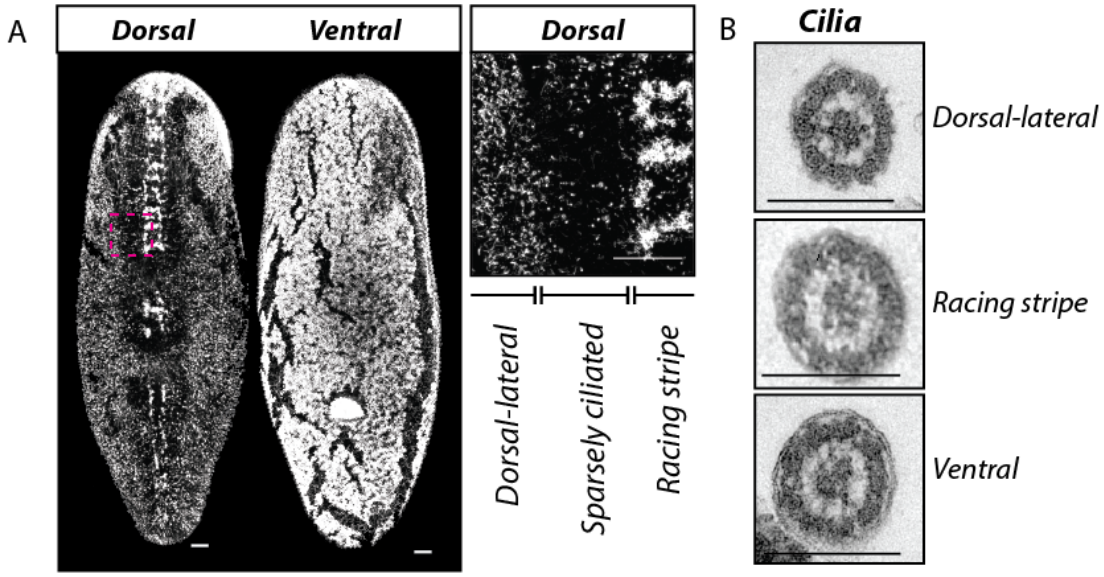

Figure 2-2. Cilia distribution along the epidermis.
Cilia covers the entire ventral surface, as well as two distinct domains within the dorsal epidermis of adult uninjured planarians: dorsal-lateral and racing stripe domains (A, acetylated tubulin staining by immunohistochemistry). Cilia in all locations have a 9+2 microtubule arrangement by TEM (B). 50 μm scale bar in A and 0.2 μm in B.

The apical and basal surface of the *S. mediterranea* epidermis is irregular. The apical surface appears rough and the basal surface does not adhere uniformly to the underlying basal membrane (Fig 2.1, A and B). Epidermal cells attach to the basal membrane at distinct domains of their basal surface (Fig 2.3, E and F). The space between these domains is filled with extracellular matrix (Fig 2.3, F and F'). Therefore, basal surface extensions are well defined, and it appears that epidermal cells rest on the basal membrane by their cytoplasmic "feet." The electron-dense spots along their points of contact with the basal membrane demarcate focal adhesions that are enriched at the tips of the basal surface extension (Fig 2.3 E).

Individual epidermal cell boundaries are often difficult to discern in electron micrographs. Nevertheless, different types of cellular junctions are recognizable at cell interfaces (Fig 2.3, A-D). Apically, cells in *S. mediterranea* are joined by septate junctions, which are tight zipper-like structures spanning more than 1.5 µm of the most apical region of the cell membrane (Fig 2.3, B). More basally, epidermal cells are joined by desmosome-like structures (Fig 2.3, C). These junctions are over 1 µm in length and the dense cytoskeletal bundles extend from their surface into the cytoplasm. In cases where neighboring cell membranes are not as tightly juxtaposed, less pronounced and sparsely distributed spot-junction-like structures could also be visualized along the lateral membrane.

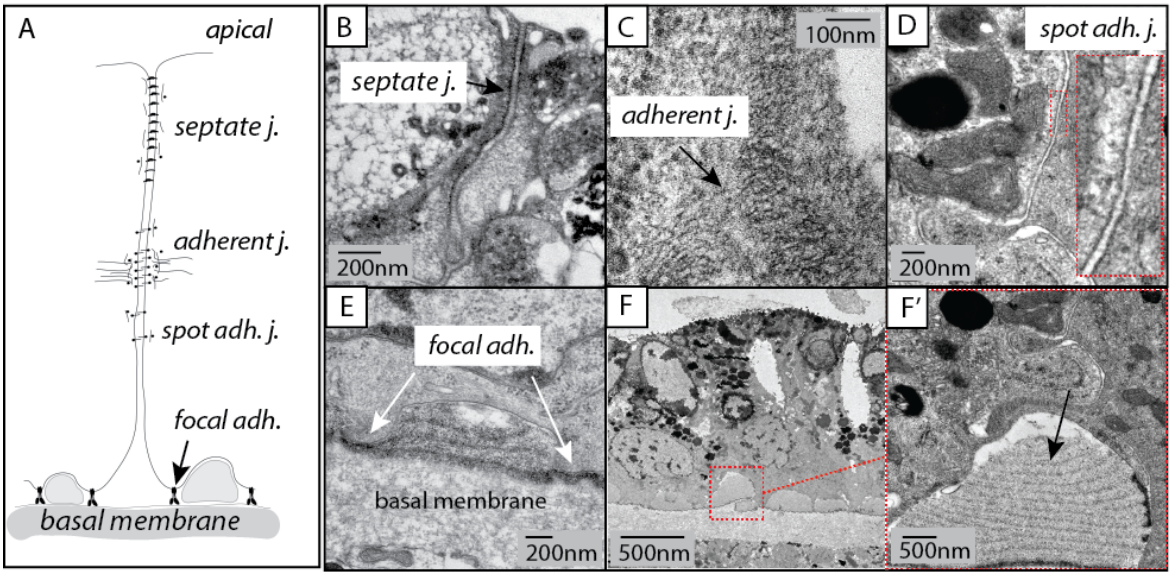

Figure 2-3. Structures along lateral and basal surface of epidermal cells of *S. mediterranea.*
Schematic representation of the described structures (A). Epidermal cells attach to each other by septate junctions (B), desmosomes (C), and spot adherens junctions (D). At the basal surface, epidermal cells attach to basal membrane by focal adhesions (E). Epidermal cells attach to the basal membrane by distinct domains of their basal surface (F and E) the space between these domains is filed with extracellular matrix structures (F', black arrow)

2.2 Response to tissue loss in S. mediterranea

Shortly after an amputation, the body wall contract at the wound site (Fig 2.4). This brings opposing wound edges together, and internal cellular debris is expelled in the process. One hour after the decapitation the tissues around wound margin begin to gradually relax, the wound surface appears smooth and expulsion of cellular debris is no longer observed. By the end of the first day after amputation, the injured body wall is no longer contracted, as it relaxes the wound tissue expands. On the second day after amputation, the blastema begins to form. The unpigmented blastemal tissue expands further as the missing tissues are regenerated over the next week. Although lost tissues are re-established within a week, the new tissue still lacks pigmentation and thus can be still distinguished from an old tissue. Within a month blastemal tissue gets pigmented (not shown) and regenerated tissue becomes indistinguishable from intact counterpart.

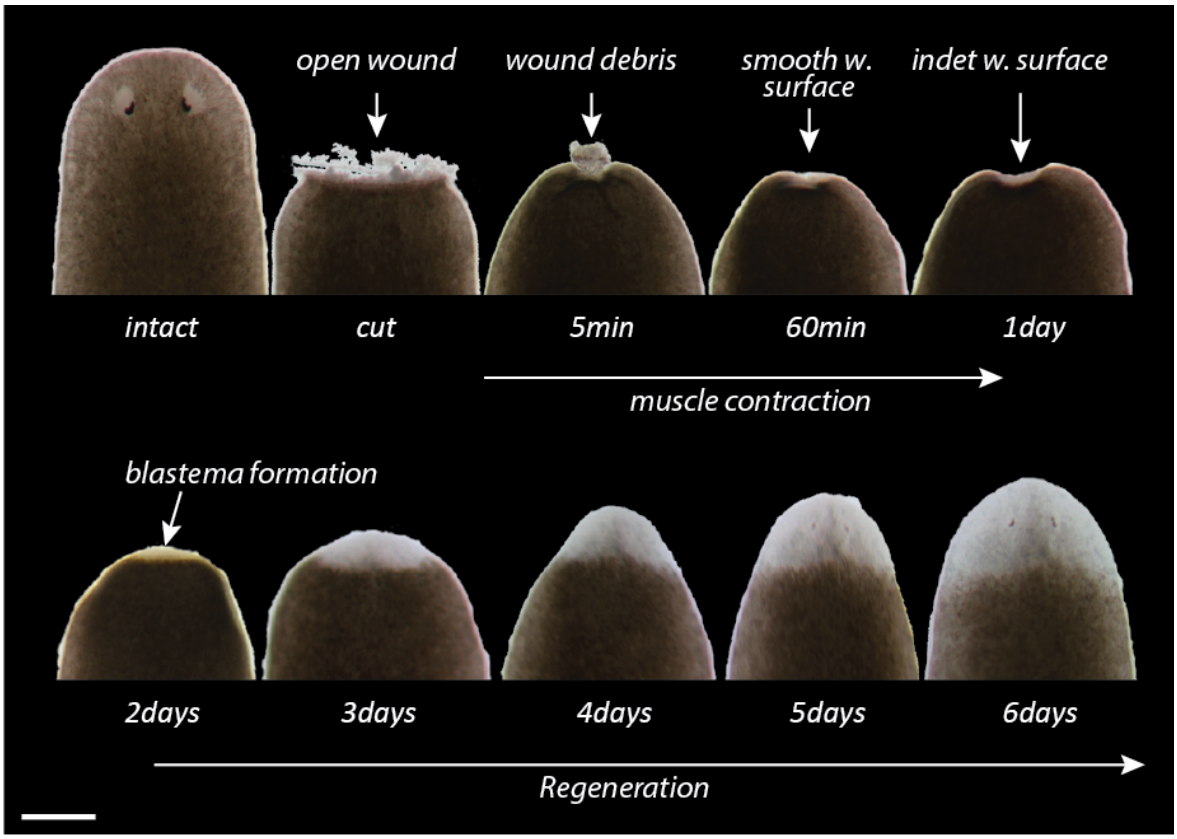

Figure 2-4. The response to tissue loss in *S. mediterranea*.
Minutes after decapitation, body wall around the wound contract and internal tissue is expelled. Within 1 hour, the wound surface closes and appears smooth. At 1 day post amputation, the body wall start to relax and an indentation is observed across the wound surface. Blastema formation is obvious by 2 days post amputation, and eye spots are visible in the regenerate within 5-6 days post amputation. 500 μm scale bar.

Cellular response to tissue loss (electron microscopy)

Our characterization of the wound response in *S. mediterranea* also examined the cellular changes occurring in the epidermis during wound healing. To visualize this process, Scanning Electron Microscopy (SEM) and TEM were performed. SEM preparation preserved the fragile cellular morphology and allowed a three-dimensional view of the epidermis during wound closure. TEM, on the other hand, complemented the SEM analysis by providing high-resolution ultrastructural information about the individual epidermal cells during wound healing and later stages of regeneration.

Wound closure dynamics visualized by SEM

SEM revealed that *S. mediterranea* displays a remarkably fast and robust cellular wound response. At 5 minutes after decapitation, a robust epidermal cell response is evident (Fig. 2.5, B), and nearly half of the wound area is already covered by stretching wound edge epidermis. The cells of the wound epithelia advance across the wound surface while displaying lamellipodia-like protrusions. At subsequent stages of wound closure, injured body wall contractions reduce the area of the wound surface by bringing opposing wound edges closer together (Fig. 2.5, C). Although wound closure duration varies slightly between samples, the entire wound surface becomes covered by a smooth layer of epidermal cells within 1-1.5 hours after decapitation (Fig. 2.5, D). Several explanations of observed variability of wound closure dynamics are possible, such as: the natural variation of wound closure speed within individual animals, the variable degree of surrounding tissue between amputations and the occasional failure to preserve wound epithelia in fixed samples.

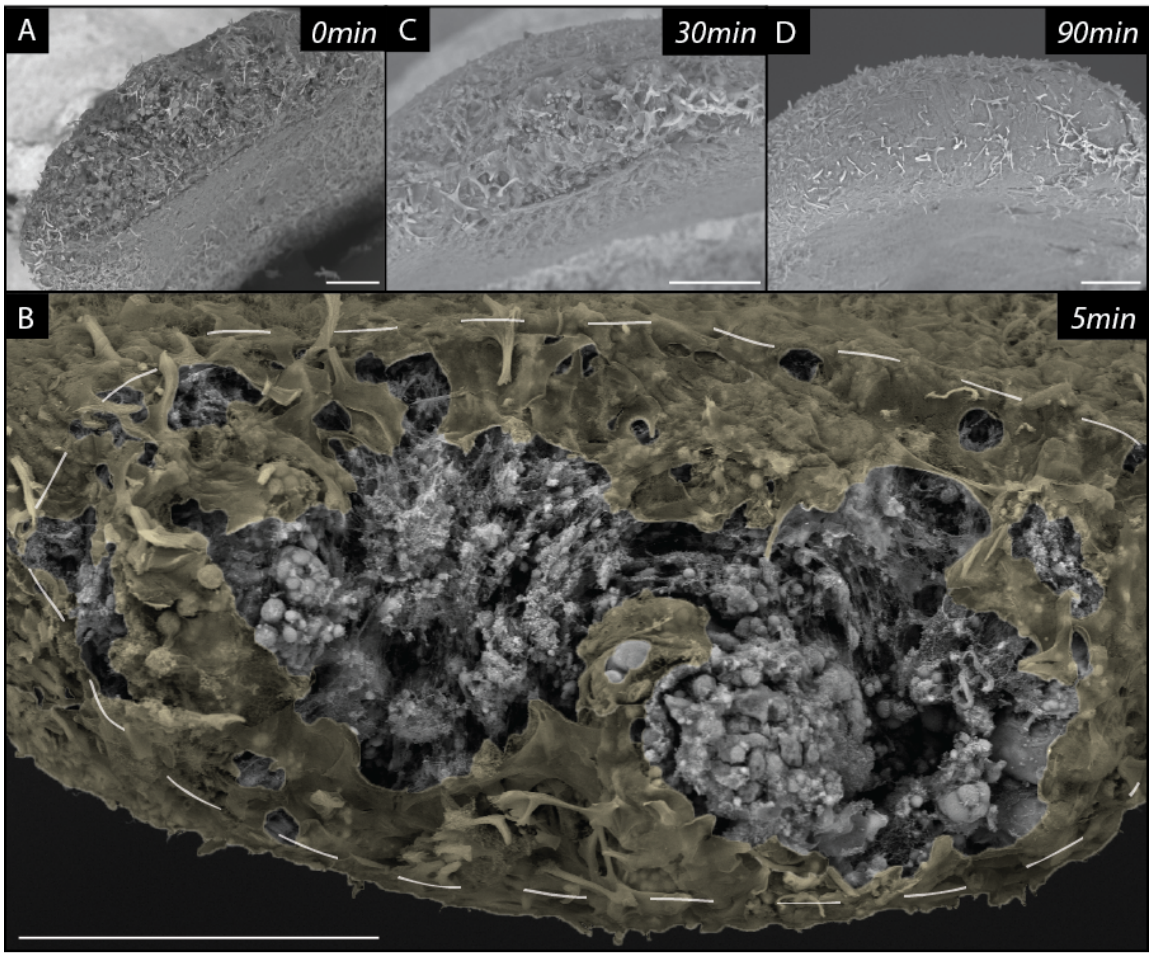

Figure 2-5. Immediate epidermal wound response and rapid wound closure in *S. mediterranea.*
SEM of wound immediately following decapitation (A). 5 min after decapitation, lamellipodia-like extensions from the wound edge epidermis (green) already cover a significant area of the wound surface (outlined by a dashed line) (B). As the wound closure progresses, body wall contraction reduce wound surface area and bring the wound edges together, 30 min (C). Wound closure is completed by 90 min. Smooth wound epithelia covers the entire wound surface. Body wall contraction at the wound site is no longer present (D). 100 μm scale bar.

Although wound closure is driven by epidermal repolarization and the extension of lamellipodia-like protrusions, distinct types of wound edge epidermis protrusions were also captured. Out of dozen animals fixed 5 min after the amputation, two specimens exhibited prominent projections of their wound edge epidermis. On the first occasion, the epidermis formed long and thin extension of epidermis (Fig, 2.6). This structure stretched 100 μm over the wound surface and interconnected the opposite wound edges. On the second occasion, the epidermal projection extended apically over the epidermal cells situated directly at the wound margin and thus connected interior epidermis with advancing wound epithelia (Fig. 2.7).

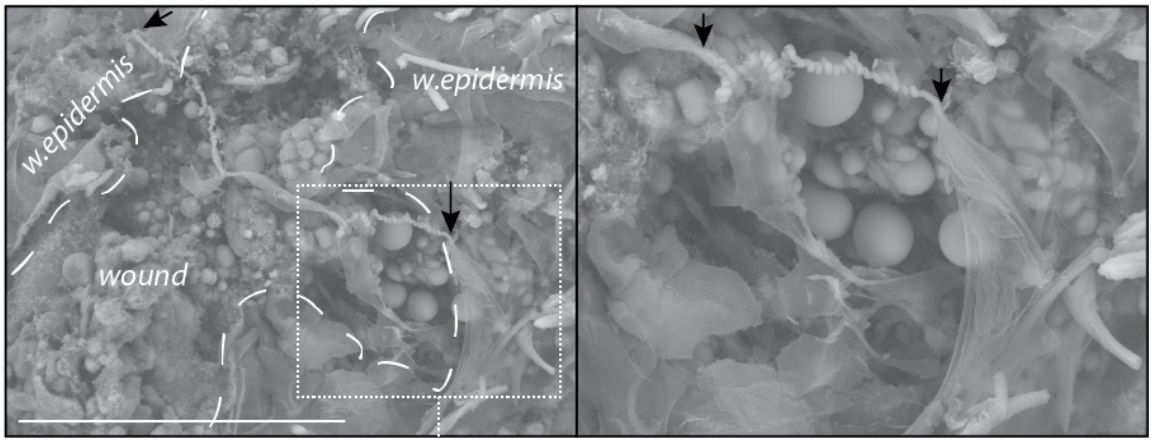

Figure 2-6. Long cellular projections invade the wound surface.

Cells of wound edge epidermis form long and thin projections (arrows) over the wound surface. These structures transverse over 100 µm distance to breach the wound surface to inter-connect opposite wound edges. 5 min after decapitation. Dashed line represents the open wound surface. 100 µm scale bar.

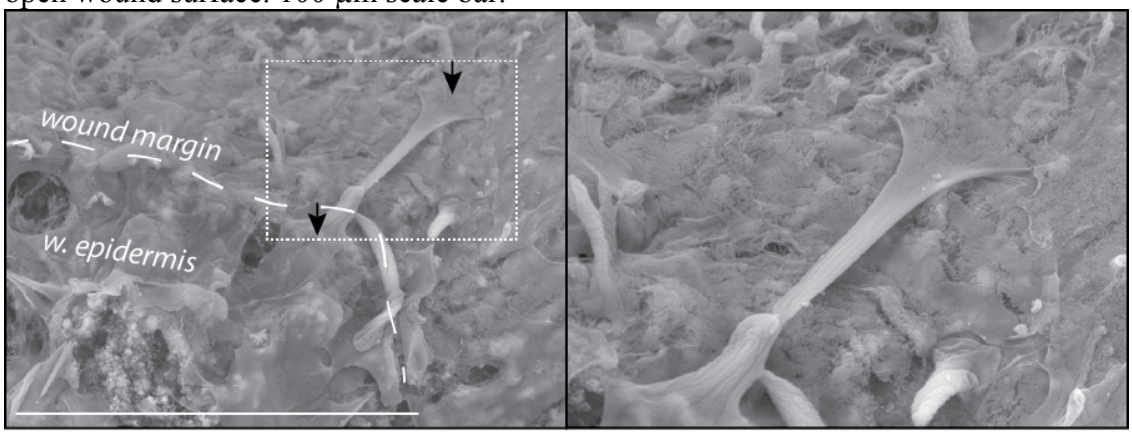

Figure 2-7. The wound epithelia is not exclusively formed by cells at the wound margin.

The apical surface of epidermal cell(s) residing further away from the wound margin and wound epithelia are connected by cellular projection (arrows). Dashed line represents the wound margin. 5 min after decapitation. 100 µm scale bar.

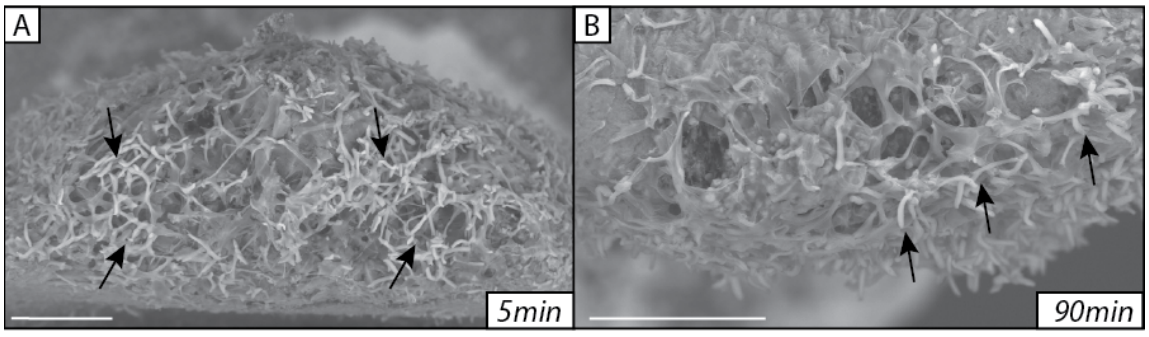

Figure 2-8. Structures of unknown nature along the wound surface.

A dense meshwork of unknown material spans the wound 5 min (A) and 90 min (B) after decapitation (B). 100 µm scale bar.

Interestingly, the early wound response might be even more complex that what was described above. Occasionally, a meshwork of finger-like structures is observed in samples at various stages of wound closure (Fig. 2.8, A and B). These structures are abundant and they do not project in a specific pattern. Although these structures seem to be associated with the wound epithelia, their origin remains to be determined.

Wound closure and epidermal regeneration visualized by TEM

The processes of wound closure and wound epithelia formation were studied by TEM. Immediately after decapitation (Fig. 2.9, A), the dramatic release of rhabdites and their contents is observed throughout the epidermis. This response is not limited to the wound edge epidermis, as rhabdite ejection is evident in cells far from the wound site. Right after injury wound edge epidermis stay attached to the remaining basal membrane, and no signs of cell repolarization towards the wound are visible. The wound edge epidermis appears disorganized with empty spaces between its cells (Fig. 2.9, A').

Shortly after decapitation (5-15 min) (Fig 2.9, B and B', C and C'), the wound tissues coalesce and become more compact. Epidermal cells at the wound margin, as well as epidermal cells several cell rows behind them, repolarize and start to extend towards the wound. Marginal epidermal cells undergo a drastic morphological conversion from apical-basal polarized columnar cells to ones that are stretched (Fig 2.9, C') and extremely flattened (Fig 2.9, C' and Fig 2.5, B). These cells maintain their attachments to each other and the basal membrane. As multiple rows of wound edge cells polarize towards the wound, some cell stretch over their anterior neighbors. As a result, the extending wound epithelia become composed of several layers of thinly stretched epidermal cells.

At later stages of wound closure (30-75 min), multiple cells of wound edge epidermis are visible along the wound surface. The advancing wound epithelia consists of 3-7 epidermal cells (Fig. 2.10, A-C). The leading cells are no longer attached to the basal membrane at the wound margin. However, they do maintain attachments to their neighboring epidermal cells. The basal surface of the epidermis is not connected to any structures at the wound surface. This suggests that re-epithelialization in *S. mediterranea* is driven by cellular extension, and not typical lamellipodial crawling along the wound surface.

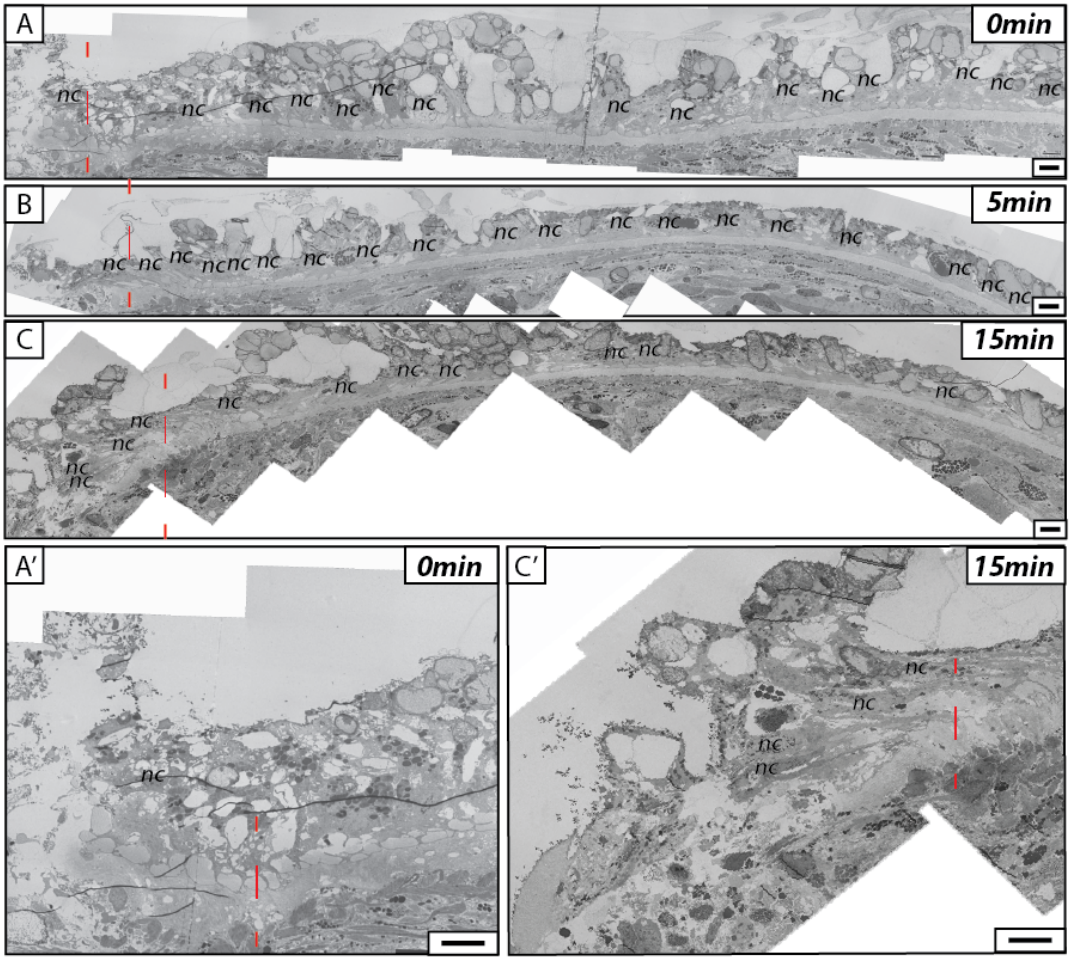

Figure 2-9. Decapitation is followed by rhabdite release and repoliarization of wound edge epidermis.
Decapitation results in robust rhabdite realease in the wound edge epidermis (A, 0 min; B, 5 min; C, 15 min). Although the wound edge epidermis appears dissorganized immediately after injury (A'), it poliarizes towards the wound within minutes (C', 15 min). 4 subsequent rows of epidermal cells stretch over each other and into the wound (C'). Red dashed line marks the wound edge. Nuclei (nc). 5 µm scale bar.

Although our previous SEM studies demonstrated that epidermal integrity is reestablished over the wound surface by around 1.5 hr, the continuous layer of wound epithelia could not be preserved in TEM samples earlier than 24 hr after the decapitation. At this point, wound epithelia covers the wound surface as an extremely stretched out, continuous cell layer (Fig. 2.11, A). At the wound margin, several epidermal cells stretch over each other (Fig. 2.11, A'). Nevertheless, most of the wound surface is covered with a layer of epidermis one cell thick (Fig. 2.11, A"). Flattened nuclei are sparsely distributed along the wound epithelium (Fig. 2.11, A'''). Although empty spaces separate the wound epithelium from the wound mesenchyme, distinct mesenchymal cells are aligned along the basal surface of the wound epithelia (Fig. 2.11, A'' and A''').

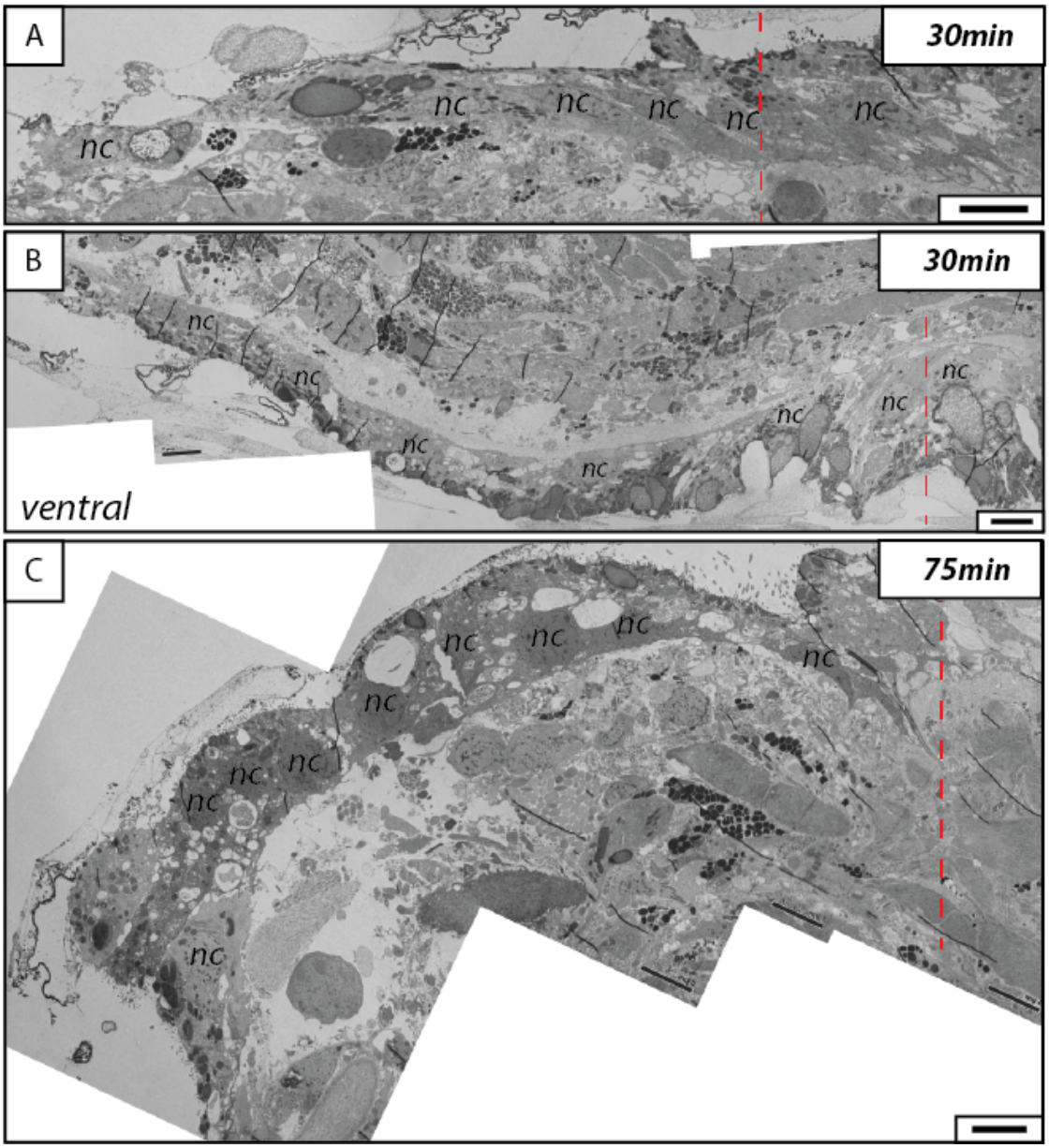

Figure 2-10. A sheet of wound edge epidermis extend over the wound surface to close the wound.
Advancing cells are no longer attached to the basal membrane at the wound egde; however, they mainatin their conatcts to each other and remain in the epidermal sheet. The wound epithelia does not associate with the wound surafce, instead appearing to extend over the wound surface rather than migrating along it (B, C). Red dashed line marks the wound edge. 30min after the decapitaion at A and B and 75min at C. Dorsal at A and C, ventral at B. Nuclei (nc). 5 µm scale bar.

Lethally irradiated animals (7 days after irradiation) formed wound epithelia which appeared indistinguishable from controls, confirming that planarian wound closure is independent of cell proliferation (Fig. 2.11, B and B'). These animals lacked mesenchymal cells underneath their wound epithelia, suggesting that these mesenchymal cells have little

to no effect on wound re-epithelization. Thus, since animals are already deprived of most epidermal progenitors by 7 days after irradiation (Eisenhoffer et al., 2008; Tu et al., 2015), indicates that the incorporation of newly differentiated epidermal progenitors into the epidermis is not necessary for planarian wound closure.

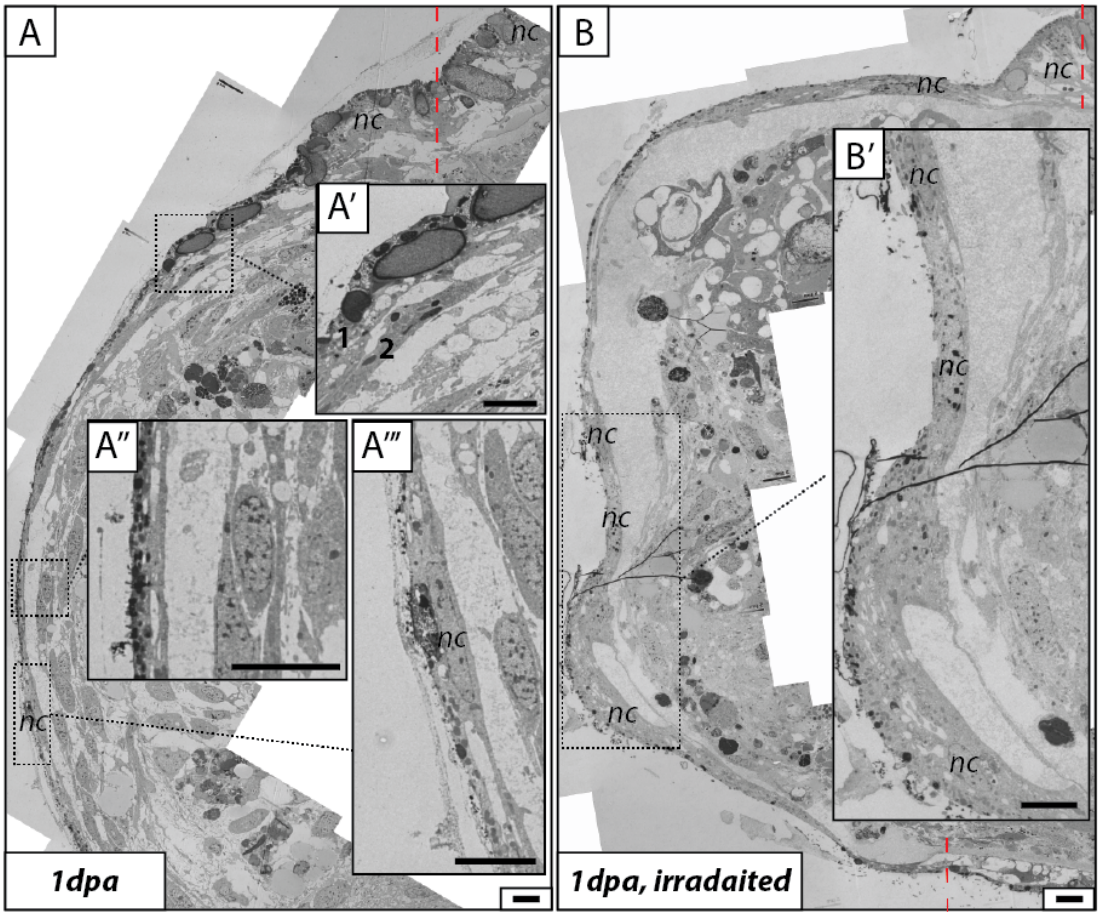

Figure 2-11. The wound is closed by a thin, stretched out epidermal layer. Wound epithelia covering the wound surface next day after injury (A). At the wound margin, multiple cells stretch over each other (A'). However, most of the wound surface is covered with a thin, stretched out epidermal layer (A'' and A'''). Wound epithelia in lethally irradiated animal next day after injury (B). Animals were irradiated one week prior the wounding. Red dashed line marks the wound edge. Nuclei (nc). 5 µm scale bar.

Epidermal tissue reorganization during blastema growth visualized by TEM

Wound closure is followed by the formation of a blastema. As regeneration progresses, the thin, stretched epidermal layer (1 day after decapitation), Fig. 2.11, A) expands further to accommodate the growing blastemal tissue (2 days post amputation (dpa), Fig 2.12, A). At 2 dpa, blastema cells accumulate underneath the wound epithelia by tightly filling the available space underneath the wound epithelia (Fig. 2.12, A, A'). Two mechanisms of epidermal tissue expansion are evident in sections examined: 1.) newly differentiated epidermal cells originating in the mesenchyme incorporate into the epidermis, and 2.) the epidermis undergoes reorganization. The evidence of mesenchymal cells entering the epidermal layer was captured because the wound epithelia thickened enough to resolve the boundaries of individual cells. By 4 dpa, newly differentiated cells enter the epidermis by squeezing between the basal lateral surface of pre-existing epidermal cells (Fig 2.12, C'). Integrating cells show some signs of epidermal differentiation, and even possess small cytoplasmic rhabdites. However, most of these cells do not stretch as far along the length of wound epithelia as the pre-existing epidermal cells, and their apical surfaces do not fully extend to the outside surface of the animal. Furthermore, an examination of the epidermis in the vicinity of the wound indicates that cells of the intact columnar epidermis also contribute to the expanding wound epithelia. Accumulating mesenchymal cells cause the epidermal layer to stretch far beyond the wound surface, and a gradual decrease in epidermal tissue height is evident in the intact columnar epidermis. By the time the blastema forms, the stretched epidermal domain was 100 μm in length (2 dpa, Fig. 2.12, A). As wound tissues expand further, the stretched epidermis domain spans 180 μm into the intact tissue (4 dpa, Fig. 2.12, C, C'', and C'''). Similar epidermal reorganization does not happen in irradiated samples because blastema formation and, thus, mechanical expansion of the wound epithelia does not occur (Fig. 2.12, B and B').

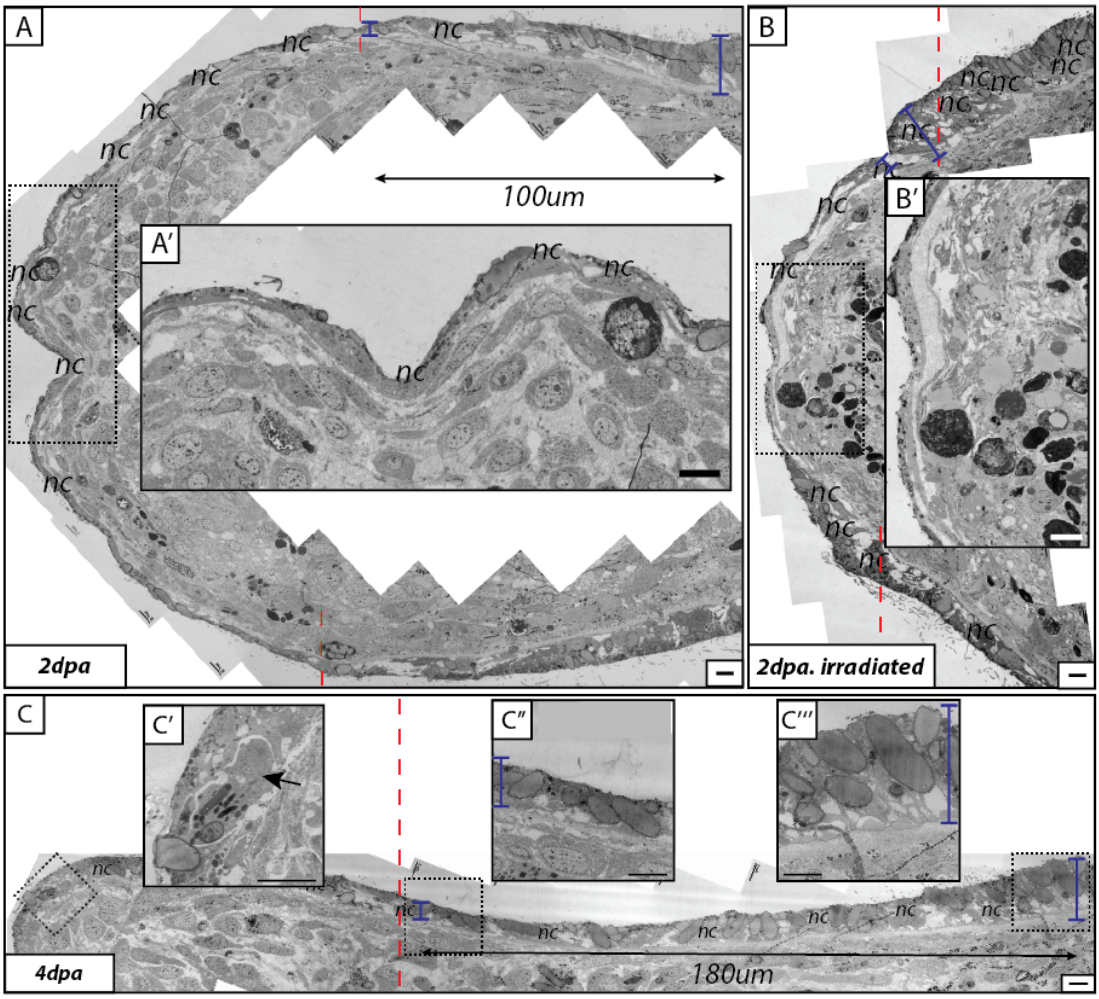

Figure 2-12. Epidermal layer reorganization over the expanding blastema. By 2 dpa, mesenchymal cells accumulate underneath the wound epithelia (A). By 4 dpa, the integrity of the epidermis covering the expanding blastema (C) is maintained by two mechanisms: new epidermal cells integrating into the wound epithelia (C') and cell recruitment from the columnar epidermis (note the change in columnar epidermis height in A versus C). The closer to the damage site, the more stretched columnar epidermis becomes (note epidermal height in C'' versus C'''). Epidermal reorganization observed in C does not occur if blastema formation is prevented by irradiation (B). Red dashed line marks the wound edge. Nuclei (nc). 5 µm scale bar.

Epidermal tissue regeneration visualized by TEM

During the subsequent days following wound closure, the wound epithelia gradually reestablishes the morphology observed in intact animals. As more cells are recruited into the wound epithelia between 1-6 dpa, the thickness of the wound epithelia increase and reacquires its typical columnar morphology (Fig. 2.11, A; Fig. 2.12, A and C; Fig. 2.13, A). By 6 dpa, the epidermis covering the blastema is indistinguishable from that of intact tissue (Fig. 2.13, A). At this time-point the basal membrane is already fully reestablished and the wound margin is no longer identifiable. The cells of the wound epithelia display a columnar morphology, and various signs of terminal epidermal differentiation are visible within this tissue. For example, the size and numbers of rhabdites is reestablished in all of the epidermal cells. The ventral surface is now covered with ciliated cells, and the specialized adhesion gland cells are easily recognizable at the body edge. In contrast, none of these epidermal characteristics could be observed in irradiated animals (Fig. 2.13, B). However, contrary to *D. japonica* (Hori, 1979), irradiated *S. mediterranea* was able to restore basal membrane, suggesting that the formation of this support structure is independent on neoblast function in this species.

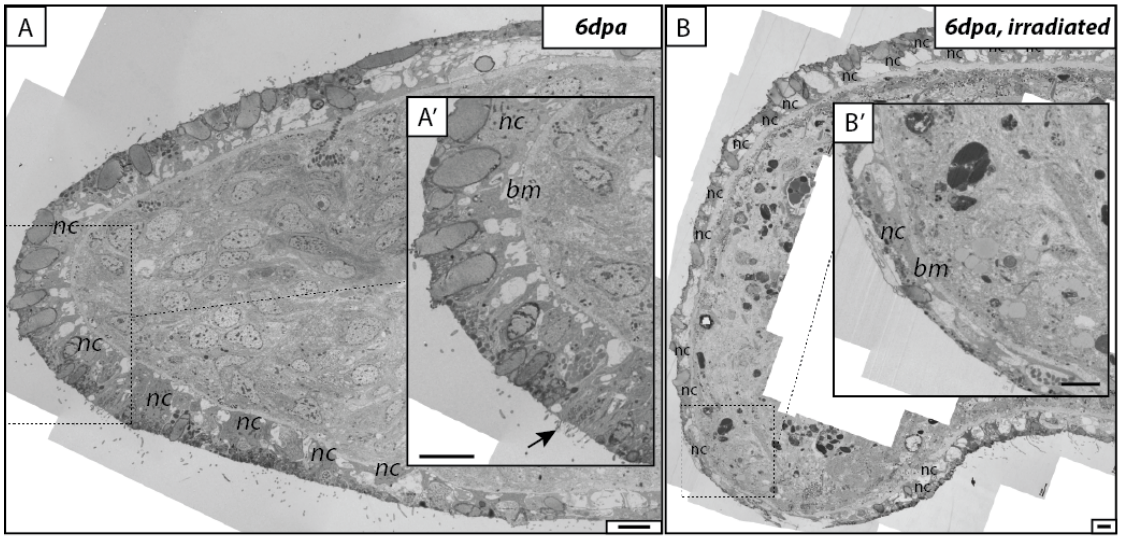

Figure 2-13. Fully reestablished epidermis.
By 6 dpa, epidermal morphology and composition is reestablished (A). Epidermal cells are columnar in shape, the basal membrane has formed, and rhabdites and cilia are abundant. The epidermal component of the adhesion gland has regenerated (arrow). Basal membrane is reestablished in irradiated animals (B). Red dashed line marks the wound edge. Nuclei (nc). 5 µm scale bar.

Summary

The wound response to tissue loss in planaria is remarkably robust and efficient, however, the cellular mechanism governing this process is not yet fully understood. Electron microscopy analysis demonstrated that wound closure in *S. mediterranea* is remarkably fast (1.5 hr; Fig. 2.5). Wound closure is mediated by drastic phenotypic transformation of differentiated columnar epithelial cells. Immediately after injury, epidermis exhibit robust exocytic wound response (rhabdite release) (Fig. 2.9, A) and starts to repolarize into extremely flat and thin wound epithelia (5 min; Fig. 2.5, B and Fig. 2.9, C`). Minutes after the tissue loss, these cells start to advance over the wound surface by extending wide lamellipodia-like structures (5 min; Fig. 2.5, B) as well as occasionally forming distinct long and thin cellular projections (Fig. 2.6 and Fig. 2.6). Wound is re-epithelialized by a one-cell thick sheet of wound edge epidermis (Fig. 2.10). The cells in advancing wound epithelia adhere to the wound surface and thus it appears that planarian wound closure is mediated by a cell extension mechanism rather than the crawling/active migration of wound edge epidermis.

Several aspects of planarian cellular wound response make it particularly interesting to study it in greater detail. Although planaria epidermis can rapidly reseal the vast wound surface after the extensive tissue damage and loss, this is achieved by epidermal cell morphology transformation rather than by increasing epidermal cell number (Hori, 1978; Hori, 1979). Intriguingly, wound closure in planaria is independent of *de novo* protein synthesis (Wenemoser et al., 2012), suggesting that the machinery endowing remarkable wound healing capacity of planarian epidermis is already present in an intact tissue. Captured novel wound responses such as long cellular projection formation suggesting that wound response in planaria is truly unconventional. However, since wound response cannot be followed in the fixed samples, neither the mechanism underpinning wound closure in planaria nor the function of observed wound responses could be interrogated.

Although planarian wound closure is a dynamic process, it was only studied in fixed samples and thus it was not directly visualized. Our work as well as previuos studies (Chandebois, 1980b; Hori, 1989; Pascolini et al., 1979; Pedersen, 1976) noted that planarian wound response might not be well preserved in fixed samples. Body wall contraction at the wound as well as delicate wound edge epithelia structures usually are not well retained within TEM samples, hence making it hard to infer the wound closure mechanism. Previously two contradictory wound closure mechanisms were proposed:

muscle contraction and cell migration mediated. Our results suggest planarian wounds are primarily closed by repolarization and extension of wound edge epidermis. However since wound close was not visualized live, the validity of either wound closure model cannot be tested. Live imaging methodology is critical for detail characterization of cellular wound response and its role in subsequent stages of wound healing. It allows to visualize wound closure, the first and critical step of wound healing, and provides the necessary tool for mechanistic studies of wound response and its contribution for subsequent wound healing steps. Thus, the ability to track cells live allows investigation of wound edge epidermis behavior and contribution to lost tissue restoration.

Chapter 3

Live imaging methodology development

Due to a lack of development of modern cell biology tools, the cellular wound response has not previously been extensively studied in an organism with high regenerative potential. No detailed live imaging studies had been performed in planaria mainly due to two hurdles: (i) the lack of efficient animal immobilization methodologies and (ii) an inability to label living cells. To provide the most comprehensive description of the cellular wound response in this system we have committed to overcoming these challenges.

3.1 Animal immobilization

Animal immobilization strategies are crucial for successful visualization of live tissue, being especially important in experiments designed to follow cellular behavior. In such cases, immobilization methodologies have to be efficient but non-deleterious to the tissue being examined throughout the extended imaging sessions. Several aspects of planarian physiology hinder the live visualization of their tissues. These animals are strongly photophobic and thus they swim away to avoid the light during microscopic examination. Remarkably, this behavior is also exhibited by body fragments from which photoreceptors or the central nervous system had been removed by decapitation. The anatomy of the planarian body makes it hard to obstruct their movements. These aquatic invertebrates do not have a firm body - the planarian body can extensively contract, stretch, and bend. In addition to extreme elasticity, these animals possess strong musculature allowing them to squeeze their mucus-covered body through tight confinements. Since the ability to maintain planarian tissue within the field of view of the microscope optics was a critical first step towards the visualization of the cellular behaviors in this system, two animal immobilization strategies were tested: chemical and mechanical.

Chemical immobilization

We investigated whether animals could be immobilized for extended time periods solely by application of bioactive compounds. A series of candidates predicted to affect animal sensory input or muscular function were considered. Despite safety concerns and compound availability limiting the number of the reagents we could test, the effectiveness of an array of candidate molecules was assessed.

The applicability of compounds with known effects on planarian motility was tested first. It has been previously reported that planarian locomotion is reduced after the exposure to chloretone (Guedelhoefer and Sánchez Alvarado, 2012) or ethanol (Stevenson and Beane, 2010). Although continuous exposure to chloretone (0.15%) completely immobilized the animal within minutes after the administration, its application for long-term animal observation was limited. Animal motility resumed shortly (5 min) after chloretone withdrawal, whereas continuous exposure to this compound (45 min) caused animal lysis. Exposure to a low concentration of ethanol (3%) was not effective. Ethanol impaired cilia-mediated "gliding" locomotion, however it did not abolish muscle-mediated locomotion and thus animals were still able to move by inching along the bottom of the dish.

Subsequently, it was investigated whether an efficient planarian immobilization reagent could be identified by screening an array of available molecules. First, compounds with known anesthetic or sedative properties in vertebrates (Ross and Ross, 2009; West et al., 2014) (tricane, eugenol, chloral hydrate, tubocurarine) were tested. However, no efficient immobilization of planarians was achieved with these compounds. Continuous exposure to aromatic alcohols, on the other hand, had a profound effect on planarian motility. 1-Phenoxy-2-propanol (10 mM) and 2-Phenoxyethanol (10 mM) led to complete immobilization within minutes after their administration. As animal motility reduced, their pharynxes extruded, suggesting that animal immobilization most likely involved musculature relaxation in these cases. Prolonged exposure (>60 min) to these molecules did not result in animal lysis and animals remained immobile long after (30 min) 1-Phenoxy-2-propanol withdrawal.

Magnesium ion-mediated muscle relaxation protocols are common in various invertebrates (Lewbart, 2011), thus their applicability for planarian immobilization was also investigated. Indeed, a brief, few-minute exposure to $MgCl_2$ (3.5%) resulted in complete animal immobilization. Although planaria remained immobile 40-60 min after acute exposure to magnesium, its effectiveness was limited to high salt concentration, which also caused occasional animal lysis. Such lysis was less prominent at lower magnesium salt concentration; however, immobilization effectiveness was not maintained in these conditions.

Efficient immobilization was also achieved by continuous exposure to a 50% solution of saturated menthol. This immobilization strategy was especially well suited for extended visualization of planarian tissues. If menthol evaporation was prevented by

mounting animals between two coverslips, intact animals could be maintained immobile for prolonged time periods (>3 hrs). Nevertheless, although menthol administration abolished muscle-mediated movements, slow animal body drift was still noticeable at higher magnifications. We reasoned that cilia-mediated locomotion is the most likely cause of the remaining motility and thus we have modified our protocol to prevent it. The tissue drift was eliminated once immobile animals were mounted within menthol solution containing viscous 6% methylcellulose matrix.

Although continuous exposure to chloretone, aromatic alcohols (1-Phenoxy-2-propanol and 2-Phenoxyethanol) and menthol could immobilize intact planaria, their applicability to injured animal visualization showed far less promise. Decapitated animals failed to contract muscles at the injury site and their wound-edge tissues started to deteriorate eventually leading to whole body lysis. Animals immobilized by acute magnesium salt treatment usually survived decapitation, however their wound closure only proceeded as the animal started to recover motility. Since none of the effective chemical immobilization regimens were compatible with wound closure, alternative immobilization strategies had to be developed.

Mechanical immobilization

We next sought to determine whether we could immobilize planarian tissue and yet preserve wound closure solely by physically restricting animal movements. Initially we attempted immobilization by embedding the animal in low melting-point agarose. However, even high percentage (>6%) agarose did not sufficiently restrict worm movements and animals swam out of the agarose as it was beginning to solidify. Next, we tried to restrict animal movements by permanently adhering one side of the animal with "wet stitches" - the adhesives commonly used to close tissue cuts after oral surgery. However, upon contact with planaria, adhesives quickly spread along the animal body and permanently engulfed its entire surface, making it unsuitable for visualization.

Custom made PDMS (Polydimethylsiloxane) devices have been successfully used to restrict animal movements in invertebrate systems (Ben-Yakar et al., 2009; Hulme et al., 2007), thus we explored their applicability in planaria. One particular PDMS device, previously designed to image fly larvae (Ghannad-Rezaie et al., 2012), seemed to be compatible with the flatworm body plan. The original device immobilized the animal by restricting its movements within an elongated 3.5x1.5 mm chamber (Fig. 3.1). Although these proportions resemble those of the planarian body, the chamber dimensions could only accommodate medium-sized planarians. Therefore, to suit the wide range of planarian

sizes, multiple separate devices with modified chamber dimensions were fabricated and subjected to testing.

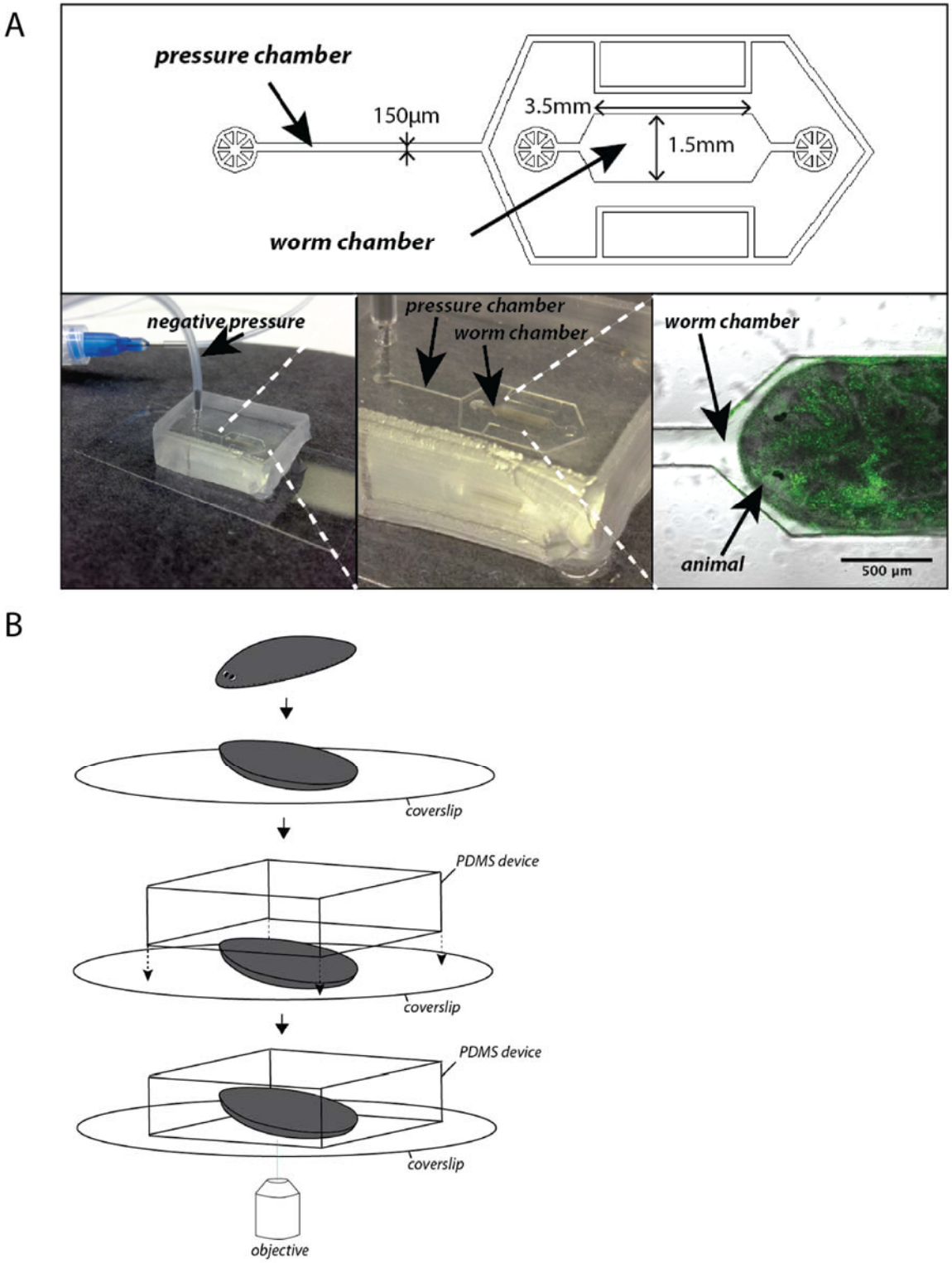

Figure 3-1. PDMS device design and its application for planarian immobilization and dorsal/ventral surface imaging.
Schematics of PDMS device design (A). Negative pressure ensures device adhesion to the coverslip. The negative pressure channel does not connect to the sample chamber (Ghannad-Rezaie et al., 2012). Schematics representing the procedure of animal mounting in PDMS device (B).

Although the adapted devices did not eliminate minor contractions of animal tissue, the nearly complete animal immobilization without tissue damage was successfully achieved when the animal body matched well with the chamber dimensions. Several device features made it well suited for prolonged and high-resolution observation of animal tissues. Since a separate channel ran along the device interface with a coverslip, the force by which the device attached to the glass surface could be adjusted. The constant application of negative pressure within this channel kept the coverslip tightly adherent to the device. As a result, the chamber remained closed and thus we were able to maintain planaria entirely flat along the coverslip surface, which made it submissive for prolonged observation with inverted microscope optics.

Next, we explored the PDMS applicability for wound response visualization. Animals with various extents of tissue damage were subjected to PDMS immobilization methodology and their wounds were subsequently visualized. Although the PDMS device did not prevent the smaller superficial wound closure, the mounting procedure was found to elicit further damage to the wound tissues. Upon application, the device pushed upon animal tissues which consequently displaced the wound edges and often tore the wound edge epidermis. This damage was most profound in the decapitated animals, in which their wounds became forced open and the cellular debris was pushed through the wound surface.

The adapted PDMS device proved to be a feasible platform for intact animal immobilization, however its design was neither suitable for large wound closure nor decapitated animal wound response visualization and thus it had to be modified. Depending on which side of the animal was mounted on the coverslip, the original device only exposed the dorsal or ventral surface of planaria. Decapitation, on the other hand, creates a wound surface which is perpendicular to the animal surface, a plane of orientation that was not accessible for observation using the available device. Thus, the PDMS device design had to be specially tailored for wound response visualization in the decapitated animal.

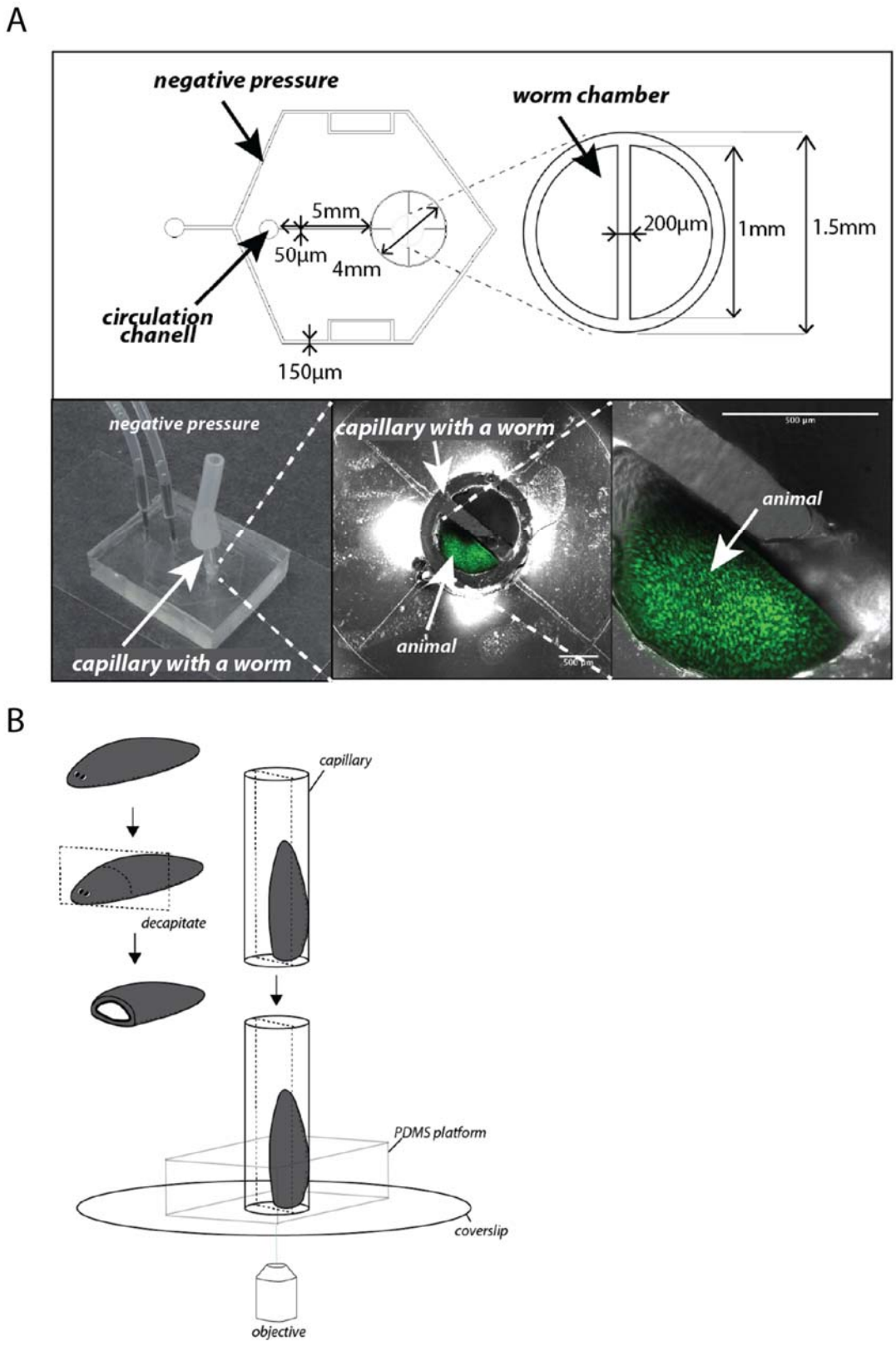

Figure 3-2. Device for orthogonally mounted sample imaging.
Schematics of device design (A). Negative pressure ensures device adhesion to the coverslip. The animal is mounted in the "theta" capillary. The circulation channel allows hydration and washing of the mounted sample. Schematics representing animal mounting in the capillary into capillary (B).

To visualize the decapitation-elicited wound surface, animals had to be mounted perpendicular to the coverslip. However, a PDMS chamber that would enable immobilization of the animals in this orientation could not be successfully designed. We reasoned that the cellular response to tissue loss could be visualized if decapitated animals were immobilized within a perpendicularly-positioned glass capillary, therefore we designed and tested a PDMS platform which allowed a capillary to be maintained in the desired orientation (Fig. 3.2). When decapitated worms were loaded into the capillary by mouth pipette it became apparent that a conventional capillary did not efficiently constrain animal movements. The “theta” capillary (the inside of which is divided into two -D-shaped channels by a septum), on the other hand, proved to be an efficient immobilization platform. The divided capillary contained two chambers, which not only better resembled the animal body shape but also allowed removal of the cellular debris by washing prior to decapitated-wound visualization.

Although the capillary approach was found to be a platform to visualize wound response in decapitated animals, it only allowed for the mounting of animals of restricted sizes and it required carefull sample positioning within the working distance of the microscope optics. Therefore, we also sought to develop a more versatile and less labor-intensive immobilization strategy. Although neither animal immobilization within solidifying low melting-point agarose (6%) nor acute exposure to chloretone (0.15%) alone were successful, the combination of both these methodologies proved to be efficient. Short exposure to chloretone maintained animals immobile long enough for low melting-point agarose to solidify over their body surface. As animals recovered after the chloretone withdrawal, they were tightly encased within agarose, which completely restricted their body movements. This strategy enabled the immobilization of large numbers of animals of various sizes. Once solidified, agarose blocks containing an animal could be trimmed and positioned in virtually any orientation along the coverslip surface (Fig. 3.3). Injured tissues did not deteriorate after mounted animal decapitation and the normal wound muscle contraction was visible at the damage site.

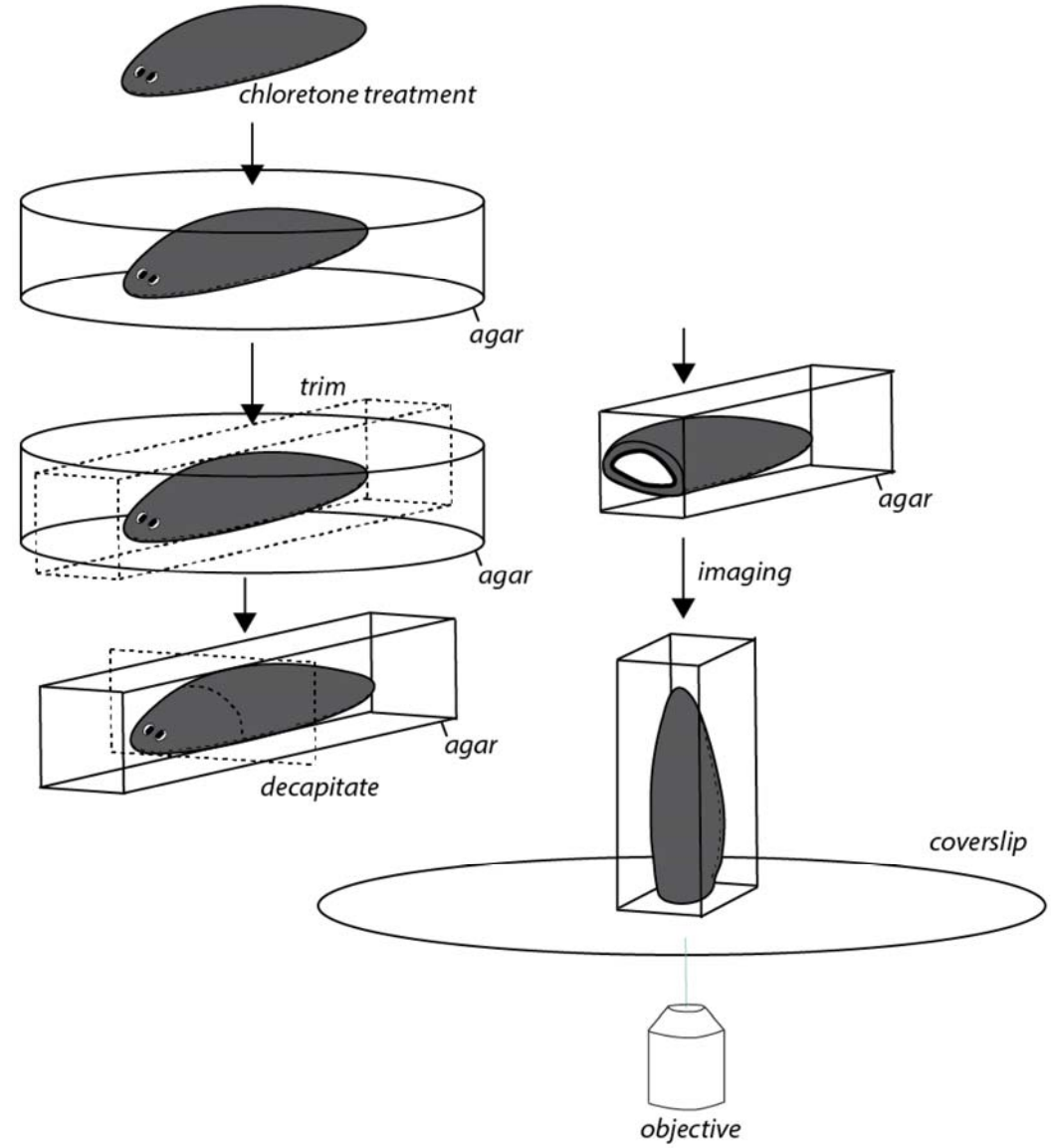

Figure 3-3. Wound response visualization in low-melting point agarose-mounted animals.
Schematics of animal immobilization in agarose procedure. Chloretone anesthetized animals are embedded in low-melting point agarose. Once agarose solidifies, excess agarose is trimmed. To follow wound response after tissue loss, animals are decapitated and their wounds positioned in front of the microscope optics.

3.2 Cell labeling

The development of immobilization methodologies allowed us to visualize the dorsal or ventral animal surface with transmitted light microscopy. However, resolving cellular behaviors within animal tissues or imaging orthogonally-mounted decapitates required fluorescent labeling of the epidermal tissue. Exogenous protein expression methodologies are not yet developed in planaria, therefore we explored the possibility of labeling planarian tissues with various commonly available fluorescent dyes.

Cell permeable organic dyes

Since the main goal of this project was to follow wound response at the epidermis, the outermost tissue of the animal, it was reasoned that soaking intact planaria in cell-permeable dyes would allow specific labelling of this tissue. The properties of the Cell Tracker and Cell Trace family of fluorescent probes (Invitrogen) made them seem well suited for this purpose. Once these cell permeable molecules enter the cytoplasm, they are converted into fluorescent probes which also covalently bind cellular proteins and therefore ensure well-retained cell labeling (Haugland et al., 2002). To label the planarian epidermis, multiple intact animals were soaked in 10 μM of dye and rinsed a few times with 1x Montjuich salt solution before imaging. Labeling with Cell Tracker dyes (Cell Tracker green and Cell Tracker orange) was the most successful approach. Robust epidermal-specific discrete cell labeling was achieved after 15 min incubation in this dye solution (Fig. 3.4, A). Extended incubation also results in the accumulation of the dye in the epidermal rhabdites, an intracellular vesicle compartments, as well as it can label the gut epithelia (not shown). Interestingly, in contrast to the Cell Tracker dyes, 15 min incubation in Cell Trace (10 μM) exclusively labels rhabdite compartment (Fig. 3.4, B) without labeling the epidermal cell cytoplasm. The robust epidermal tissue nuclei staining was achieved by soaking animals for 45min in Draq5 (10 μM) (Fig. 3,4, C).

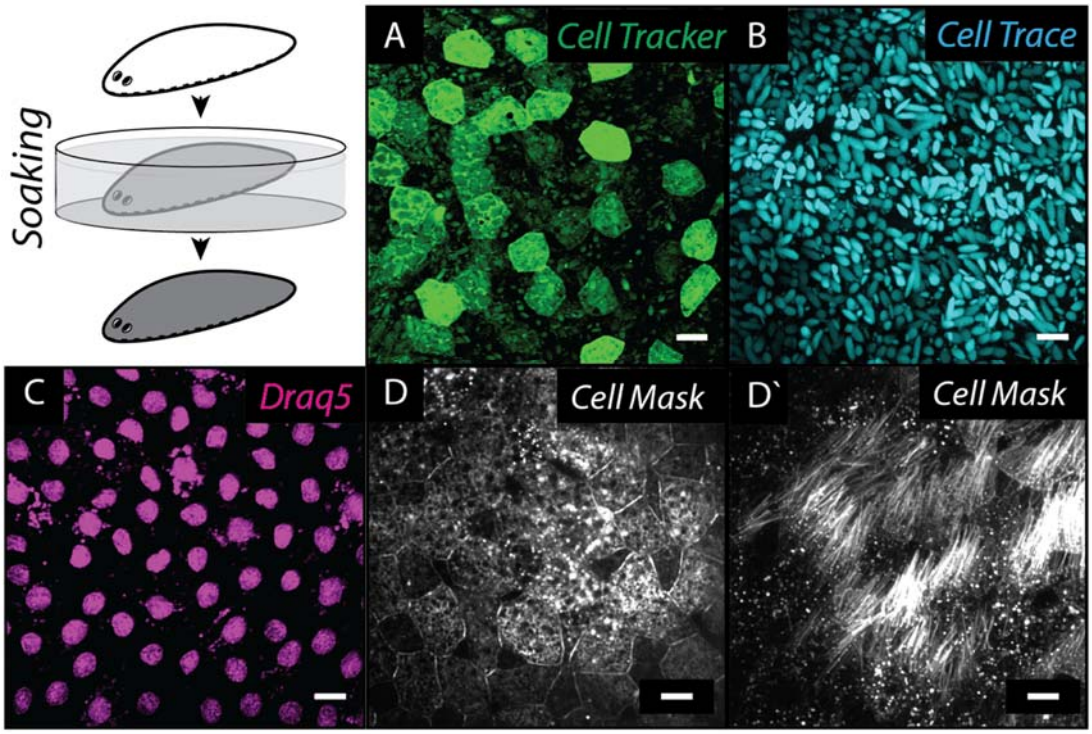

Figure 3-4. Live epidermal tissue labeling with cell permeable dyes.
Epidermal cell labeling with Cell Tracker Green (A), rhabdite labeling with Cell Trace Far Red (B), nuclei labeling with Draq5 (C), cell membrane (D) and cilia (D`) labeling with Cell Mask dye. 10 µm scale bar.

Although Cell Tracker dyes allowed visualization of live epidermis, the comprehensive analysis of epidermal cell behavior required cellular membrane labeling methodologies. Traditionally, DiI or its derivatives are used to label the cellular membrane of various organisms (Terasaki and Jaffe, 2004, Haugland, 2002 #3616). However, soaking animals in these lipophilic dyes did not label the planarian epidermis. Alternative dye delivery strategies were also tested; however, neither exposure to an oily dye suspension, nor placing dye crystals into the epidermal layer were effective. Although soaking of the animal in Cell Mask dye (Invitrogen) labeled the epidermal cell membrane (Fig. 3.4, D) and cilia (Fig. 3.4, D'), the staining was not robust and resulted in high background staining.

DiOlistics

Molecule delivery by high velocity particle bombardment (biolistics) has been successfully used in various organisms (Christou et al., 1988; O'Brien and Lummis, 2004; Praitis, 2006; Sambrook and Russell, 2006). Although biolistics is primarily used to deliver nucleic acids, this method can also be used to deliver a broad variety of molecules. Several authors have used this approach for DiI or its derivative molecule delivery and cell labeling (DiOlistics) (Gan et al., 2000; O'Brien and Lummis, 2004; O'Brien and Lummis, 2007; O'Brien and Lummis, 2006). Successful application of DiOlistics in other systems, encouraged us to adapt this technique for planarian cell labeling. The particle labeling and loading methodology was specifically adapted for a PDS-1000/He (Biorad) instrument, and thus the optimal parameters for robust epidermal tissue labeling were established (Fig 3.5). Specifically, 0.5mg of labeled 0.7 µm tungsten particles were loaded into the instrument by drying their ethanol (or methylene chloride) suspension onto a macro-carrier disk, a 10 psi vacuum was created inside the instrument, and the dry animal surface was bombarded from 9 cm by accelerating labeled particles with a 1100 psi burst of helium gas.

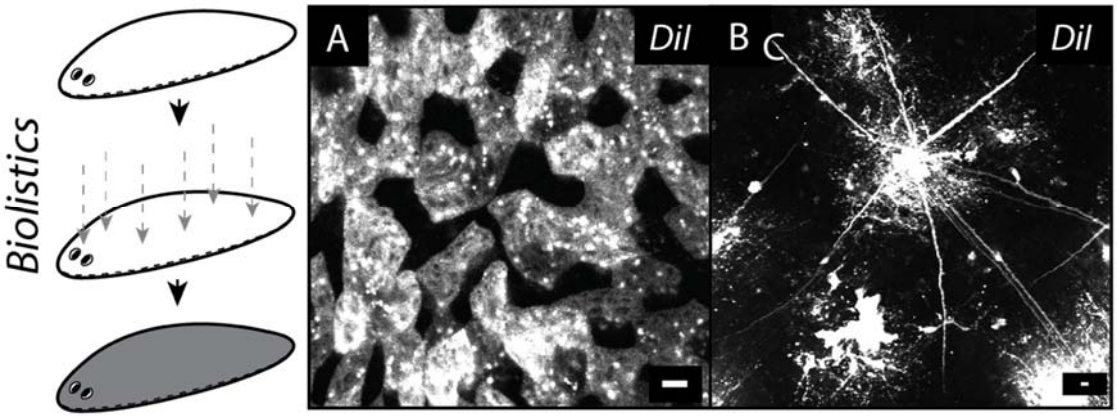

Figure 3-5. Planarian tissue labeling by DiOlistics.
Robust epidermal cell (live) labeling by DiI labeled particle bombardment (A), sub-epidermal muscle fiber (live) labeling (B). 10 µm scale bar.

Dynamic interaction in intact epidermis

To demonstrate the efficiency of our newly developed suite of live imaging methodologies, we followed cellular dynamics within intact planarian tissue. One day after the dorsal epidermis labeling with DiOlistic (DiI), a handful of intact animals were mounted into PDMS device (Fig 3.1) and their epidermal tissue was visualized live. Since this labeling strategy robustly outlined the cellular membrane of discrete cells scattered along the animal surface, the shape of basolateral surface of individual epidermal cells could be visualized. Intact epidermis behavior was analyzed in a few dozen animals and vast majority of the cells (hundreds) stood straight within columnar epithelia with their entire lateral surface perpendicular to the basal membrane. To our surprise, the morphology of several cells (n=4) within a few animals was considerably different. Specifically, although these few cells were still part of the epidermal layer, their basolateral surface protruded far into the surrounding epidermis (Fig. 3.6). At the basolateral surface these cells formed prominent lamellipodia-like or invadopodia-like protrusions as well as multiple smaller filopodia. It appeared that extended protrusions intervene between the neighboring epidermal cells or project under the neighbor interface with the basal membrane. Filopodial projections were extended and retracted on multiple sides of the cells, consistent with the possibility that cells are probing their environment rather than trying to migrate in any specific direction.

The biological significance of observed behaviors still has to be characterized more vigorously. The fact that a vast majority of diolisticaly labeled cells did not exhibit protrusive behaviors suggests that latter is not a response to labeling technique used. The rarity of this cellular protrusion activity might have several explanations: epidermal cells exhibit these behaviors only for a short period of time; it is associated with rare homeostatic event (e.g. new cell incorporation into the epidermal layer or reorganization of epidermis); or these behaviors are restricted to scarcely distributed epidermal cell population. So far, protrusive cell behaviours were not observed in cell permeable dye labeled epidermis. Cell Tracker dyes predominately label cell cytoplasm in a labeling pattern that is not conducive for fine cellular membrane extension visualization. Thus, contrary to biolistics, cell permeable dye labeling provides a relatively uniform epidermal staining, which might make it difficult to discriminate lateral surface of an individual cell and its protrusions within the tissue.

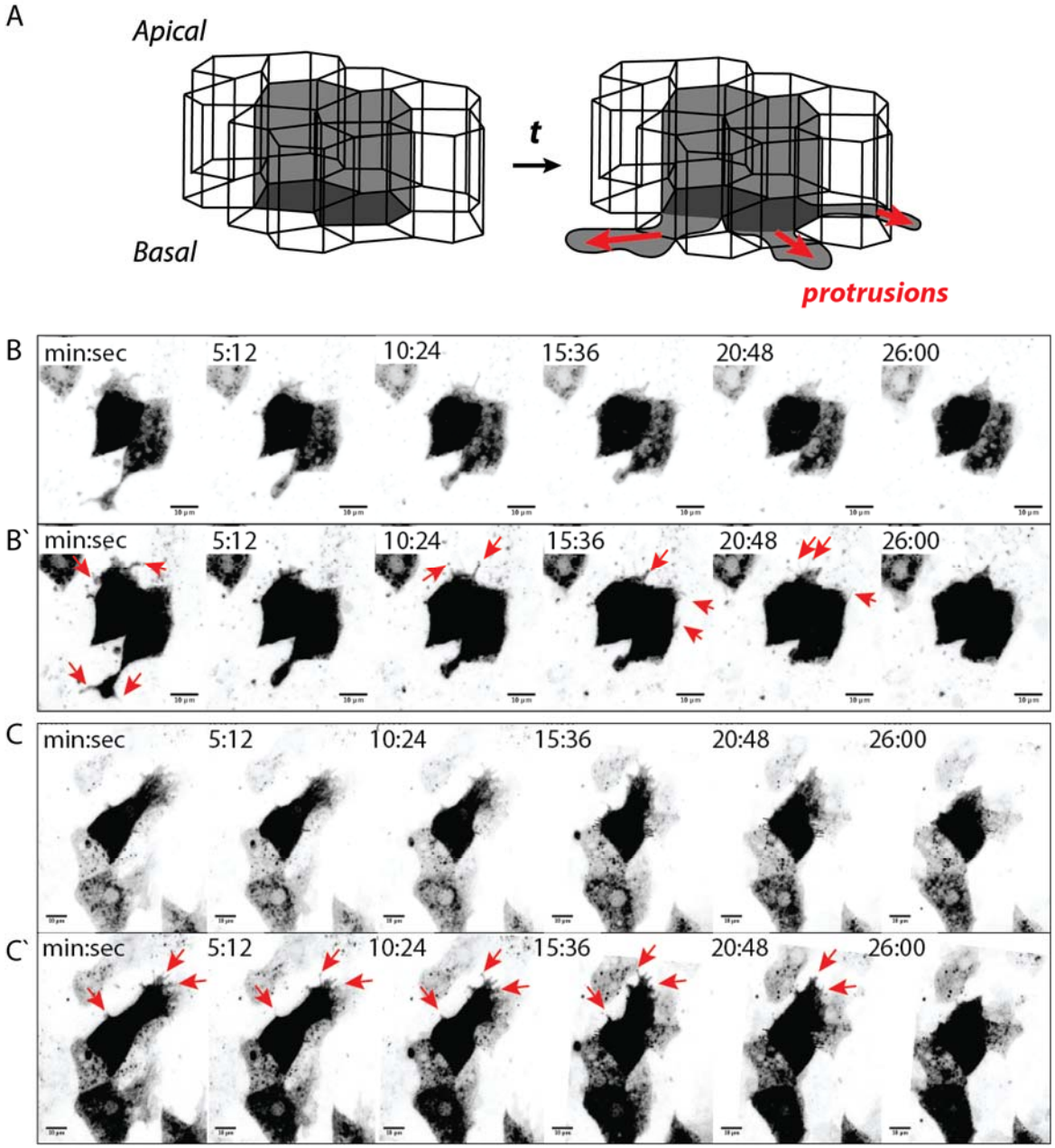

Figure 3-6. The dynamic cellular bahaviuor within inatct epidermis.
Schematic representation of the observed behaviors (A): epidermal cells exhibit protrusive behaviors along their basal lateral surface (B and C). DiI labeling (dark) within unlabeled tissue. Enhanced contrast at the lower panels (B` and C`). 10 µm scale bar.

Chapter 4

Cellular wound response in *S. mediterranea*

4.1 Cellular response to tissue damage

To describe the response of the epidermis in *S. mediterranea* to tissue damage, we performed laser mediated tissue ablation. Since the extent of epidermal damage can be controlled to some degree in this assay, we visualized the epidermal response to different size wounds. Interestingly, the epidermal wound response varied with the extent of epidermal damage (Fig. 4.1).

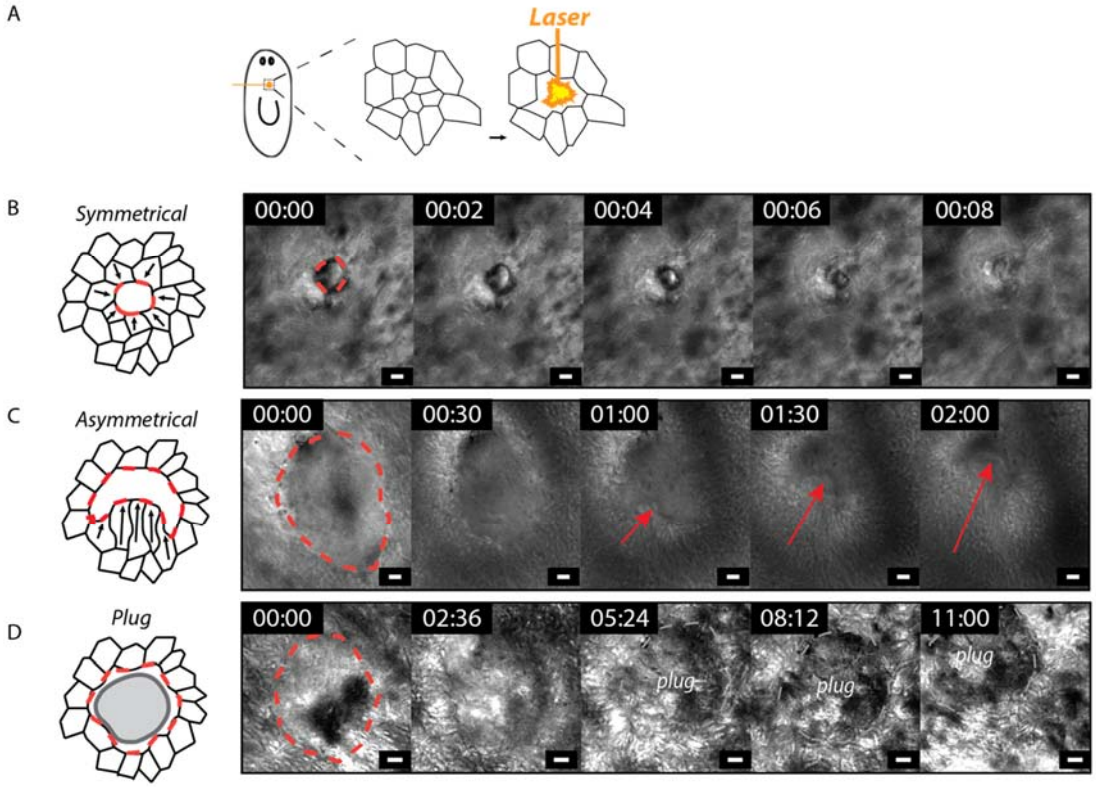

Figure 4-1. Diverse cellular wound responses to superficial tissue ablation. Schematic representation of the wounding paradigm (A). Laser elicted wounds close either by symmetric (B) or asymmetric (C) response of wound edge epidermis as well as by plug formation (D). The ablated tissue area is marked by red dashed line: (B) symmetrical wound response after 550 μm^2 ablation (~ 4 cells ablated), (C) asymmetrical wound response after 9500 μm^2 ablation (~ 70 cells ablated), and (D) plug formation after 6000 μm^2 ablation (~ 44 cells ablated). The average epidermal cell occupies 134.13 μm^2 area (Appendix 3). 10 µm scale bar. Time scale is minutes:seconds

The smallest wounds (around 550 μm^2 tissue or 4-cell ablation) closed within seconds by a rapid and uniform contraction of the wound margin (2/2) (Fig. 4.1, A). Visually, this response resembled that of actin cable mediated contraction wound closure. However, the mechanism of small wound closure could not be further characterized using light microscopy. We were not able to discern whether small wounds close by epidermal wound response and/or underlying muscle contraction.

To visualize epidermal response to more severe tissue damage we ablated 6000-10000 μm^2 (roughly 44-77 cells) of epidermis. In 3/9 cases epidermal wound response was not uniform along the circumference of the wound (Fig. 4.1, B). Shortly after tissue damage (<2 min), the epidermis at one edge (or several edges) of the wound flattened and extended over the wound surface. Its cells collectively migrated over the wound surface, like a multicellular tongue. This structure reached the opposing wound edge and thus covered entire wound surface within 3 min after injury. In 6/9 cases no cellular behaviors were visible at the wound edge epidermis (Fig. 4.1, C). Minutes after damage, the wound surface became irregular and the wound edge could no longer be identified. Over the next few minutes the appearance of the wound surface continued to change. It gradually darkened and, as the animal contracted its tissues (>10 min), it became apparent that a scab/plug structure formed over the damaged area.

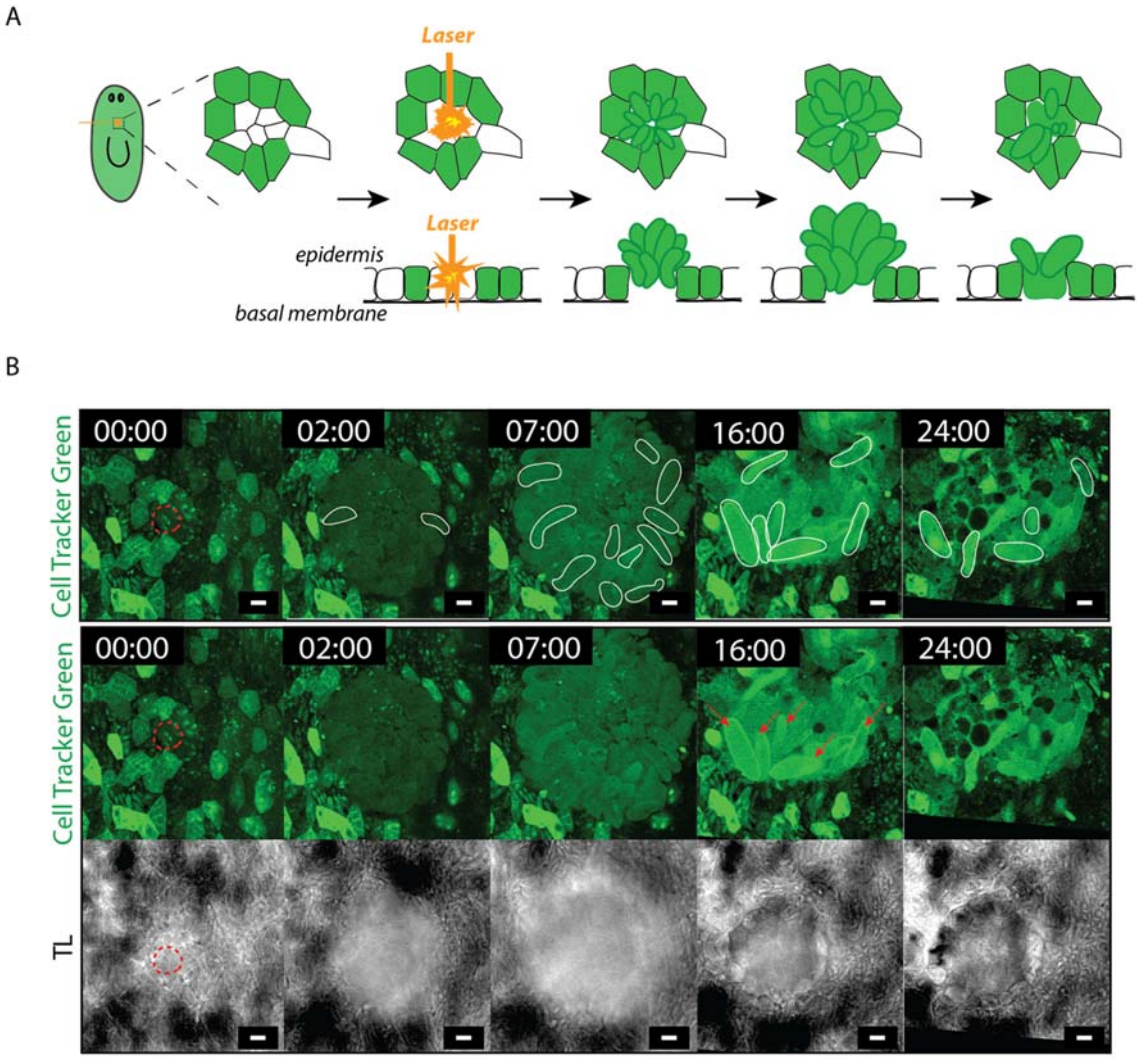

Figure 4-2. Exocytic wound response after tissue ablation.
Schematic representation (A): rod-shaped particles are released from a wound surface (B). Upon released particles expand and diffuse along wound surface. 550 μm^2 ablation (~ 4 cells). Minutes. 10 µm scale bar.

The *S. mediterranea* response to tissue damage was also visualized using florescence microscopy (Fig. 4.2). Shortly after the laser ablation (minutes) an amorphous, fluorescent cloud of particles was released from cells near the damage site (5/5). These structures quickly expanded over the damage site and thus interfered with our ability to visualize the cellular wound response at the wound edge epidermis. As they expanded, the shape of individual particles got better defined. By 7-16 min the particles were elongated, rod-like structures, suggesting that they were likely rhabdites released from the damaged tissue. Subsequently (7-24 min), the expanded particles started to disintegrate and their contents dispersed further over the wound surface.

4.2 Cellular response to tissue loss

The *S. mediterranea* response to tissue loss was characterized by monitoring the cellular behaviors of fluorescently labeled epidermis cells in the decapitated animals (pre-pharyngeal amputation). Capturing the cellular behavior along the entire wound edge epidermis in high resolution and through the entire wound closure proved to be extremely challenging. To visualize cellular wound response live, around one hundred animals were immobilized in agarose and decapitated (Fig. 3.3; pharyngeal amputation). Specimens which maintained tissue integrity after immobilization as well as remained immobile after the decapitation (roughly the fourth of immobilized animals) were subjected for live imaging. To make sure that manipulation had not interfered with animal's ability to respond to wound, we attempted to follow wound closure only in the specimens (n=9) which exhibited the body wall muscle contraction along the entire wound circumvent, the first and stereotypical wound response. Re-occurring tissue movements, poorly defined wound edge epidermis as well as fluorescent debris impeded our ability to follow wound response in most of the specimens (8/9). Nevertheless, the entire wound edge epidermis of one specimen was successfully visualized and its cellular behaviors were followed through the wound closure in high resolution for a first time in planaria (Fig. 4.3).

The wound edge epidermis exhibited dynamic cellular behaviors throughout the wound closure process (Fig. 4.3). Shortly after the decapitation, epidermal cell protrusions were visible along the entire circumference of the wound. Lamellipodia and filopodia-like structures continuously extended into the wound, but they did not make stable contacts with its surface. Live imaging revealed that decapitated animal wound re-epithelialization is driven by epidermal cell extension rather than cell migration. Wound closure started (7 min) close to the intersection between the dorsal and ventral wound edges. The gap between opposing wound edges was the narrowest in this region and epidermal cell extensions breached it first. As dorsal and ventral epidermis protrusions reached each other, they made prominent contacts which pulled the opposing wound edges closer together. The narrowing wound surface allowed subsequent contacts between the dorsal and ventral epidermis, and the opposing wound edges continued fusing inwards in a zipper-like fashion (zipper-like closure; Fig. 4.3, B).

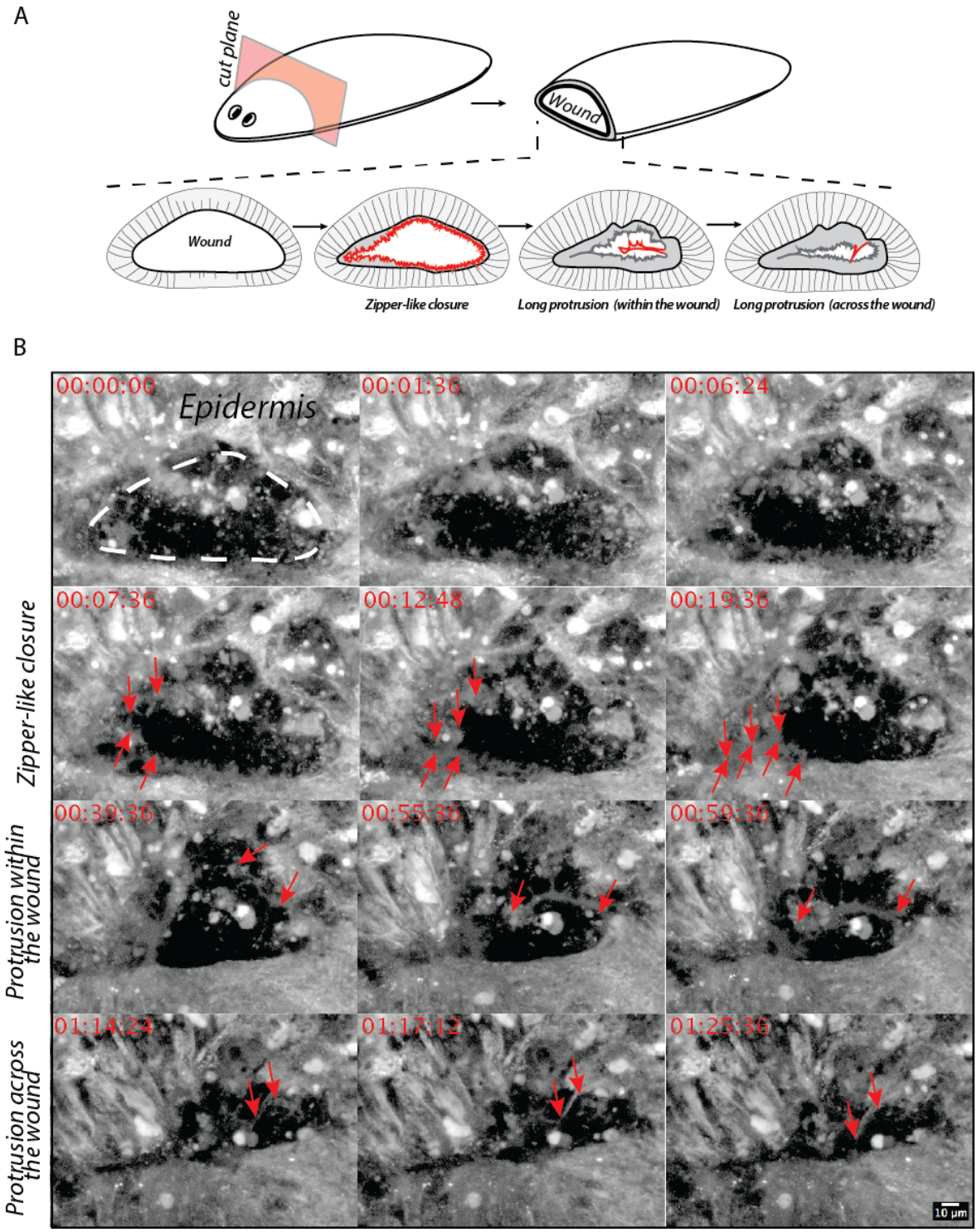

Figure 4-3. The mechanism of wound closure in decapitated animals.
Schematic representation (A) and live imaging (B). Wound closure by filopodia zipper and long extension of wound edge epidermis (arrows). Cell Tracker Green labeled epidermis (white), wound surface (dark). Time scale is hours:minutes:seconds. 10 µm scale bar.

Epidermal cell interactions were not limited to closely juxtaposed wound edges. Occasionally, opposing wound edges interacted via long epidermal cell projections. Pronounced multicellular ventral epidermal extensions extended far (~80 μm) across the wound surface (protrusions across the wound; Fig. 4.3, B). Although these epidermal structures projected parallel to the advancing wound edges, they exhibited dynamic filopodia, which interacted with the dorsal epidermis wound edge. Narrower and less complex extensions projected from the dorsal epidermis (protrusions within the wound; Fig. 4.3, B). These structures extended over the wound surface (~50 μm) and made permanent contacts with the ventral wound edge. Upon contact, opposite wound edges were brought closer together and thus wound closure was nearly completed within 1.5 hrs. The wound closure time in the agarose immobilized animal corresponded to the time of wound surface smoothening during gross tissue wound response visualization observed in non-immobilized animals (Fig. 2.4) as well as to electron microscopy study results (Fig. 2.5), suggesting that wound closure dynamics were not altered by agarose immobilization methodology or florescent tissue labeling.

Cellular response was also followed in diolisticaly labeled epidermis. We labeled dorsal epidermis in around hundred animals and subsequently subjected them to agarose immobilization strategy to visualized their wound response. The wound contraction was clearly present in five specimens, however the wound edge epidermis could be visualized and successfully followed for an extended time period only in a single animal (Fig. 4.4). In response to tissue loss, epidermis formed long and thin extensions of wound edge epidermis analogues to the one captured in wound SEM analysis (Fig. 2.6).

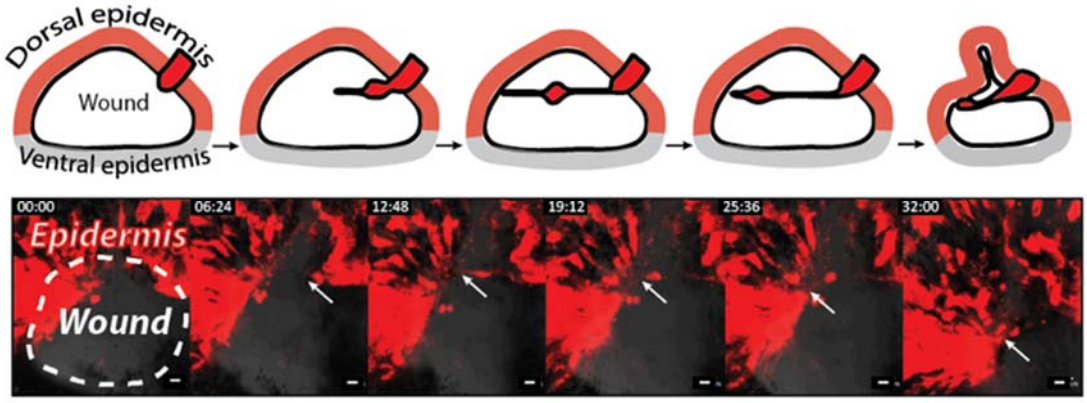

Figure 4-4. Epidermal cells migrate and breach the wound surface.
Occasionally cells extend from the one wound edge, migrate along the wound surface to incorporate into the opposing wound edge (arrow) epidermis. Cells remain attached to their original location throughout the migration. Schematics at the upper panel, live imaging snapshots at the lower panel. DiI labeled dorsal epidermis (red). Time scale is minutes:seconds. 10 µm scale bar.

During the wound closure a few epidermal cells at wound edge epidermis extended from the wound margin and migrated over 100 µm to reach the opposite wound edge (Fig, 4.4). Throughout this process, the migrating cell(s) remained attached to the wound edge by the fine stretch of their cytoplasm, which got increasingly thinner as epidermis moved further along the wound surface. As migrating cell(s) reached the wound edge they incorporated into the opposing epidermal layer. At the same time, the recently breached wound margins moved closer together and wound closure advanced further.

To demonstrate that long epidermal extensions formation is not specific to agarose immobilization methodology, we attempted to visualize them in capillary immobilized animals. We also sought to provide the detail description of this novel structure behaviour, thus we followed wound response in cytoplasmic (Cell Tracker) and nuclear (Draq5) dye labeled epidermis. Around hundred labeled animals were decapitated and subjected to immobilization in capillary. Wound surface could be visualized in 20 specimens, however due to animal movements or poorly defined wound edge epidermis the wound response could not be followed live in most of them (19/20). The cellular wound response of wound edge epidermis was successfully followed in one specimen (Fig. 4.5) and its epidermis formed long projections on two separate occasions (Fig. 4.5, A and B). The extensions of wound edge epidermis were either retracted (Fig. 4.5, A) or reached over the wound and extended further until they became too thin and hence the fluorescent label of their cytoplasm was too weak to detect it (Fig. 4.5, B). Epidermal nuclei labeling (Draq5) demonstrated that these structures are multicellular (Fig. 4.5, B and B`). Intriguingly,

tracking these nuclei further captured cell translocation along epidermal projections (Fig. 4.5, B`) indicating that these long structures are not simply the protrusions of wound edge epidermis: they represent a distinct mode of cellular migration over the wound surface. Therefore, we call these discrete, long range, uni- or multi-cellular extensions of the wound edge epidermis “cellular bridges”.

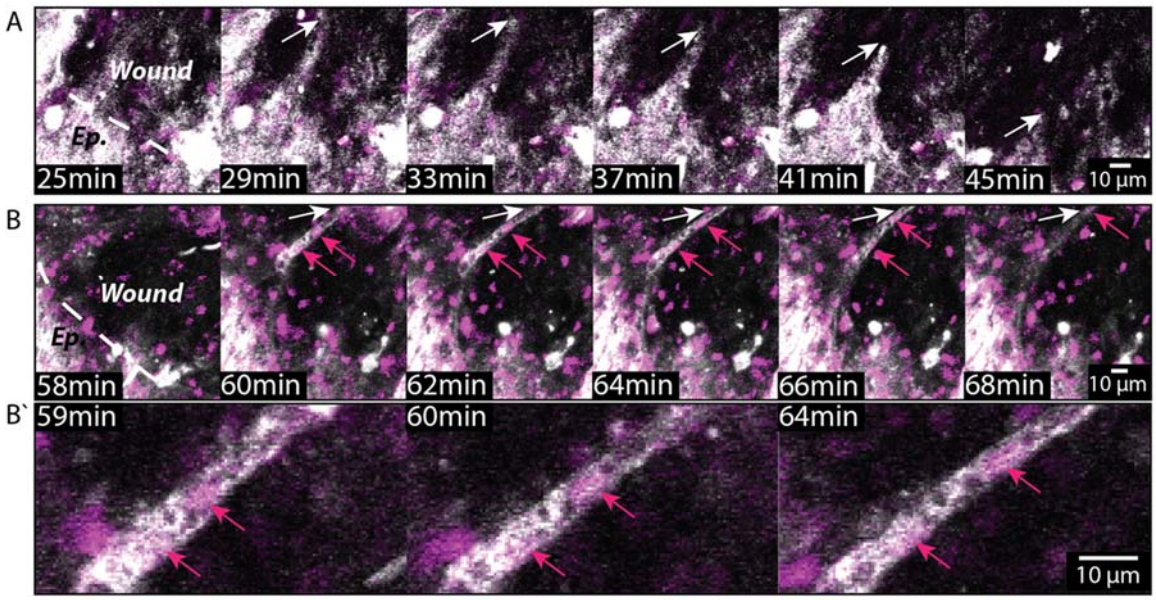

Figure 4-5. Cellular migration along the wound edge epidermis extension.
Long multicellular extensions of wound edge epidermis were followed live in decapitated and capillary immobilized animals. Wound edge epidermis (white) extend long multicellular projections (white arrow) over the decapitated animal wound (no label, dark). Epidermal extensions are either retracted (A) or are extended further (B) and mediate cell translocation over the wound surface (nuclei, magenta arrows) (B and B`). Snapshots form a time-lapse movie. Epidermal cells labeled with Cell Tracker Green (white), nuclei labeled with Draq5 (magenta). 10 µm scale bar. wound surface (dark). 10 µm scale bar.

4.3 Epidermal tissue regeneration

Due to the inability to label live, differentiated cells, neither the fate of the wound epithelia after wound closure nor its cell contribution to planarian tissue regeneration was observed previously. Our electron microscopy study has showed that differentiated epidermis can rearrange and contribute to the cellular pool of re-growing tissues. To better describe this process, we applied live cell labeling to follow terminally differentiated epidermal cells during head regeneration (Fig. 4.6). Epidermal tissue labeling results were consistent with our previous observations. The regenerating epidermis consisted of both newly incorporated, unlabeled cells as well as labeled, and thus differentiated wound edge epidermis-derived cells. Labeled cells were found far beyond the amputation site; they were scattered over the entire regenerated surface. By 5-7 dpa, when most head tissues had regenerated, labeled cells accounted for roughly half of the epidermal layer, indicating that differentiated cells were a major contributor to the regenerated epidermis. The presence of wound edge epidermis within reestablished columnar epidermis shows that although the wound epithelia is a temporary tissue, the fate of its cells is not limited to this tissue formation. Epidermal cells that participate in wound healing can re-differentiate into columnar epidermis, thus remaining part of epidermis for more than two weeks after wound closure. Throughout this time the number of epidermal wound edge derived cells gradually decreases with kinetics that seem consistent with that of the normal epidermal cell turnover rate (Tu et al., 2015; van Wolfswinkel et al., 2014).

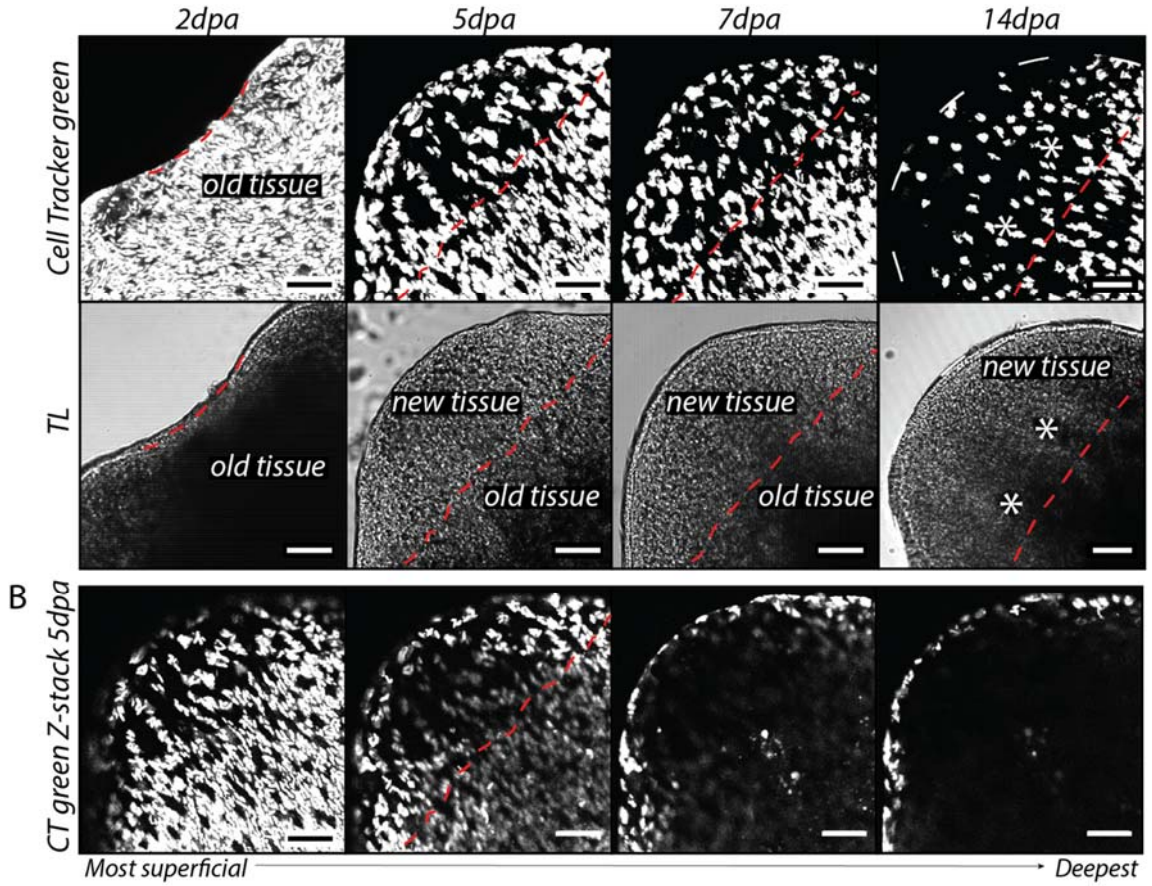

Figure 4-6. Wound edge epidermis contributes to loss tissue regeneration.
After wound closure, cells of wound edge epidermis incorporate into the regenerated columnar epidermis and remain in this tissue form more than two weeks following decapitation **(A). A,** upper panel: cells that resided in epidermal layer at the time of decapitation, Cell Tracker Green (white); newly incorporated epidermal cells (dark, no labeling). **A,** lower panel: transmitted light images of upper panel. **B.** Optical sections demonstrate that live cell labeling is epidermis specific (5 dpa); Cell tracker cells (white) are found in epidermis (most superficial tissue) and absent in mesenchyme.
Red dashed lines represents decapitation site. 50 μm scale bar.

Chapter 5

Molecular characterization of *S. mediterranea* epidermis

5.1 Epidermal dissection

A molecular description of the planarian epidermis required the development of an epidermal dissection protocol which would allow for the precise dissociation of the animal epidermis away from the underlying tissues. During the development of animal immobilization techniques, we discovered that high salt treatment can cause epidermal layer detachment from the underlying basement membrane. Immediately after exposure to 1M NaCl, animals have curled their body ventrally and released rhabdite material. Subsequent animal movements ceased and the changes within the epidermis became apparent. Within 4-7 min of NaCl treatment, the normally translucent epidermal tissue started to become opaque, a transition which is marked by the epidermal layer detachment from the basal membrane (Fig. 5.1, B). Although animals did not survive past this point, their tissues did not disintegrate and epidermis remained as a continuous opaque layer along the animal surface. Therefore, we reasoned that the detached epidermal tissue could be surgically dissected and removed from the animal surface.

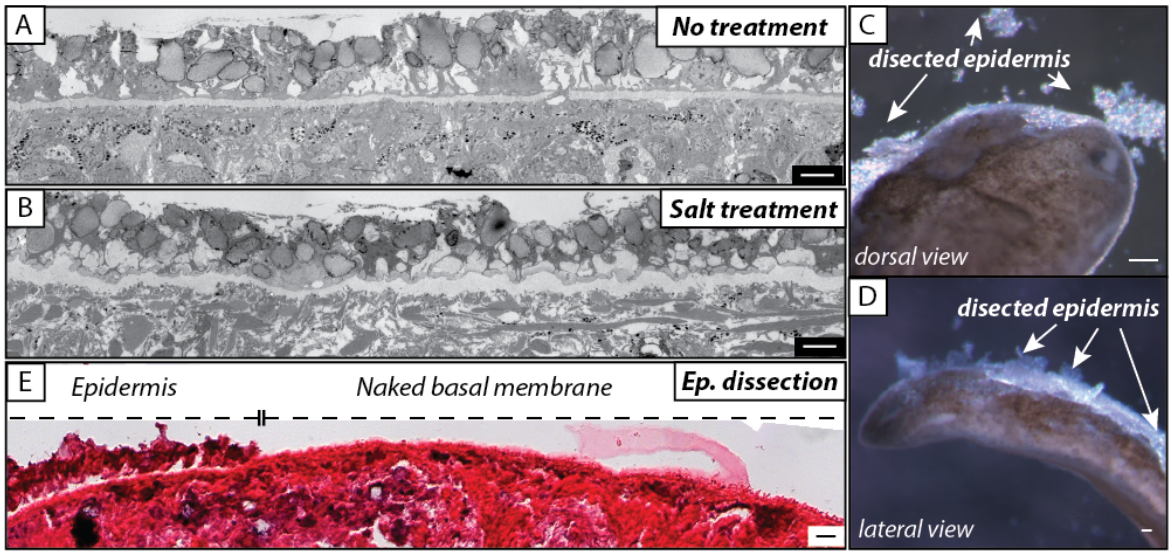

Figure 5-1. Epidermal dissection methodology.
Salt treatment (7min, 1M NaCl) causes epidermis detachment from basal membrane. Epidermal cross-section before (A) and after salt treatment (B). Epidermal layer is dissection (C and D). Basal membrane remains intact after epidermal dissection, H&E staining (E). Scale bar is 5 µm in A and B, 50 µm in C and D, 20 µm in E.

Once detached from the basal membrane, the entire dorsal or ventral epidermis can be harvested from the animal surface (Fig. 5.1, C and D) by a fine insect pin (total procedure time 10min). Due to the flexible nature of the instrument, the gentle application of its longitudinal surface allows one to scrape the pieces of epidermal sheets without obvious damage to the underlying tissues (Fig. 5.1 E). This procedure does not damage the underlying basal membrane and the sub-epidermal pigment layer remains intact after epidermal cell collection.

We further assessed whether our epidermal dissection methodology is compatible with any downstream molecular characterization approaches. Specifically, we subjected dissociated epidermal samples to protein and RNA isolation protocols. The precipitated proteins were difficult to solubilize and thus the amenability of epidermal samples to proteomic approaches was limited. However, nucleic acid purification was successful and up to 210 ng total RNA was isolated from the individual animal dorsal or ventral epidermis. Total RNA concentration was higher than 75 ng in 5/10 dorsal and 6/10 ventral samples. The integrity of isolated RNA was confirmed by electrophoretogram (Bioanalyser, Agilen): samples had well defined ribosomal RNA peaks with no signs of RNA degradation (smear).

5.2 Transcriptional profile of S. mediterranea epidermis

Our newly developed tissue isolation methodology was subsequently applied to characterize the transcriptional profile of *S. mediterranea* epidermis. In order to identify epidermal-specific transcripts, epidermal samples need to be compared to a control sample representing all animal tissues excluding the epidermis itself. However, harvesting the entire dorsal and ventral epidermis (dorsal and ventral) proved to be technically challenging. Considering that epidermal tissue represents only a small fraction of the entire animal body, epidermal transcripts should be underrepresented in an all-tissue context. Therefore, we reasoned that epidermally enriched transcripts could be identified by differential gene expression analysis between dissected epidermis and whole worm (all tissues) (Fig. 5.2). It was also decided that a separate analysis should be performed for dorsal and ventral epidermal samples. Dorsal columnar and ventral cuboidal epidermis are morphologically distinct and hence their molecular signatures should also differ.

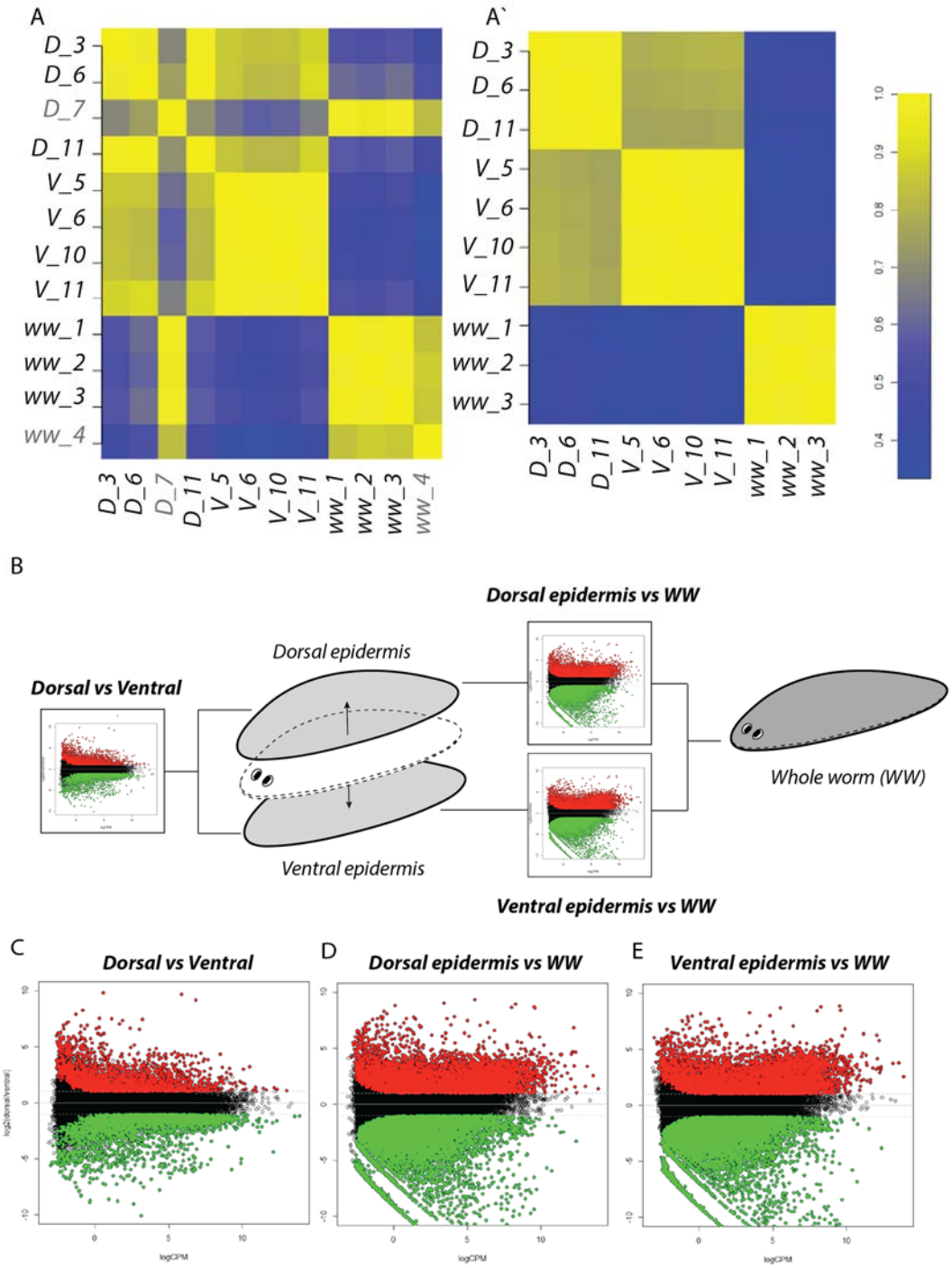

Figure 5-2. Epidermal expression profile analysis
Epidermally enriched genes were determined by comparing expression signatures of dissected epidermis and whole worm (WW) samples.Correlation between quadruplicates expression profiles (A and A`). Sample "D_7" and "ww_4" (E) data were excluded form subsequent analysis (A`). Schematic representation of the expression profile comparisons (B). MA plots of differential expression analysis results (adjusted p value < 0.01 and fold change > 2): dorsal epidermis vs ventral epidermis (C), dorsal epidermis vs WW (D), ventral epidermis vs WW (E). between quadruplicates expression profiles (A and A`). Sample "D_7" and "ww_4" (E) data were excluded form subsequent analysis (A`). Schematic representation of the expression profile comparisons (B). MA plots of differential expression analysis results (adjusted p value < 0.01 and fold change > 2): dorsal epidermis vs ventral epidermis (C), dorsal epidermis vs WW (D), ventral epidermis vs WW (E).

comparison	*up*	*down*
Dorsal/ww	6189	8568
Ventral/ww	5886	8744
Dorsal/Ventral	2478	3140

Table 1. Differential expression analysis summary.
Gene number in Fig. 5.2. Adjusted p value < 0.01 and fold change > 2.

Samples (quadruplicates) representing dorsal and ventral epidermis of single worm were collected and their transcriptional profile determined (Fig. 5.2). The transcription profile analysis of most quadruplicates showed high degree of correlation (Fig. 5.2, A) and these samples were used for subsequent analysis (Fig. 5.2, A'). To determine epidermally expressed transcripts, the expression profiles of dorsal and ventral epidermis samples were compared to a dissection buffer treated whole worm (WW), all-tissue reference (Fig. 5.2, B). Differential expression analysis between epidermal samples and WW reference identified 6189 dorsal-enriched and 5886 ventral- enriched genes (adj. p value<0.01 and fold change >2). Subsequently, different tissue markers were used to demonstrate the specificity of our epidermal-enrichment approach. Genes with published epidermal expression patterns, but not markers of other sub-epidermal tissues (differentiating progenitors, gut, nervous system, muscle) (Eisenhoffer et al., 2008; Tu et al., 2015; van Wolfswinkel et al., 2014), had at least two-fold enrichment either in dorsal or ventral epidermis samples compared to WW samples (Fig. 5.3). Therefore, we were able to validate the specificity of our dorsal and ventral tissue-enrichment approach. Genes with known dorsal-specific expression patterns such as *bambi* (Gavino and Reddien, 2011) and *slc-26a-4* (Vu et al., 2015), were over four-fold enriched in dissected dorsal epidermis when compared to ventral samples.

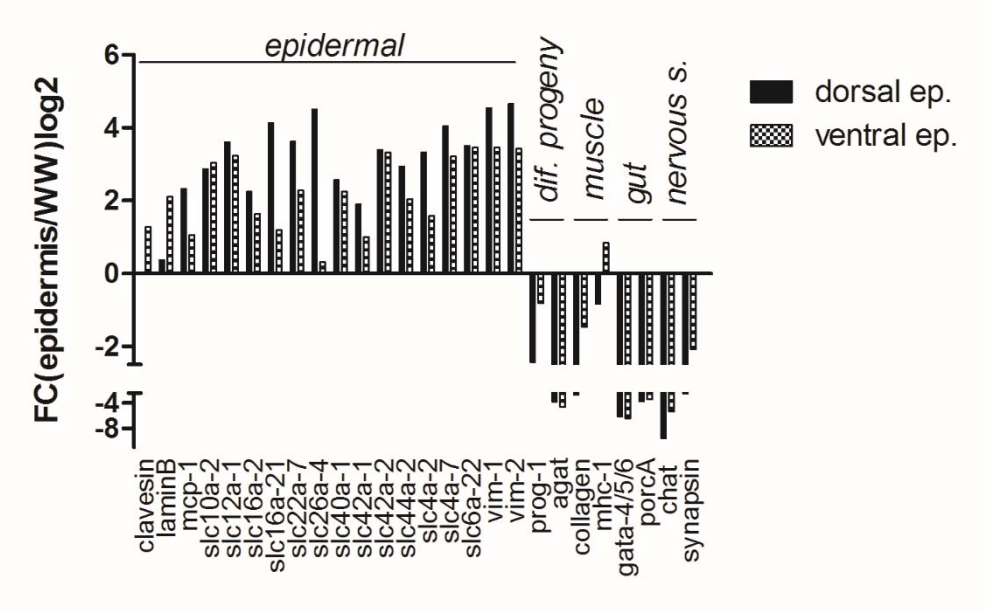

Figure 5-3. Epidermal expression profile validation.
Epidermal markers, but not other tissue markers, are enriched in dissected epidermis samples (epidermal/whole animal sample comparison).

Next, we sought to perform gene ontology (GO) analysis to describe the processes and the structures represented in the epidermal transcription profiles. The epidermal transcription profile analysis (Fig. 5.2) have identified extensive list of epidermally enriched genes (Table 1). To reduce gene number for subsequent GO term analysis we focused on epidermal genes with highest enrichment in respect to whole animal samples (FC>8 and p. value <0.01). Reduced gene list included genes enriched in both dorsal and ventral samples (790), dorsal sample specific genes (585) and ventral sample specific genes (1045). GO analysis of these datasets identified 1880 terms enriched in both dorsal and ventral datasets and 1894 terms enriched in ventral specific dataset (p.value > 0.01). No terms were significantly enriched in dorsal sample specific gene dataset. The dorsal and ventral dataset contained terms associated with various epithelia structures (e.g. various cellular junctions, cilia) as well as terms associated with an array of signaling pathways (Table 2, A). Specifically, Notch, JNK, STAT, NF-kappaB and integrin signaling as well as positive regulation of non- and canonical Wnt signaling pathways. The ventral sample specific terms included TOR, Erbb, Slit-Robbo and Smoothened signaling pathways, negative regulation of non-canonical Wnt signaling pathway as well as chromatin modifying machinery associated terms (MLL3/4, Set/Compass, SAGA) (Table 2, B).

Table 2 Gene ontology terms represented in epidermal samples.
Datasets representing epidermally enriched genes (FC>8 and p. value<0.01 in respect to whole animal samples) were analyzed. The selected gene ontology terms and their enrichment p. value displayed: enriched in both dorsal and ventral sample (A), enriched and specific to ventral sample (A).

A

GO terms enriched in both Dorsal and Ventral samples	***p. value***
integrin-mediated signaling pathway	1.62E-13
intermediate filament cytoskeleton	4.04E-13
apical cortex	9.02E-13
basal plasma membrane	1.29E-12
positive regulation of non-canonical Wnt signaling pathway	3.45E-11
dorsal/ventral pattern formation, imaginal disc	2.58E-10
epithelial cell type specification, open tracheal system	6.79E-10
Notch signaling involved in heart development	1.39E-08
establishment or maintenance of epithelial cell apical/basal polarity	1.60E-08
1. intermediate filament	2.39E-08
apical junction complex	3.00E-08
cation channel complex	5.08E-08
adherens junction	1.81E-07
bicellular tight junction	3.45E-07
JNK cascade	4.04E-07
positive regulation of protein kinase B signaling	5.62E-07
cilium morphogenesis	1.91E-06
toll-like receptor signaling pathway	2.09E-06
regulation of insulin receptor signaling pathway	1.29E-05
regulation of GTPase activity	5.54E-05
positive regulation of exocytosis	7.79E-05
I-kappaB kinase/NF-kappaB signaling	8.29E-05
focal adhesion	1.52E-04
regulation of JAK-STAT cascade	1.85E-04
protein kinase B signaling	2.40E-04
positive regulation of canonical Wnt signaling pathway	4.54E-04

B

2. ***Ventral sample specific GO terms***	***p. value***
positive regulation of TOR signaling	2.37E-10
3. smoothened signaling pathway	8.79E-10
negative regulation of non-canonical Wnt signaling pathway	1.30E-08
MLL3/4 complex	1.09E-07
SAGA complex	2.56E-07
Slit-Robo signaling complex	4.15E-07
Set1C/COMPASS complex	2.92E-06
regulation of ERBB signaling pathway	1.01E-03

Epidermally enriched gene library

Differential expression analysis has provided an extensive list of epidermally-enriched genes for further molecular and functional characterization of the *S. mediterranea* epidermis. To create a comprehensive resource for further studies, a specific cohort of these genes (~460) were selected and cloned to generate an "epidermally-enriched gene library".This collection was composed of epidermal genes (dorsal and/or ventral) which had the highest fold change or mostly significant enrichment (smallest p. value) in over the all tissue-whole worm reference. Thus, since transcription factors are crucial regulators of epidermal biology (Tu et al., 2015; van Wolfswinkel et al., 2014), an array of epidermal genes which contained predicted DNA binding domain were also included into the library.

We characterized the range of expression patterns represented within the generated library by performing an *in situ* hybridization (ISH) screen. We were able to detect expression patterns of nearly one third of the genes cloned (>28%). Virtually all of these genes were expressed at the most superficial tissues. Although expression within deeper animal tissues staining was rare, some of the genes were expressed broadly throughout the animal mesenchyme, outer surface of the pharynx, or within the cells surrounding the central nervous system (CNS).

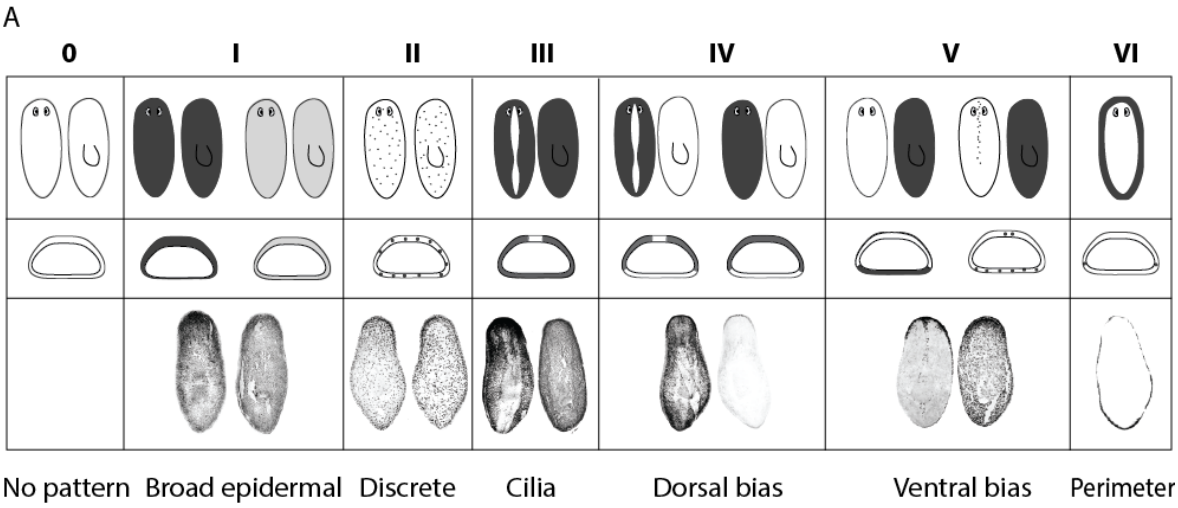

Figure 5-4. Summary of expression patterns represented within "epidermally enriched gene library".
Group I: no expression pattern detected; Group II: strong or weak expression pattern along animal surface; Group III: expression in discrete epidermal/sub-epidermal cells; Group IV: expression pattern resembling ciliated cell distribution; Group V: expression pattern bias to dorsal surface; Group VI: expression pattern bias to ventral surface; Group 6: expression along dorsal/ventral tissue interface (body edge/perimeter);

Table 3. Gene number within each expression pattern group (Fig. 5.4)

	Groups							
	0	**I**	**II**	**III**	**IV**	**V**	**VI**	*total*
genes in a group	335	128	23	12	12	7	2	463
strong probes in a group	0	6	21	11	10	7	2	57
TFs in a group	50	28	2	2	0	0	0	82

Based on their expression patterns, the cloned genes were classified into 6 categories (Fig. 5.4; Table 3): (I) ubiquitous, usually weak expression throughout the epidermis; (II) expression within discrete sub-/epidermal cells; (III) ciliated cell-like expression pattern (lateral domains of dorsal epidermis and ventral surface); (IV) dorsal biased expression; (V) ventral biased expression; (VI) expression at the dorsal and ventral epidermis intersection (animal body edge or perimeter).

The epidermally-enriched genes exhibiting the strongest expression patterns were subjected for more detailed characterization with fluorescent in situ hybridization (FISH) methodology. The expression patterns of approximately 50 genes were assessed by FISH and the expression of 24 genes could be successfully visualized for further characterization. Although the expression of most of these genes resembled the expression patterns associated with already defined epidermal cell populations (ciliated cells, adhesion glands, newly differentiated epidermal cells), some of the patterns appeared to be more specific (Fig. 5.5). For example, SMED30006763 was expressed in a subset of ciliated epidermal cells, SMED30026425 was expressed in the ventral ciliated epidermis and racing stripe cilia, but not in the dorsal-lateral ciliated epidermis. SMED30019993 and caveolin (SMED30003024)-encoding transcripts were specifically expressed in the dorsal epidermis, whereas another putative caveolin (SMED30003024) gene was specifically localized to the ventral epidermis. An Na+/K+-ATPase alpha-subunit (SMED30010071) gene had an expression that was enriched in the dorsal epidermis, however it seemed to be specifically absent in the ciliated cells of the racing stripe.

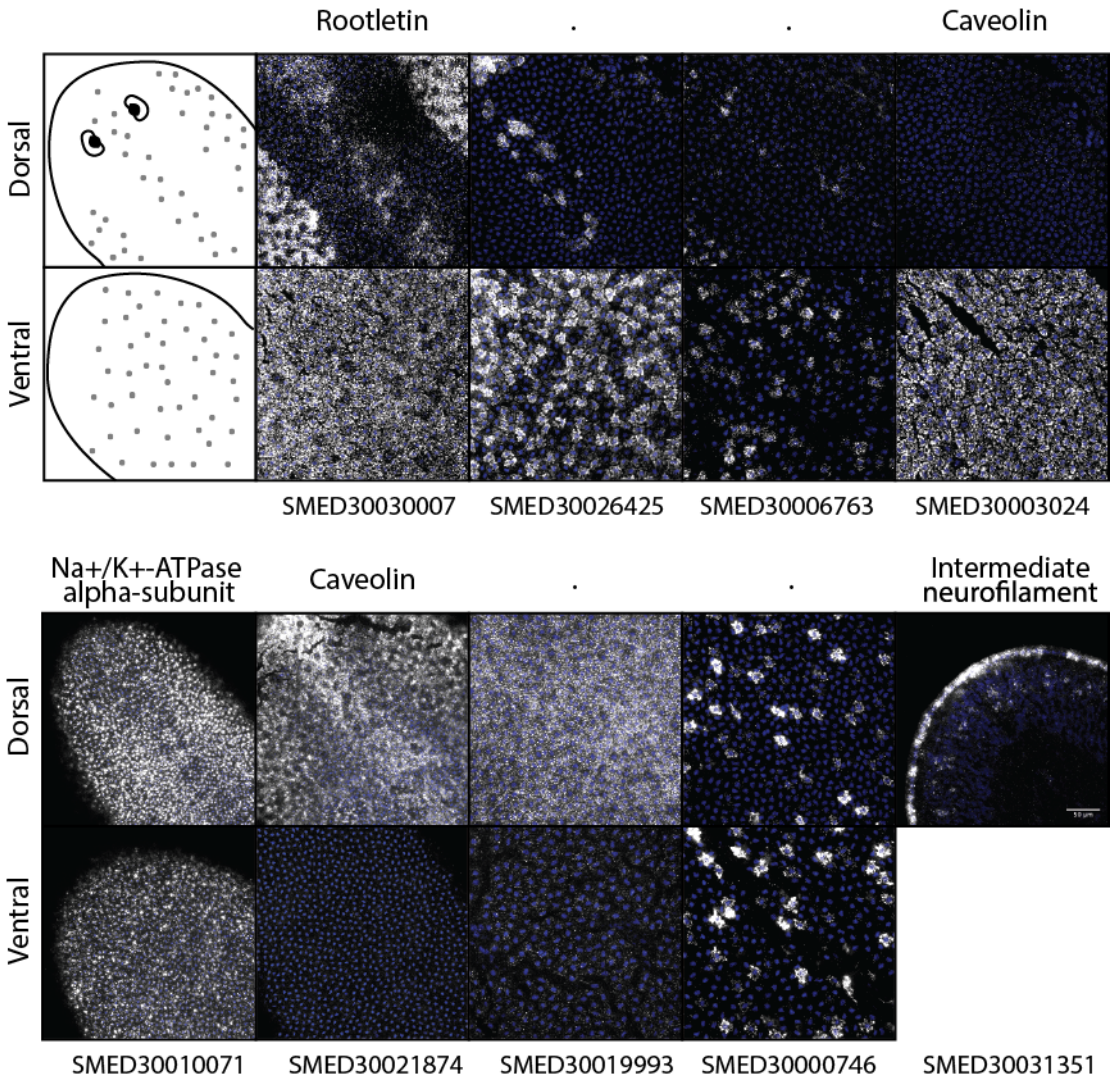

Figure 5-5. Expression patterns of most robust epidermal markers.
Dorsal and ventral epidermis at the head region. If gene homology could be determined it is represented above the expression pattern. Transcript number below the expression pattern. Expression pattern (white), DAPI (blue). 50 µm scale bar.

The potential overlap between some of the identified and previously published markers of distinct epidermal cell populations (Tu et al., 2015), specifically *zpuf-6*, *vim* and *rootletin*, were assessed next (Table 3). All markers which were expressed in both epidermis as well as the discrete sub-epidermal cells overlapped to some extent with *zpuf6* expression pattern, a marker of newly differentiated epidermal cells within sub-/epidermis (Tu et al., 2015). Thus, our results showed no alternative, zpuf-6 negative epidermal progenitor population in *S. mediterranea*. Epidermal- specific expression patterns which did not overlap with *zpuf6* were either broadly expressed throughout the epidermal layer or were co-expressed with the ciliated cell marker *rootletin*, suggesting that their expression coincides with terminal stages of epidermal differentiation.

Table 4. Identification of markers that overlap with published markers of distinct epidermal cell populations.

zpuf-6^{+}- newly differentiated epidermal cells in the mesenchyme and epidermis; *rootletin*$^{+}$- ciliated cell marker; *vim*$^{+}$ - marks the transition along *zpuf-6*$^{+}$ differentiation into ciliated (*rootletin*$^{+}$) cells; Group number corresponds to marker expression pattern group at Fig.5.5 and Table 1.

id	**group**	***zpuf6***		***vim***	***rootletin (cilia)***
		mesenchyme	*epidermis*		
SMED30025672	I	no	no	no	
SMED30030663	I	no	yes		
SMED30005345	I	yes	yes	yes	yes
SMED30022344	I	yes	yes	yes	yes
SMED30028069	I	yes	yes		yes
SMED30006268	II	no	no	yes	
SMED30032199	II	no	yes	yes	
SMED30000746	II	yes	yes		
SMED30024850	II	no	no	no	yes
SMED30029019	II	yes	yes	yes	
SMED30030007	III	no	no	no	
SMED30019305	III	no	no		
SMED30012136	III	no	no		
SMED30006763	III	no	no	no	yes
SMED30029546	III	no	no	no	
SMED30021874	IV	no	no	no	yes
SMED30010071	IV	no	yes	yes	yes
SMED30034787	IV	yes	yes		yes
SMED30012786	IV	yes	yes		no
SMED30021589	IV	yes	yes		
SMED30019993	IV	no	no	no	yes
SMED30000158	V	no	yes	yes	
SMED30026425	V	no	yes	no	yes
SMED30003024	V				yes

Chapter 6

Functional screen

6.1 Phenotype summary

The generation of an epidermally-enriched gene library has provided candidate gene sequences for functional studies in order to determine whether any of them may play a role in planarian tissue homeostasis or wound repair. An extensive list (~463) of epidermal transcript sequences within the generated clone library provides templates for dsRNA synthesis and thus enabled subsequent functional characterization via RNAi mediated knock-down. To explore the mechanism underpinning various aspects of planarian epidermal biology, we designed a screening strategy capable of identifying epidermal genes important for tissue homeostasis, wound closure and regeneration (Fig. 6.1). Since our epidermal gene library list was too extensive for a feasible functional RNAi screen, we decided to focus on genes containing a putative (or predicted) DNA-binding domain. We reasoned that knock-down of transcriptional regulator would perturb a vast array of downstream targets and thus would yield the highest chance of causing a noticeable and quantifiable phenotype. More than hundred epidermally enriched genes contained putative DNA binding domain (zinc finger, helix loop helix, homeobox, forkhead-box and etc.). This list (Table 5) included transcription factor homologues as well as genes typically not associated with transcription regulation but yet containing DNA binding domain-like sequences (e.g. homoebox domain in ceramide synthetase 2). We have selected 46 of these genes for subsequent functional studies. dsRNAs corresponding

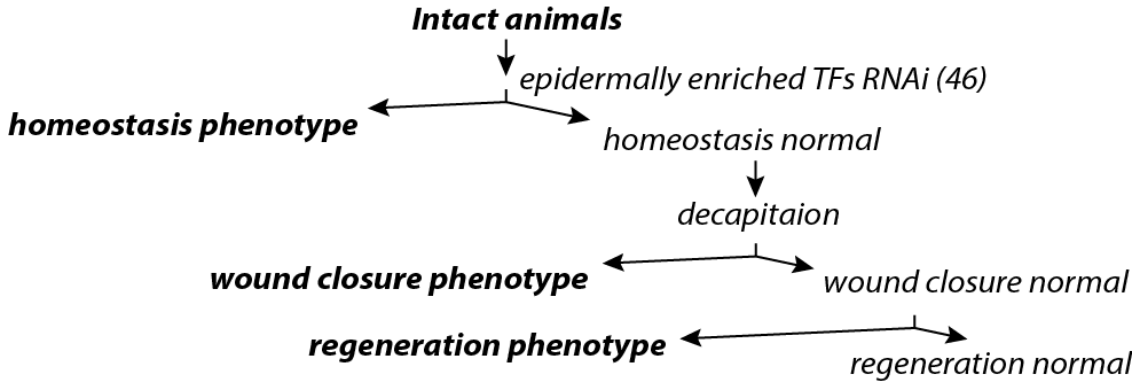

Figure 6-1. Functional screen (RNAi) screening strategy to identify genes with a role in tissue homeostasis, wound closure and regeneration.
Multiple doses of dsRNA are administered to intact animals. Any resulting intact tissue defects are classified as homeostasis phenotypes. Subsequently animals are decapitated and their ability to close wounds and regenerate lost tissue are assessed.

to candidate gene sequences were fed to animals every 4 days at least 8 times over a course of 36 days and any intact tissue defects (lesions, lysis, reduction in locomotion etc.) were classified as homeostasis defects. Genes without any obvious homeostasis defects after 36 days were subjected to amputation (head and tail) and further screened for wound and regenerative response defects for a duration of 12 days after amputation. Animal lysis or persistent muscle contraction at the wound site 12-24 hrs after amputation would be indicative of a wound closure defect, whereas surviving animal fragments with an inability to reestablish anterior and/or posterior tissues would indicate the candidate gene plays a potential role in regeneration.

Intact tissue phenotypes (homeostasis defects)

Multiple genes (10/46) from our candidate list were identified as giving intact tissue phenotypes in our RNAi screen (Fig. 6.2; Table 5). Identified defects included previously described (Reddien et al., 2005) as well as novel phenotype classes. The most abundant phenotype in our screen (4/46) was whole body lysis, however the severity and length of this phenotype progression varied. The phenotype of fork-head domain containing gene SMED30006455 as well as zinc-finger domain containing gene SMED30011041 progressed the fastest, causing complete penetrance and entire animal body lysis after just 3-4 doses of dsRNA administration. SMED30000740, a helix-turn-helix containing gene exhibited similar phenotype after 6-8 doses of dsRNA (Fig 6.2). Although the knockdown of zinc finger protein SMED30001601 with sequence similarity to mouse Growth factor independent 1 (Gfi-1) transcription factor eventually also caused animal lysis, the phenotype progression was distinct from those mentioned above (Fig 6.2; further description at Fig. 6.4). Initially, small lesions appeared above the pharynx on the dorsal side of the animal body. As the phenotype further progressed these lesions healed, however, the animal body started to curl ventrally, the behavior stereotypical to neoblast function perturbation (Reddien et al., 2005). Our screen also identified a phenotype class not reported in any previous studies - anterior-posterior axis-specific tissue failure. Knockdown of Microphthalmia-associated transcription factor (MITF) - like SMED30020410 gene resulted in anterior (head) tissue lysis, whereas fork-head box containing gene SMED30035239 RNAi predominantly caused posterior (tail) tissue lysis (Fig 6.2).

Several RNAi conditions caused very specific tissue defects without animal lysis. Knockdown of Forkhead box protein P4 (SMED30032631) resulted in loss of body

pigmentation (Fig. 6.2), a rare phenotype class which was also identified in previous large scale functional screens (Reddien et al., 2005). FoxP4 (RNAi) phenotype progressed from the anterior to posterior end of the animal. Worms remained devoid of pigmentation even weeks after the last RNAi administration, suggesting either extremely slow pigment cell turnover or pigment synthesis. The Fork-head SMED30014407 RNAi knockdown caused animal body edema, a common phenotype due to excretory system failure from cilia and solute carrier gene perturbation (Reddien et al., 2005; Vij et al., 2012; Vu et al., 2015)(Fig. 6.2). Knock-down of homeobox gene SMED30016301 with sequence similarity to the vertebrate Nk 6.1 transcription factor had a profound effect on animal locomotion/behavior (Fig. 6.2). Although these worms exhibited photophobic behavior and tried to avoid the light, they could not detach their ventral tail surface from the substrate. Hence, these animals extensively extended the anterior portion of their body and exhibited very thinned body column, therefore resembling rare "stick and stretch" phenotype reported after hepatocellular-associated antigen (NBE.8.11C) RNAi treatment (Reddien et al., 2005).

Nearly half of identified phenotypes (4/10) were caused by knockdown of forkhead box (Fox) transcription factor proteins, indicating that this family plays various distinct roles in planarian tissue homeostasis. These evolutionary conserved transcription factors (Golson and Kaestner, 2016) are crucial for both metazoan tissue development and maintenance and the deletion of even a single Fox transcription factor is usually lethal. In vertebrates Fox family members regulate specification, differentiation and maintenance of trophectoderm, liver, pancreas, ovaries, intestine, lung, kidney, prostate, brain, thyroid, skeletal and heart muscle, skeleton, vascular tissue and immune cells (Golson and Kaestner, 2016; Zhu, 2016). Although other phenotype causing genes in our screen belonged to different families of transcription regulators (eg. hoemobox, leucine zipper, zinc finger), their homologue's roles in tissue establishment or maintenance have been also characterized in vertebrates. NK6 homeobox protein has an important role in beta cell establishment in pancreas (Iype et al., 2004) as well as neuronal fate specification (Sander et al., 2000). MITF is a basic helix-loop-helix leucine zipper transcription factor involved in lineage-specific pathway regulation of many types of cells including melanocytes, osteoclasts, and mast cells (Hershey and Fisher, 2004; Watanabe et al., 1998). MITF mutations are implicated in Waardenburg and Tietz syndromes, which result in deafness, bone loss, small eyes, and poorly pigmented eyes and skin in vertebrates (Moore, 1995; Smith et al., 1997; Watanabe et al., 1998). In vertebrates Gfi-1 zinc-finger protein is essential transcription repressor for hematopoiesis (Person et al., 2003) as well as inner ear

cell maintenance (Hertzano et al., 2004). Its mutation perturbs myeloid differentiation (Person et al., 2003)and results in inner ear hair cell loss (Hertzano et al., 2004).

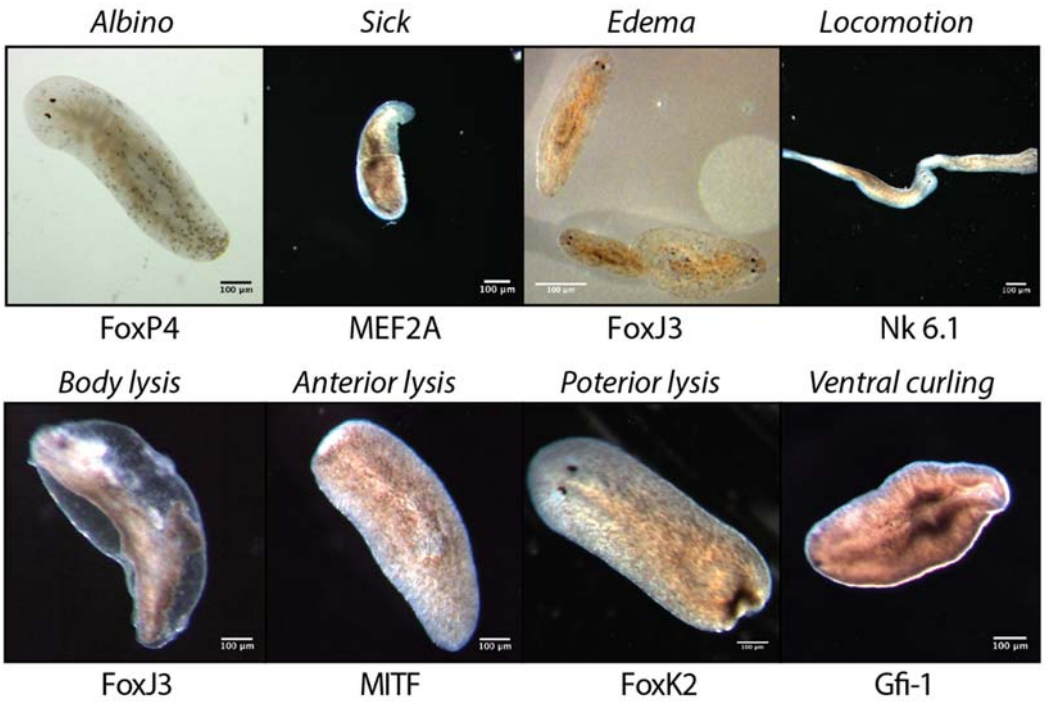

Figure 6-2. RNAi screen identified diverse homeostasis phenotypes

Table 5. Epidermally enriched genes with putative DNA binding domain (putative transcription factors) and their phenotypes.

smed id	*homology to vertebrate (mouse) proteins*		*Log2FC*		*Adj.p-value*		*RNA i.*	*Phenotype*		
	description	*E.value*	*D/ww*	*V/ww*	*D/ww*	*V/ww*	*4.*	*Homoestasis*	*W. healing*	*Regeneration*
Enriched at Dorsal and Ventral epidermis (FC>2):										
SMED30010536	distal-less homeobox 5	7.E-14	3.25	3.41	7.E-54	1.E-61	+			
SMED30014407	forkhead box J3	3.E-16	2.23	3.87	5.E-33	1.E-89		Edema		
SMED30002934	forkhead box J1	4.E-42	2.54	3.24	4.E-43	3.E-69	+			
SMED30015041	retinoic acid receptor, beta	3.E-24	2.95	2.57	4.E-58	5.E-49	+		Lysis	
SMED30000740	E74-like factor 2	7.E-18	2.78	2.62	7.E-28	7.E-27	+	Lysis		
SMED30015704	homeobox A10	3.E-17	2.87	2.46	5.E-35	2.E-28				
SMED30011754	E74-like factor 2	5.E-07	2.51	2.75	1.E-43	7.E-55	+			
SMED30016301	NK6 homeobox 1	4.E-36	2.33	2.92	2.E-30	2.E-48	+	Locomotion		
SMED30016899	.	.	2.24	2.73	1.E-26	5.E-40	+			
SMED30035514	ankyrin repeat domain 50	3.E-09	2.00	2.85	2.E-23	3.E-47				
SMED30027170	HIV type I enhancer binding protein 3	1.E-12	2.38	2.35	2.E-17	4.E-18				
SMED30032625	.	.	2.00	2.65	6.E-16	2.E-28				
SMED30006454	.	.	2.16	2.38	8.E-16	6.E-20	+			
SMED30025473	MAX interactor 1, dimerization protein	4.E-06	1.87	2.64	2.E-25	5.E-50	+			
SMED30024319	SAM pointed domain containing ets TF	4.E-20	1.94	2.45	2.E-26	1.E-42				

smed id	homology to vertebrate (mouse) proteins		Log2FC		Adj.p-value		RNAi	Phenotype		
	description	E.value	D/ww	V/ww	D/ww	V/ww		Homoestasis	W. healing	Regeneration
SMED30009043	forkhead box J2	4.E-28	2.01	2.35	4.E-20	3.E-28				
SMED30018339	.	.	2.29	1.95	3.E-21	3.E-17				
SMED30000458	E1A binding protein p300	0.E+00	2.22	1.92	5.E-09	1.E-07	+			
SMED30028553	zinc finger, BED type containing 4	1.E-64	2.14	1.97	3.E-34	2.E-31				
SMED30002579	E74-like factor 3	7.E-07	1.46	2.53	2.E-08	7.E-23				
SMED30018122	myocyte enhancer factor 2C	4.E-09	1.65	2.25	7.E-16	2.E-29				
SMED30029242	LIM homeobox protein 2	3.E-29	1.22	2.60	2.E-12	2.E-53	+			
SMED30019262	heat shock factor 1	5.E-36	1.67	1.99	5.E-19	4.E-28				
SMED30003975	ceramide synthase 2	2.E-72	2.41	1.13	4.E-31	5.E-09	+			
SMED30023587	.	.	1.34	1.95	6.E-13	3.E-27				
SMED30019431	D site albumin promoter binding protein	2.E-09	1.86	1.42	2.E-23	2.E-15	+			
SMED30013043	runt related transcription factor 2	6.E-40	1.77	1.36	8.E-20	1.E-13				
SMED30020022	E74-like factor 5	2.E-06	1.34	1.71	8.E-12	1.E-19				
SMED30023819	.	.	1.25	1.66	1.E-11	6.E-21				
SMED30020090	zinc finger protein 541	1.E-21	1.43	1.44	1.E-16	3.E-18	+			
SMED30005237	predicted gene 14401	4.E-17	1.59	1.27	4.E-14	2.E-10	+			
SMED30028898	.	.	1.32	1.51	6.E-11	6.E-15	+			
SMED30001601	Growth factor independent 1 (Gfi-1)	7.E-13	1.65	1.11	7.E-20	9.E-11	+	Curling/Lysis		
SMED30005073	zinc finger, BED type containing 5	9.E-124	1.53	1.22	6.E-16	2.E-11				

smed id	homology to vertebrate (mouse) proteins		Log2FC		Adj.p-value		RNAi	Phenotype		
	description	E.value	D/ww	V/ww	D/ww	V/ww		Homoestasis	W. healing	Regeneration
SMED30016927	.	.	1.40	1.23	7.E-11	3.E-09				
SMED30031794	myocyte enhancer factor 2A	7.E-41	1.08	1.49	1.E-08	1.E-16	+	Sick		
SMED30006392	Zn finger and BTB domain containing 40	9.E-08	1.17	1.26	5.E-06	4.E-07				
SMED30008041	.	.	1.13	1.27	1.E-07	4.E-10				
SMED30014937	ELK1, member of ETS oncogene family	4.E-10	1.01	1.28	1.E-07	2.E-12				

Enriched at Dorsal epidermis (FC>2):

SMED30026019	msh homeobox 1	5.E-37	4.14	0.05	6.E-34	9.E-01	+			
SMED30031351	GATA binding protein 3	3.E-49	4.00	-0.25	2.E-33	4.E-01	+			
SMED30032395	T-box 3	2.E-118	3.89	-0.42	4.E-18	3.E-01	+			
SMED30032592	ovo like zinc finger 1	4.E-47	3.42	0.34	1.E-37	2.E-01	+			
SMED30000485	PR domain containing 1, with ZNF domain	4.E-55	3.17	-0.82	3.E-17	2.E-02	+			
SMED30013810	teashirt zinc finger family member 2	2.E-06	2.96	0.92	1.E-28	2.E-04				
SMED30011553	T-box 2	3.E-72	2.62	-1.34	2.E-32	5.E-10	+			
SMED30010268	forkhead box D3	7.E-44	1.32	-2.23	9.E-03	3.E-04				
SMED30029873	early growth response 1	8.E-28	2.41	0.68	2.E-38	1.E-04	+			
SMED30031744	forkhead box K1	9.E-47	1.95	0.70	2.E-25	9.E-05				

smed id	homology to vertebrate (mouse) proteins		Log2FC		Adj.p-value		RNAi	Phenotype		
	description	E.value	D/ww	V/ww	D/ww	V/ww		Homoestasis	W. healing	Regeneration
SMED30014326	ovo like zinc finger 1	9.E-50	1.36	-1.41	2.E-08	7.E-08	+			
SMED30022030	early growth response 4	3.E-25	1.74	0.32	3.E-04	5.E-01				
SMED30020689	E74-like factor 4	3.E-27	1.56	0.77	1.E-19	2.E-06	+			
SMED30009224	early growth response 1	2.E-24	1.62	0.33	2.E-03	5.E-01				
SMED30032631	forkhead box P4	3.E-23	1.46	0.59	4.E-16	6.E-04	+	Albino		
SMED30029780	early growth response 4	7.E-26	1.51	0.24	7.E-04	6.E-01				
SMED30003389	serum response factor	1.E-28	1.45	0.25	4.E-15	2.E-01				
SMED30026666	zinc finger protein 341	4.E-42	1.08	0.94	7.E-07	5.E-06				
SMED30017247	.	.	1.28	0.40	2.E-03	4.E-01				
SMED30029253	.	.	1.12	0.70	1.E-03	4.E-02				
SMED30027272	CREB binding protein	0.E+00	1.11	0.70	3.E-11	1.E-05				
SMED30006455	forkhead box J3	2.E-17	1.16	0.54	8.E-13	6.E-04	+	Lysis		
SMED30028733	Pbx/knotted 1 homeobox 2	1.E-61	1.16	0.35	5.E-08	9.E-02	+			No anterior reg.
SMED30014280	l(3)mbt-like 3 (Drosophila)	1.E-88	1.07	0.40	9.E-06	9.E-02	+			
SMED30017865	nuclear transcription factor-Y alpha	3.E-26	1.01	0.51	7.E-09	3.E-03				

smed id	homology to vertebrate (mouse) proteins		Log2FC		Adj.p-value		RNAi	Phenotype		
	description	E.value	D/ww	V/ww	D/ww	V/ww		Homoestasis	W. healing	Regeneration
Enriched at Ventral epidermis (FC>2):										
SMED30026741	Kruppel-like factor 4 (gut)	2.E-42	-5.53	2.01	2.E-04	2.E-03	+			
SMED30008131	orthodenticle homeobox 1	1.E-17	-3.36	4.46	1.E-20	6.E-82				
SMED30013740	forkhead box D1	2.E-44	-4.50	2.01	5.E-21	2.E-11				
SMED30032163	regulatory factor X, 4	5.E-46	-1.40	4.58	2.E-07	6.E-61				
SMED30030504	Iroquois related homeobox 6 (Drosophila)	6.E-38	-2.92	2.69	2.E-10	9.E-14				
SMED30018592	ovo like zinc finger 2	4.E-35	-3.35	1.58	2.E-04	4.E-03				
SMED30033757	forkhead box J1	1.E-34	0.69	3.49	7.E-03	1.E-44	+			
SMED30000893	NK2 homeobox 4	3.E-27	-1.14	2.80	1.E-01	6.E-05	+			
SMED30016788	zinc finger protein of the cerebellum 2	8.E-81	-1.71	2.28	1.E-07	2.E-15	+			
SMED30026965	TEA domain family member 1	3.E-71	0.21	2.56	3.E-01	3.E-43	+			
SMED30003390	.	.	0.92	2.09	4.E-05	2.E-22				
SMED30021262	RAB GEF 1	1.E-72	0.96	1.81	4.E-08	1.E-26	+			
SMED30001802	.	.	-1.60	1.12	6.E-06	7.E-04				
SMED30001785	RAR-related orphan receptor alpha	3.E-19	-0.90	1.52	8.E-04	2.E-10	+			
SMED30001207	calmodulin binding transcr.activator 2	1.E-27	0.48	1.65	1.E-02	1.E-19				
SMED30032613	homeobox A4	6.E-33	0.92	1.39	2.E-03	6.E-07				
SMED30021694	heat shock factor 1	1.E-26	-0.67	1.46	3.E-03	4.E-12				

smed id	homology to vertebrate (mouse) proteins		Log2FC		Adj.p-value		RNAi	Phenotype		
	description	E.value	D/ww	V/ww	D/ww	V/ww		Homoestasis	W. healing	Regeneration
SMED30006028	.	.	-1.09	1.07	3.E-02	2.E-02	+			
SMED30000346	.	.	0.38	1.45	4.E-02	2.E-16				
SMED30011041	.	.	0.07	1.42	8.E-01	3.E-08		Lysis		
SMED30011885	cAMP responsive element BP 3-like 4	3.E-23	0.93	1.08	6.E-08	4.E-11				
SMED30032477	endothelial differentiation-related 1	2.E-51	0.58	1.25	3.E-03	2.E-11				
SMED30032935	scratch family zinc finger 1	4.E-31	-0.53	1.18	4.E-01	3.E-02				
SMED30003001	signal transducer and activator of transcrip. 5A	9.E-14	-0.26	1.25	3.E-01	1.E-09				
SMED30035662	regulatory factor X, 1	1.E-156	0.59	1.06	3.E-04	6.E-12	+			
SMED30032427	.	.	0.24	1.16	6.E-01	9.E-03				
SMED30029528	zinc finger protein 90	6.E-07	0.52	1.05	6.E-03	2.E-09				
SMED30030829	Y box protein 3	2.E-27	0.35	1.03	2.E-01	3.E-06				

smed id	homology to vertebrate (mouse) proteins		Log2FC		Adj.p-value		RNAi	Phenotype		
	description	E.value	D/ww	V/ww	D/ww	V/ww		Homoestasis	W. healing	Regeneration
Enriched in Dorsal and/or Ventral epidermis (FC<2):										
SMED30033237	nuclear receptor subfamily , F, 1	6.E-31	0.99	0.79	4.E-09	1.E-06	+			
SMED30020410	microphthalmia-associated TF	1.E-12	0.60	0.59	5.E-03	4.E-03	+	Lysis (head)		
SMED30001441	lysine (K)-specific demethylase 5C	0.E+00	0.69	0.51	5.E-05	2.E-03	+			
SMED30033789	one cut domain, family member 1	3.E-70	0.98	0.68	6.E-10	8.E-06	+			
SMED30035239	forkhead box K2	7.E-48	0.42	0.45	1.E-02	4.E-03	+	Lysis (tail)		
SMED30021726	zinc finger, AN1-type domain 5	8.E-29	0.65	0.68	5.E-04	1.E-04	+			
SMED30014114	myocyte enhancer factor 2C	3.E-47	0.62	-0.22	4.E-03	3.E-01	+			
SMED30019046	TEA domain family member 1	3.E-111	0.94	0.52	1.E-06	5.E-03				
SMED30027645	zinc finger protein 768	2.E-17	0.81	0.56	3.E-06	7.E-04				
SMED30012510	early growth response 1	2.E-34	0.77	-0.12	4.E-05	5.E-01				
SMED30029241	RAR-related orphan receptor alpha	2.E-22	0.67	-0.41	3.E-04	2.E-02				
SMED30035670	zinc finger, AN1-type domain 6	1.E-19	-0.04	0.69	9.E-01	1.E-04				

Wound response phenotypes

RNAi knockdown of Transcription factors which did not result in severe intact tissue phenotypes were selected for subsequent functional studies in injury repair. To investigate whether candidate genes are important for wound response, RNAi animals were subjected to amputation (head and tail) and scored for their ability to close wounds and regenerate missing tissue.

We expected the RNAi conditions affecting wound closure would result in prolonged wound muscle contraction and/or injured tissue lysis within the first 24hrs after amputation. Although RNAi knockdown of most of the transcription factors gave no obvious wound-closure phenotype in our assay, knockdown of nuclear hormone receptor (SMED30015041) resulted in injured tissue lysis. Interestingly, this gene did not show a severe phenotype in intact animals, suggesting that it may have a wound closure-specific function which could be subsequently analyzed with live imaging techniques. Nevertheless, although the SMED30015041 (RNAi) wound closure phenotype was reproduced once after the initial screen, we could not reproduce it in subsequent RNAi attempts.

To identify regeneration-specific phenotypes, we examined the ability of animal fragments to reestablish lost anterior and posterior tissues after transverse amputations. The knock-down of homeodomain containing gene SMED30028733 resulted in a penetrant anterior-tissue-specific regeneration defect. Nevertheless, closer SMED30028733 sequence analysis revealed that this gene function has been previously described. SMED30028733 clone sequence matched to *Smed-prep* (Felix and Aboobaker, 2010), already published regulator of anterior tissue specific regeneration.

6.2 Smed-Gfi-1 phenotype characterization

Our functional screen identified an array of homeostatic defects. Some of these defects resembled previously characterized planarian phenotypes. For example edema formation after FoxJ3 knockdown phenocopied cilia function perturbation (Reddien et al., 2005; Vij et al., 2012; Vu et al., 2015), ventral curling after the Gfi-1 (RNAi) was stereotypical to neoblast function and epidermal lineage maintenance perturbation (Reddien et al., 2005; van Wolfswinkel et al., 2014; Wagner et al., 2012). The mechanism behind novel phenotypes progression was harder to infer. Some phenotypes were either

novel (eg. anterior-posterior specific lysis) or were not previously characterized in detail (eg. stick and stretch, depigmentation). Therefore, due to time limitation we were not able to pursue their characterization.

The Gfi-1 knockdown caused complete and 100% penetrant tissue maintenance failure and its phenotype progression (ventral curling followed by lysis) closely resembled epidermal lineage maintenance defects (Reddien et al., 2005; van Wolfswinkel et al., 2014; Wagner et al., 2012). Therefore Gfi-1 phenotype was selected for more detail characterization. In our initial epidermally-enriched ISH screen failed to detect an expression pattern for Gfi-1 (group 0), thus we decided that its expression pattern analysis had to be revisited. Extended signal development (overnight) revealed that Gfi-1 (FC(1.65)log2 and FC(1.11)log2 in dorsal/ww and ventral/ww samples respectively) was also expressed throughout the animal mesenchyme (Fig. 6.3, A). We followed the *gfi-1* expression pattern of these undifferentiated mesenchymal cells in irradiated animals to determine their cell turnover kinetics. The mesenchymal expression pattern was reduced one day after irradiation and continued to diminish within next 7 days, indicating that *gfi-1* is expressed in a subset of neoblasts as well as their mesenchymal progeny (Eisenhoffer et al., 2008). As mesenchymal staining was reduced, *gfi-1* expression in the differentiated tissues became more apparent. This gene was revealed to be expressed in the gut epithelia, sensory neurons at the anterior region of the brain as well as epidermis.

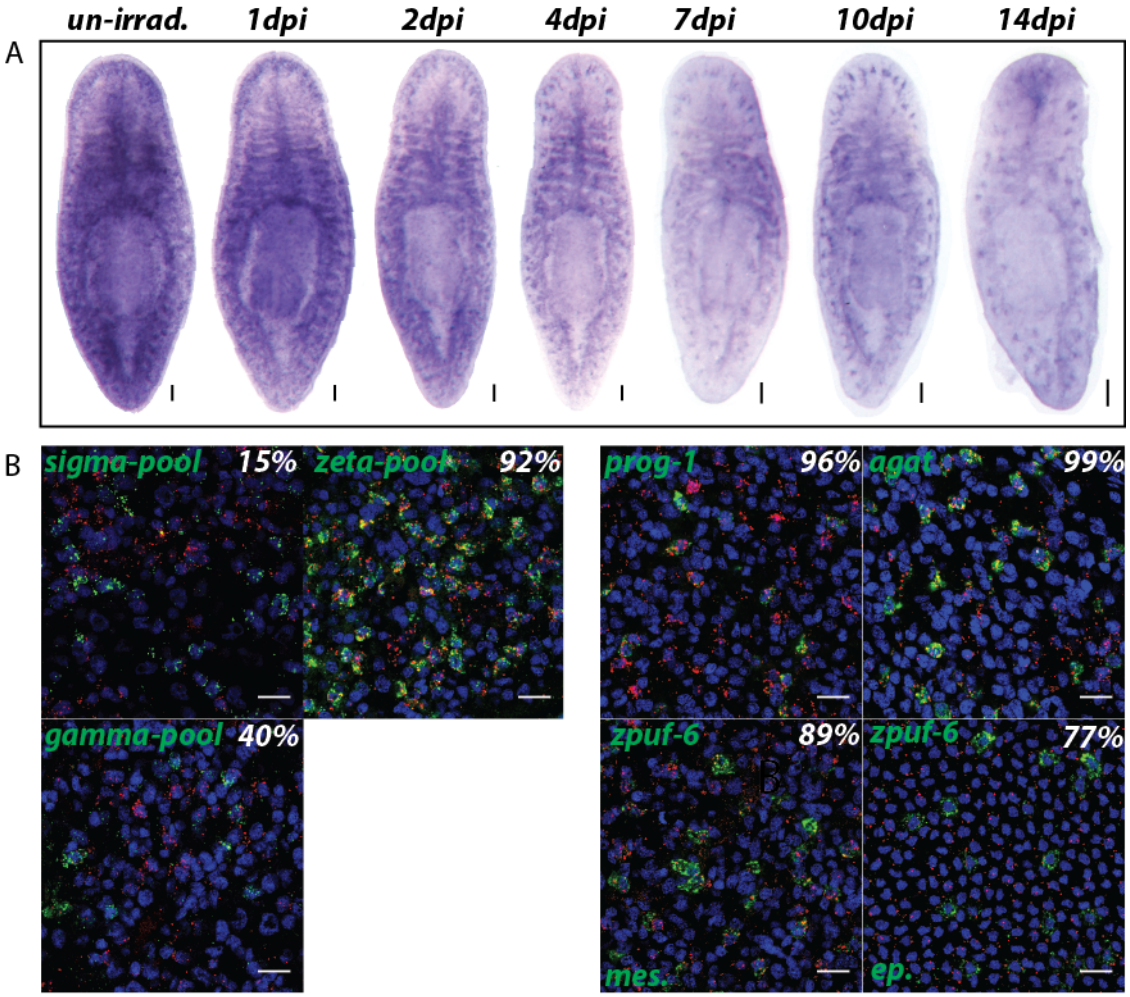

Figure 6-3. *gfi-1* expression in epidermal lineage. *gfi-1* is expressed throughout mesenchyme, gut and epidermis.
Expression pattern analysis in irradiated animals (A). Within mesenchyme *gfi-1* is mainly expressed in zeta, epidermal lineage, neoblasts as well as early (*prog-1*) and late epidermal lineage progenitors (*agat* and *zpuf-6*). Neoblast lineage marker pools (van Wolfswinkel et al., 2014): zeta (*fgfr-1, zfp-1, soxP-3, and egr-1*); gamma (*hnf-4, gata456, and nkx2.2*); sigma (*soxP-1 and soxP-2*). 10 µm scale bar.

To provide a more comprehensive description of the *gfi-1* expression pattern, we performed co-localization studies with established neoblast and their mesenchymal progeny markers (Fig. 6.3, B). Within the neoblast compartment, *gfi-1* expression overlapped with epidermal lineage zeta-class (van Wolfswinkel et al., 2014) cells (96%), whereas co-localization with sigma- and gamma-class neoblasts (van Wolfswinkel et al., 2014) was much lower (15% and 40% respectively). Consequently, we determined *gfi-1* to be expressed within differentiating epidermal progenitors. *gfi-1* transcripts were present in nearly all early (*prog-1*, 96%) and late (*agat*, 99%) epidermal progenitors as well as most of the *zpuf-6*$^{+}$ cells in mesenchyme and epidermal layer (89% and 77% respectively).

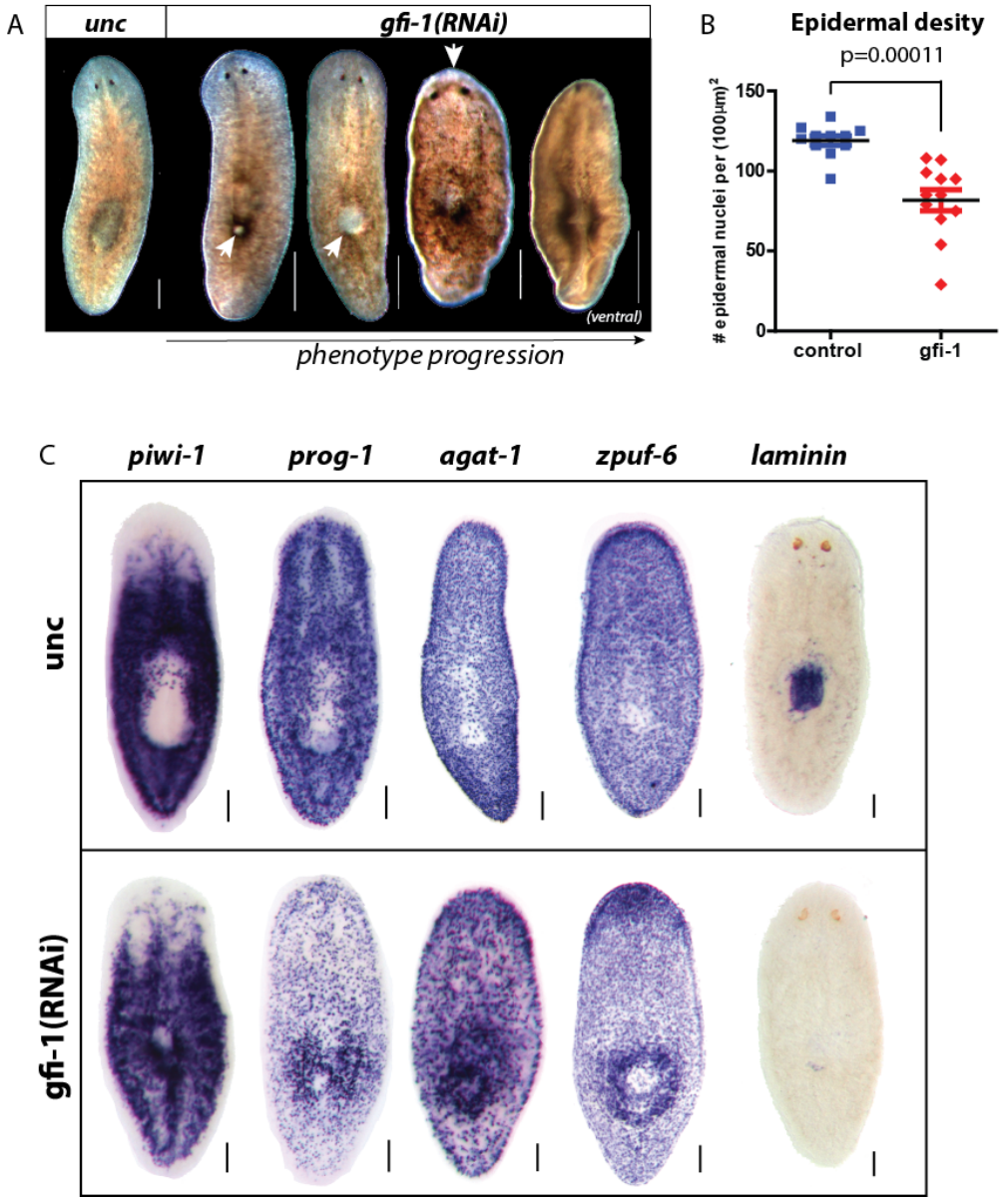

Figure 6-4. *gfi-1*(RNAi) phenotype characterization.
gfi-1(RNAi) causes dorsal lesions, head regression and ventral curling phenotypes (arrows) (A); Epidermal density decreases after *gfi-1*(RNAi). Epidermal nuclei (DAPI) density quantification within ventral epidermis, 20 days after the first dsRNA feeding (B); *gfi-1*(RNAi) have reduced early epidermal progenitors (*prog-1*) and lose their pharynx by 16 days after the first dsRNA feeding. Scale bar is 200 µm in A and 100 µm in C.

We then sought to investigate the role of Gfi-1 in planarian tissue maintenance. At the time-point (12 after the first dsRNA feeding) when knock-down animals developed dorsal lesions and stopped eating (Fig. 6.3, A), they completely lacked pharynges (*laminin*; Fig. 6.4, C). Although the neoblast (*smedwi-1*) number decrease was modest (*piwi-1*; Fig. 6.4, C), the density of epidermal lineage cells was increased at the dorsal lesion site and overall their numbers decreased. Gfi-1 RNAi knock-down animals had a significant

reduction of early epidermal progenitor number (*prog-1*; Fig. 6.4, C), whereas the decrease in late epidermal progenitor (*agat*; Fig. 6.4, C) and *zpuf-6*$^{+}$ cells numbers was modest at the time-point examined (16 days after the first dsRNA). As the phenotype progressed further and animals started to curl ventrally (20-24 days after the first dsRNA), we were able to quantify the *gfi-1*(RNAi) effect on epidermal maintenance. Epidermal cell density was significantly decreased (median 85±6,9 and 122±3 per 100 μm^2; p.value 0.0001) at the ventral epidermis (Fig. 6.4, C), demonstrating that the final stages of *gfi-1*(RNAi) phenotype progression are indeed a result of epidermal maintenance failure.

Chapter 7

Discussion

While all animals appear capable of healing their wounds, wound closure mechanisms can nevertheless vary widely between species, tissues and/or developmental stages. Despite the observed variability of the Metazoan wound response, mechanistic cellular wound response studies have been primarily done in few Ecdysozoan models, *i.e.*, *Drosophila* and *C. elegans* (Galko and Krasnow, 2004; Lesch et al., 2010; Millard and Martin, 2008; Xu and Chisholm, 2011), with large Metazoan groups like the Lophotrochozoa remaining virtually unexplored. It is unlikely that the breadth of Metazoan wound healing mechanisms is well represented within the few Ecdysozoans thus far examined, for example. In fact, the epidermis of flies and Nematodes is rather specialized, as both are covered by a cuticule, and in the case of *C. elegans*, it is also syncytial. Hence, it is unclear how well the Ecdysozoan epidermis may inform the wound responses of other animals or of other tissues such as mucosal epithelia.

Although regeneration is widespread among the Metazoa, it is not understood why such capacity has been lost/reduced in numerous species, tissues and/or developmental stages. Studies have suggested that the epidermal wound response is crucial for initiating regeneration (Brockes and Kumar, 2008). For instance, the regenerative response is abolished if wound epithelia formation is perturbed in salamanders or humans (Goss, 1956; Illingworth, 1974; Mescher, 1976). In fact, the discrete mechanisms underpinning the initiation of regeneration is yet to be determined. Therefore, wound healing studies across diverse animal groups that vary in regenerative capacity might help reveal factors associated with the initiation and/or loss of response to regenerative processes.

Studies in planaria offer an opportunity to significantly expand our understanding of metazoan wound healing for several important reasons. Planaria can survive extensive tissue damage, nevertheless the mechanism endowing such robust and efficient healing capacity remains elusive. The wound closure capacity of planarian epidermis is even more remarkable if one considers that it is capable to repopulate wound surface without proliferation and increase in its cell number. Furthermore, several observations also suggest that re-epithelialization in planarian is achieved by proteins that are already present in the intact epidermis: wound closure is remarkably fast, it is neither perturbed by exposure to the protein synthesis inhibitor cycloheximide nor by knock-down of wound induced genes (Wenemoser et al., 2012). Wound closure in planarians is followed by

regenerative program activation and complete lost tissue reestablishment. Thus, planaria model allows to characterize wound response in organism with high regenerative capacity and, unlike other wound healing models, provides an opportunity to compare cellular wound response to tissue loss and tissue damage.

Live visualization of cellular wound response to laser ablation of epidermis demonstrated that cellular response to tissue damage in planaria is almost instantaneous (seconds). Although the exact mechanism of wound re-epithelization is yet to be determined, the observed symmetric and asymmetric wound closure patterns imply that several wound closure mechanisms might be utilized in planarian epidermis. In case of asymmetric wound response, advancing wound epithelia is flat with wide lamellipodia forming at the leading edge. This wound closure pattern resembles collective cell migration, nevertheless it still has to be determined whether this re-epithelialization is driven by lamellipodia crawling or re-poliarization and extension of wound edge epidermis. The ability of epidermis to immediately respond to tissue damage suggest that epidermal cells might be competent to engage in wound response even before injury. Alternatively, wound response might be initiated by mechanical cues resulting from the loss of epidermal integrity or contraction of injured body wall. In light of this hypothesis, observed dynamic protrusive behaviors in intact epidermis might indeed represent the innate ability of epidermal cells to respond to tissue damage or their capacity to probe epidermal tissue integrity thus immediately respond to its damage.

Established wound healing models only allow to study wound response to tissue damage, whereas planaria can also survive and recover after extensive tissue loss. Nevertheless, the mechanism endowing such a robust and efficient wound healing has not been characterized in detail. Electron microscopy analysis as well as development and application of live imaging methodologies allowed us to visualize planarian wound response to decapitation and reassess the validity of two previously proposed wound closure mechanisms. First, the more accepted view postulated that planarian wounds are closed by active migration of wound edge epidermis, whereas, the second argued against cell migration and suggested wounds are re-epithelized by muscle contraction. Although both the body wall contraction contribution and occasional cellular migration-like behaviors of wound edge epidermis were observed in our studies, neither the typical lamellipodial crawling mediated cell migration or muscle contraction is the primary mechanism of planarian wounds closure. Inconsistent with lamellipodial crawling mechanism (Hori, 1989; Morita and Best, 1974; Pascolini et al., 1984; Spiegelman and

Dudley, 1973), cells of advancing wound edge epidermis do not establish prominent contacts with wound surfaces and thus do not seem to grasp over the underlining wound tissues. Instead, these cells maintain intracellular junctions and remain within epidermal sheet rather than acquiring typical migratory mesenchymal cell-like state. Furthermore, fixed and live wound visualization also contradicted the notion that planarian wounds are closed within minutes solely by muscle contraction (Chandebois, 1980a). In our experiments, wounds remained open even after body wall contraction which suggests that this wound response may aid, but is not sufficient to complete wound closure.

Our work shows that wounds of decapitated animals are closed by extension of the wound edge epidermis and subsequently by filopodia-mediated fusion of opposing wound edges. Minutes after the decapitation, the wound edge epidermis loses its columnar morphology, repolarizes and extends flat lamellipodia-like protrusions into the wound surface while remaining attached to the basal membrane. Later, the leading wound edge cells depart from the basal membrane, but remain attached to their epidermal neighbors at the wound margin. The advancing epidermal cells do not appear to establish contacts with wound surface indicating that planarian epithelialization is not driven by lamellipodial crawling mediated cell migration. As wound epithelia advances over the wound surface it does not seem to be supported by extracellular structures or cellular debris, thus it appears that planarian wounds are closed as wound edge epidermis repolarizes and extends over the wound surface. Wound edge epidermis advances over the wound surface as multicellular extension, which morphologically resembles Chamdebois' (1980) proposed epidermal spurs.

Live imaging demonstrated that the final stages of wound closure in decapitated planarians is mediated by filopodial interactions between opposing wound edge epidermis, a mechanism not entirely dissimilar to the epidermal sheet fusion reported during *Drosophila* embryonic dorsal closure. Initially filopodia interactions are observed in the lateral wound edges, areas where the distance between opposing wound edges are the shortest. As filopodia pull the epidermal sheets closer together, new interactions are formed along the interface of juxtaposed epidermal cells and thus wound closure continues to gradually progress inward in a zipper-like fashion. This process in *Drosophila* embryonic dorsal closure involves actin cable contraction, but it still has to be investigated whether such structures are also formed during planaria wound closure. Thus, in *Drosophila* filopodia also conduct spatial surveillance along juxtaposed epidermal edges to ensure that the correct body plan will be established after dorsal epidermal sheet fusion

(Millard and Martin, 2008). It would be interesting to investigate whether filopodia function analogously during planarian wound closure. In contrast to the longitudinal axis of the Arthropod body, planaria are not clearly segmented, however thier bodies have a well defined dorsal-ventral boundary which needs to be re-established after tissue loss. Subsequent wound closure analyses could test if filopodia behavior is affected in entirely dorsalized or ventralized animals (after BMP pathway perturbation)(Gavino and Reddien, 2011; Molina et al., 2007; Orii and Watanabe, 2007; Reddien et al., 2007) and help determine whether filopodia also play spatial recognition roles in planaria.

Although planarian wound response shares some resemblance with *Drosophila* embryonic dorsal closure, it encompasses additional complex cellular behaviors. In planarians, interaction between fusing epidermal sheets is not limited to filopodia protrusions. The long, unicellular or multicellular projections of the marginal epidermis occasionally reach over the wound surface to contact the opposite wound edge. As these structures extend they always remain attached to their original location at the marginal basal membrane. Morphologically, these structures vary from being extremely thin and likely unicellular to being wider and multi-cellular. When these structures are formed, the cellular bodies and nuclei migrate along their length, traverse over the wound surface and reach the opposite wound edge. Similar cellular wound responses have yet to be described in established wound healing systems; however, we suspect that this type of cellular behavior might be also present in other Metazoans given that long actin projections have been also reported in cnidarian wounds (DuBuc et al., 2014). Currently, analogous cellular migration has been only visualized in primary cultures of human mucosal epithelia, specifically bronchia and mammary epithelia (Zani and Edelman, 2010; Zani et al., 2010). Human mucosal epithelia cells can form extremely long (up to one millimeter) “epithelial bridges” or projections between neighboring colonies. These uni- and multi-cellular structures hover freely above the underlying substratum and mediate single or multiple cell migration, as well as intra-cellular communication. Although the physiological significance of these structures remains to be investigated in much greater mechanistic detail, epithelia bridge formation in other systems is known to be stimulated by inflammatory pathways, the inhibition of nuclear factor (NF)-kB or cyclooxygenase (COX) pathways, as well as increased reactive oxygen species (ROS) (Zani et al., 2010).

Planarian wound closure is dependent on neither proliferation nor mesenchymal cell intercalation into epidermis. Hence, irradiated (and thus neoblast and epidermal progenitor depleted) animals are still able to close their wounds. This process is relatively

fast. After decapitation, for instance, *S. mediterranea* closes its wounds within 1-2 hours. As the wound edge epidermis meets along the wound surface, a thinly stretched sheet of wound epithelium is formed. Although wound epithelium covers the wound as a single-cell-layer sheet, multiple wound epithelia cells are initially stretched over each other at the wound margin. Epidermal cells continue to be recruited to the wound epithelium after wound closure: cells depart from the basal membrane to intercalate into the wound epithelium, the integrity of which is maintained by intracellular connections between epidermal neighbors rather that attachment to the wound tissues. Although wound epithelium is directly exposed to the wound mesenchyme, both tissues remain separated by empty spaces up until blastemal formation. As the expanding blastema starts to stretch the wound epithelial monolayer, more cells are observed being recruited into the wound epithelia from the surrounding, intact columnar epidermis. At around 4 days after the decapitation, epidermal progeny starts to intercalate into the epidermal layer from the mesenchyme. As cell numbers within the wound epithelium increase, the tissue become thicker. After the basement membrane is restored (5-6dpa), the epidermis reacquires its intact morphology and reestablishes its composition. Live tracing demonstrated that thinly stretched wound epithelia revert to columnar morphology and reintegrate into the regenerated epidermis. Therefore, the regenerated epidermal layer consists of both newly differentiated cells as well as cells recruited from the wound edge epidermis. Our studies have also uncovered that contrary to *D. japonica* (Hori, 1979), *S. mediterranea* can reestablish basal membrane even after lethal irradiation, suggesting that different mechanism of lost tissue reestablishment might be present even among different planarian species.

Developed epidermal dissection methodology and subsequent transcriptional profile analysis provided a list of epidermally expressed genes. Expression of some of these genes were restricted to certain domains of epidermis, therefore suggesting that planarian epidermis is more heterogonous than it was previously recognized. These transcripts provide useful markers for subsequent studies of planarian epidermis biology. They can be applied to measure epidermal cell specification during homeostasis as well as to follow epidermal cell fate throughout the wound response and regeneration. In response to tissue loss differentiated wound edge epidermis undergoes morphological transformation into the thin sheet of wound epithelia, which gradually resumes its columnar shape and contribute to tissue restoration. Identified markers allow to begin investigating whether these terminally differentiated cells maintain their fate throughout

this morphological transformation and to assess whether dedifferentiation occurs during planarian regeneration.

The identified epidermal expression profile analysis provided a list of genes for subsequent mechanistic studies of epidermal maintenance, function and wound response. We reasoned that knockdown of epidermally enriched transcription regulators has the highest chance of causing the epidermal phenotypes for the following reasons. Transcription factors are the key for differentiation, therefore targeting these molecules has a high chance of causing homeostasis or regeneration phenotypes. Thus, their knockdown ultimately should also cause the depletion of an array of their target genes in intact epidermis, some of which might be crucial for epidermal ability to respond to wound. Although none of the selected genes had reproducible wound healing phenotypes in our pilot screen, nearly a fifth (19.1%, 11/47) of assessed transcription factors yielded homeostasis defects. The identified phenotypes included a range of tissue maintenance defects. We characterized Smed-Gfi-1 (RNAi) phenotype in greater detail and demonstrated that this gene indeed has a role in epidermal maintenance. The subsequent characterization of other identified homeostasis phenotypes will allow to further investigate transcription regulator role in epidermal maintenance. The follow up studies should also interrogate the signaling cascade role in epidermal homeostasis. Wnt, Notch, STAT, JNK and NF-kappaB signaling pathway components were enriched in transcriptional profile of planarian epidermis, yet their contribution to planarian epidermis has not been explored.

Planarian re-epithelization starts immediately after injury and it is independent on *de novo* protein synthesis (Wenemoser et al., 2012), therefore it must be executed by proteins that are already present in intact tissue. Since these molecules likely are represented in epidermal sample expression profile, they could be identified by knockdown screen of selected epidermally expressed genes. Various conserved metazoan wound response mediators are enriched in epidermis and hence they are good candidates for the functional studies. Knockdown of receptors (transmembrane domain containing proteins), MAPK kinases, small GTPases and proteins implicated in cytoskeleton remodeling (e.g. actin polymerization machinery) will help elucidate their role in planarian wound healing. Developed live imaging methodology will allow to measure target gene role in wound healing and would allow to compare it to other metazoans.

Elucidating the mechanism responsible for remarkable wound healing capacity in planaria might also require investigating the function of structures or processes which are

unique to planarian epidermis. Several features differentiate planarian epidermis form other wound healing models: the irregular epidermal cell morphology, the dynamic protrusive behaviors, the formation of prominent cytoplasmic feet along their basal surface as well as the abundant intracellular rhabdite vesicle formation. The robust rhabdite release in response to injury raises the intriguing but yet investigated possibility that exocytic response might play an important role in planarian wound healing. Rhabdites could contain cues, which are normally sequestered in intact tissue and quickly released in response to injury. Developed rhabdite isolation and proteomic characterization methodology (Appendix 3) allows to perform molecular characterization of these organelles and provides an opportunity to assess their content role in would healing. Exocytic wound response in planaria could also be a part of the mechanism allowing to expand the surface epidermis and thus rapidly close the wound. Post-mitotic epidermis must have a mechanism allowing re-epithelialize the wound without an increase in epidermal cell number. Adult arthropod epidermis expands its surface by cell fusion and syncytium formation (Losick et al., 2013). It would be interesting to investigate whether rhabdite exocytosis and their membrane incorporation into epidermal cell plasma membrane acts to expand the surface of wound epithelia and thus is required for wound closure. The potential rhabdite membrane contribution to wound epithelia surface expansion is truly impressive. Per our estimates the intracellular rhabdite surface is equal to the plasma membrane surface (Appendix 3). Analysis of wound closure dynamics after exocytic machinery perturbation (genetic or pharmacological) will allow to assess whether rhabdite membrane incorporation indeed is a novel strategy for wound epithelia surface expansion and therefore fast wound closure in post-mitotic epidermis.

Chapter 8

Methods and materials

Animal husbandry

The CIW4 clonal line of *Schmidtea mediterranea* was maintained at 20°C in 1× Montjuich salts (1.6 mM NaCl, 1.0 mM CaCl2, 1.0 mM MgSO4, 0.1 mM MgCl2, 0.1 mM KCl and 1.2 mM NaHCO3prepared in Milli-Q water) (Cebria and Newmark, 2005). 1 week starved animals were used for all experiments.

Electron microscopy

Transmitted electron microscopy was done as previously described (Vu et al., 2015): (1) 6-7mm specimens were fixed overnight in cold fixative (2.5% glutaraldehyde, 2% paraformaldehyde, 1% sucrose, 1 mM CaCl2 in 0.05 M sodium cacodylate buffer pH 7.36); (2) washed in wash buffer (0.1 M sodium cacodylate buffer; 1 mM CaCl2; and 1% sucrose) for 1 hr (3–4 exchanges); (3) fixed in 1% osmium tetroxide in 0.1 M sodium cacodylate buffer (containing 1 mM CaCl2) for 2 hr; (4) washed in wash buffer for 1 hr (3–4 exchanges) and in Milli-Q water for 30 min (3–4 exchanges); (5) fixed overnight in 0.5% aqueous uranyl acetate (in dark); (6) washed in Milli-Q water for 30 min (3–4 exchanges), and (7) dehydrated in acetone 30% (20 min), 50% (20 min), 70% (overnight), 90% (20 min, 2 times), and 100% (20 min, 3 times). Specimens were then embedded in epon-araldite or Spurr's resin as follows: 25% resin/acetone for 3 hr; 50% resin/acetone for 2.5 hr; 75% resin/acetone overnight; 100% resin without accelerator with microwave at 350 W for 3 min on/3 min off/3 min on for 1 day (2 exchanges); 100% resin with accelerator with microwave at 350 W for 3 min on/3 min off/3 min on for 1 day (2 exchanges) and placed in 60°C oven for polymerization for 2 days. Ultra-thin 50–100 nm sections were collected using a Leica UC6 Ultramicrotome. TEM specimens were stained with Sato's lead (3 min)/4% uranyl acetate in 70% methanol (4 min)/Sato's lead (6 min) prior to imaging on a FEI Technai BioTwin at 80 kV equipped with a Gatan UltraScan 1000 digital camera. Captured images were stitched by FIJI (Schneider et al., 2012) stitching plugins.

For scanning electron microscopy (1) 6-7mm samples were fixed overnight in cold 2.5% glutaraldehyde in 0.05 M sodium cacodylate (containing 1 mM CaCl2), (2) rinsed in Milli-Q water, (3) treated overnight with 2% aqueous osmium tetroxide in 4°C, (4)

dehydrated in a graded series of ethanol and (5) dried in a Tousimis Samdri-795 critical point dryer. Samples were mounted on stubs and sputter coated with gold palladium. Imaging was done with a Hitachi TM-1000 tabletop SEM.

Gamma irradiation

For irradiation experiments, animals were exposed to 10000 rads of γ-irradiation on a GammaCell 40 Exactor (Best Theratronics) irradiator. Animal amputations were done 7 days after irradiation.

Animal immobilization: chemical

Animal chemical immobilization was done by one of the following methods: exposure to 0.15% Chloretone (112054, Sigma), 0.25% Menthol (W266590, Sigma),10 μM 1-Phenoxy-2-propanol (484423, Sigma), 10 μM, 2-Phenoxyethanol (56753, Sigma) or acute treatment with 3.5% Magnesium chloride hexahydrate (M2670, Sigma). Menthol treatment effectiveness was improved by limiting its evaporation throughout the imaging sessions and by mounting immobilized animals in 6% methyl cellulose (9004-65-3, Acros organics) 0.25% menthol ointment.

Animal immobilization: mechanical

Microfluidic chips were fabricated using conventional photolithography as previously described (Ghannad-Rezaie et al., 2012). A silicon wafer was first coated with SU-8 (Microchem) using a spin coater. Films of various thickness were manufactured, so the spin procedures were performed as suggested on the SU-8 product literature. The wafer was then pre-baked according to product literature. The microfluidic design was achieved by UV exposing through a custom drawn mask. The mold was then post-baked and placed in the SU-8 developer for the suggested time. Chips were then replica molded from the SU-8 mold using Polydimethylsiloxane (PDMS)(Sylgard 184, Dow Corning) in a 10:1 (prepolymer to curing agent) ratio. The device was then baked at 80°C for 20 minutes. A borosilicate theta capillary (1mm ID x1.5mm OD x 0.2mm septum, Friedrich & Dimmock) was inserted into an orthogonal immobilization device through a hand punched hole. Tubing was connected to the vacuum chamber with 19-gauge stainless steel needle. A tight seal between the PDMS chip and the coverslip was created by applying weak vacuum

inside connected tubing. Vacuum was generated either manually, using a 10cc syringe, or by using a mechanical pump (Pico plus, Harvard apparatus).

Animal immobilization within agarose was done by the following procedure: chloretone (5-7min, 0.15%) anesthetized animals were submerged within solidifying 6% low melting point agarose (50084, Lonza) in 1x Montjuich salt solution. As agarose solidified, animals were decapitated and subsequently positioned on the coverslip for subsequent visualization with inverted microscope optics (Fig. 3.3).

Animal immobilization with adhesives was performed by sticking ventral side of the animal on a PeriAcryl 90 (P-ACRYL5, GluStitch) or GluSeal (GLUSEAL5, GluStitch) covered plastic surface.

Live cell labeling:

Animals were labeled by 15-30min incubation in 10 μM Cell Tracker Green (C7025, Life Technologies) or Cell Tracker Orange (C7025, Life Technologies), 5 μM Cell Trace Far Red (C34564, Life Technologies), 1-2x Cell Mask Deep Red stain (C10046, Life Technologies). Epidermal nuclei were labeled by 60min incubation in 10 μM DRAQ5 (DR05500, Biostatus). After labeling, animals were rinsed a few times in 1x Montjuich salt solution. Unless specified otherwise (Fig. 4.6), labeled animals were imaged shortly after the tissue labeling.

Live cell labeling: Diolistics

Tungsten micro-carriers (0.7 micron; 1652266, BioRad) were covered with DiI (D282, life technologies) as previously described (Gan et al., 2000). 0.5mg of labeled micro-carriers were re-suspended in small volume (10-20 μl) ethanol (64-17-5, Fisher) or methylene chloride (494453, Sigma), spread and dried along the center of macro-carrier disk (1652335, BioRad). Macro-carrier disc was loaded into the PDS-1000/He instrument (1652257, BioRad) as recommended by manufacturer (M1652249 user manual, BioRad). Prior to bombardment, 10-20 (8mm) animals were placed in the center of a 60mm petri dish. After water was removed from animal surface, the dish was placed onto the target shelf of the instrument set at 9 cm from micro-carrier launch assembly. The 10 psi vacuum was created inside the instrument and labeled micro-carriers were accelerated by burst of 1100 psi (rupture disk 1652329, BioRad) helium. Immediately after bombardment, labeling animals were rinsed and left to recover in 1x Montjuich salt solution. Animals were imaged 2-24hrs after tissue labeling.

Epidermal dissection

Medium size animals (8mm) were placed in a spot test plate (Pyrex) and incubated in 100 µl dissection buffer (1M NaCl, 100 mM Tris pH 8.0, 5mM EDTA pH 8.0) at room temperature for 4-7min. As epidermal tissue became opaque, the pieces of epidermal sheet were dissected from the animal surface by gently applying the side of the fine insect pin (size 000; 654300, Carolina Biological Supply). The dissected epidermis (single animal dorsal or ventral epidermis) containing buffer was collected and subjected to RNA isolation by the following methodology: (1) tissue containing dissection buffer (~100 µl) was mixed with 1200 µl Trizol (15596018, Invitrogen) and snap frozen in liquid nitrogen; (2) samples were thawed in room temperature, mixed with 346ul chloroform (X205, Amersco), shaken by hand for 15 seconds and let sit at room temperature for 3 minutes; subsequently, (3) samples were spun at 12000G for 15min (4C°); (4) aqueous phase was collected and mixed with 1040 µl isopropanol (I9516, Sigma) and 7.5 µg linear acrylamide (AM9520, Ambion); (5) samples were precipitated overnight at -20C°; (6) the next day, spun at 12000G for 15min at 4C°; (7) the resulting pellet was washed twice with 1ml of ice cold 75% ethanol; (8) air dried and re-suspended in 7.5 µl RNAse free water. The quality of RNA sample was assessed by Qubit (Invitrogen) and 2100 Bioanalyzer (Agilent Technologies) platform.

RNAseq

For RNAseq analysis the biological replicates of dissected dorsal epidermis samples, dissected ventral epidermis samples as well as whole animal (all tissue) samples were collected and subjected to Trizol RNA isolation. mRNAseq libraries were generated from 84-100 ng of high quality total RNA, as assessed using the Agilent 2100 Bioanalyzer. Libraries were made according to the manufacturer's directions for the TruSeq Stranded mRNA LT Kit (Illumina, RS-122-2101). Resulting short fragment libraries were checked for quality and quantity using the Bioanalyzer and Qubit Fluorometer (Life Technologies). Equal molar libraries were pooled, requantified and sequenced as 50 bp single read on the Illumina HiSeq 2500 instrument using HiSeq Control Software 2.2.38. Following sequencing, Illumina Primary Analysis version RTA 1.18.61.0 and Secondary Analysis version CASAVA-1.8.2 were run to demultiplex reads for all libraries and generate

FASTQ files. Genes were defined as exhibiting altered expression in RNAseq analysis if they had a minimum fold change of 2 and an adjusted p-value < 0.01.

Protein isolation

Proteins were isolated from rhanbdite particles by the following procedure: (1) 2-4 animals (8mm) were placed in the spot test plate; (2) exposed to 200 µl of dissection buffer (1M NaCl, 100 mM Tris pH 8.0, 5mM EDTA pH 8.0) for 5-10min at room temperature; (3) once rhabdite particles were released, the buffer was collected by pipette without touching the animal surface; (4) samples were mixed with 200 µl 2x RIPA buffer (300mM sodium chloride, 2% NP-40, 1% sodium deoxycholate, 0.2% SDS, 100 mM Tris pH 8.0) and rotated 1hr at 4°C; (5) samples were treated with 0.1U of Benzonase (E8263, Sigma); (5) mixed with 100µl 100% trichloroacetic acid (91226, Sigma) and precipitated overnight at 4C°; (5) spun at 14,000rpm for 30 min at 4°C; (6) the resulting pellet was washed twice with 500 µl of ice cold acetone (65051, Sigma) and spun 14,000rpm for 10 min after each wash; and (8) pellet was air dried. A Small amount of sample was re-suspended in 100 µl 100mM Tris-HCl (pH 8.5), ran on SDS-PAGE gel and stained with silver nitrate as previously described (Chevallet et al., 2006). The remaining sample was subjected for proteomic analysis by Multidimensional Protein Identification Technology (MudPIT) as previously described (Florens and Washburn, 2006). The protein abundance was evaluated by calculating Normalized Spectral Abundance Factor (NSAF) metrics:

$$NSAF = \frac{u.spectra}{length\ of\ protein}\ of\ X \Big/ sum\left(\frac{u.spectra}{length\ of\ protein}\right) of\ all\ non\ redundant\ proteins$$

Cloning

Primers with overhangs (CATTACCATCCCG in forward and CCAATTCTACCCG in reverse primer) homologous to pPR-T4P vector (J. Rink) were used for PCR amplification from a cDNA library generated with SuperScriptIII (18080051, Life Technologies). PCR products were treated with T4 polymerase (M0203, New England BioLabs), mixed with linearized vector (digested with SmaI and treated with T4 polymerase) and incubated for 10 min at room temperature. Constructs were transformed into *Escherichia coli* strain DH5alpha, clones were selected by colony PCR and verified by sequencing. Primers used for cloning are described in Table 5.

In situ hybridization

Antisense riboprobes were synthesized and colorimetric or fluorescent *in situ* hybridization was performed as previously described (King and Newmark, 2013; Pearson et al., 2009). The published in situ hybridization protocols were optimized for epidermal expression pattern detection: fixation time increased to 1hr at room temperature, no DTT reduction step was performed, animals were bleached (5% formamide, 0.5X SSC, and 1.2% H_2O_2) for no longer than 1.5hr and extended colorimetric signal development times (up to 8hr at room temperature and overnight at 4°C) were used. NBT/BCIP developed whole-mount in situ specimens were mounted in mounting media containing 80% glycerol. Fluorescent whole-mount in situ specimens were mounted in modified ScaleA2 containing 20% glycerol, 2.5% DABCO and 4 M urea (Hama et al., 2011).

RNAi

RNAi feedings were performed as described previously (Gurley et al., 2008) with the following modifications: soft-serve RNAi food for all genes was prepared 4 times more concentrated. Animals were fed 8-12 times every 4 days prior to amputation. For all RNAi experiments, animals were cut 4-5 days after the last feeding.

Immunostaining

Animals were fixed as previously described (Pearson et al., 2009) rehydrated, blocked with 5% horse serum in PBS 0.5% Triton X and incubated with primary antibody overnight at 4°C. Primary antibodies used in this study: pERK (1:400; 4370 Cell Signaling Technologies), Ezrin (1:400; CPTC-Ezrin-1, DSHB), acetylated tubulin (1:1000; T7451, Sigma). The next day, samples were five times 15 min washed with PBS 0.5% Triton X and incubated with alexa-conjugated secondary antibodies (1:1000; Abcam) for 2 hours at room temperature, five times 15 min washed with PBS 0.5% Triton X, and mounted in Aqua-Poly/mount (18606, Polysciences).

Microscopy

Colorimetric in situ images were captured on Zeiss Lumar stereoscopes. Confocal and live images were captured on a Zeiss LSM510-PRO, LSM700 Falcon, LSM 780 inverted microscopes with a 10x 0.45 Plan-Apochromat, 20x 0.8 Plan-Apochromat or 40x

1.1 LD C-Apochromat objectives (all Zeiss). Image processing was done by FIJI (Schneider et al., 2012), Zen (Zeiss) or Imaris (Bitplane) software.

Tissue ablation experiments were performed on LSM510-PRO microscope (Zeiss) equipped with C-Apochromat 40x/1.20 W objective (Zeiss) and tunable two photon laser (Chamelion, Coherent) set at 720 μm (1.125mW).

Western blot analysis

Animal tissue was snap frozen in liquid nitrogen and subsequently lysed by incubating in loading buffer (50 mM TrisHCl pH6.8, 2% SDS, 6% Glycerol, 0.1M DTT, 0.004% bromophenol blue, 1x cOmplete protease inhibitor Cocktail (0589279100, Roche) and 1x phosphatase inhibitor Phosstop (4906845001, Roche)) for 10min at 90°C. Tissue lysates were subjected to western blot analysis as previously described (Liu et al., 2014). The following primary antibodies were used: pERK (1:1000; 4370 Cell Signaling Technologies), Hsp60 (1:1000; 12165, Cell Signaling Technologies) and alpha-tubulin (1:10000; T5168, Sigma). Primary antibodies were either detected by HRP conjugated antibodies and signal developed with ECL Prime Western Blotting Detection Reagent (RPN2232, Amersham) or fluorophore conjugated antibodies (1:1000; Rockland Immunochemicals) and imaged on an Odyssey imager (Li-Cor).

Pharmacology

Animals (8mm) were exposed to 5 μM trametinib, selumetinib, vemurafenib (all BioMed Valley Discoveries) or U0126 (1144, Tocris) for 1hr at room temperature, cut into 5 fragments and subjected for western blot analysis 30 minutes after injury.

Table 6. Primers of the gene sequences used in this thesis

id	*forward primer*	*reverse primer*
SMED30000732	GGCCTTAGTGATAACTGCTG	TCTCTGCCCATTCAACATAC
SMED30001032	CTCGAACCTTAATGATCTGC	GGCTTCACTCGAAGACATAG
SMED30001049	CTTATCGAAAACCGCTCTC	AGGCATATGGGTGTATTCTG
SMED30001115	CGGCTACGCTGTAAAAATAG	TGTAGTTGCAGACATTGGAG
SMED30001248	ATCACCTGACCGATAGAATG	GGACAAAACTGGAGTGAGAC
SMED30002304	TCTCTGGAAAACTGTGAAGC	TTTGGTACTTGGAGTTCCTG
SMED30002382	CTGTTTGGTCTGATGACCTC	CATTAGATCCAGGTAGTCCG
SMED30003537	ACGGATAACCTACCATTGTG	CTCCTATAATGGTTTCGACG
SMED30003685	TAAATGCCATCCAGTAGAGC	TTCTTCTGTCTAGTCCCTCG
SMED30003823	AATTACGGGACAGTAACGTG	GTCTTTCAGCTGATTAACCG
SMED30003953	ATCAAGCTCCATCAAGAACC	TAAGTGTGCGAATACAGACG
SMED30005904	CAGGAGAGGAAATCACTTTG	TGGATGAGATCATCGTGTAG
SMED30006006	GGAACGTAAAGTTGGACTTG	CGTTGGATCTTTCAGCATC
SMED30006193	ATTAGCTGTGCTGTTTGACC	CGCAATTCCAGAGACTTATC
SMED30006335	AAACTCAACTCTTGCAGCTC	GTACTTCCCTCCCATAAACC
SMED30006857	CCAGAGACTCCAATTTTGAC	TATGATTCTGGAGGTTCCTG
SMED30007095	GATCAAGTTAGATGGCAAGC	ACGTTCTGATCTGGTATTGG
SMED30007302	TATACCATGGAGAAGGGATG	GTGGTGAACTTTCGTAGGTC
SMED30008678	CATTCGGGTTCTCGTTATAG	GATGACGTACAAAAAGGAGG
SMED30008700	GATGTGCAAATGATAGTCCC	GTAGCCGATTTCGTTCTTAC
SMED30009081	GTTCAGCTATATTCAACGGG	CATTCTCTTTGTCTCTTCGG
SMED30009121	ATACGAGGAATAATGAGCGG	CAACGTCTCCCTTTGATTTC
SMED30009166	GCAATGAAAACACTACCGAG	GTTTAACTGCCAATCTCCAG
SMED30009277	GAATTGCAGTCCAAAGTAGC	TGAGTATCCTGGTCCATTTC
SMED30009865	AAGCAACTAAGGGCGTATG	AGTCAAGAGCTTTGGCTTG
SMED30010702	AGTGAATACATTACAGCCGC	CTCTACTTCCGATAACACGG
SMED30011027	TGGAAGAGCTAGAAGAATGG	ATCCAAAAGACCCTCTGTG
SMED30011096	AGATAAACTTAGCCCCAACC	TATCCCATAGGCCAATACAC
SMED30011449	CTTATCGAAAACCGCTCTC	AGGCATATGGGTGTATTCTG
SMED30012759	CAAATGTGTTAGCACGTCAC	GACCAAACTTGACTTTCTGC
SMED30012836	GCAATACGAATCGGAGATAG	GTGCTTTCTGGAGTTGTAGC
SMED30013041	ACTGCTCAGTTCTTTAACGC	GATTGCGTCGTAACTTCTTC
SMED30013197	AACCACTAGTCGAAATTCCC	TAACCGAGTCTTTCTGTTGG
SMED30013615	CGAGGAGTCAGAAAATTGAC	ACCGTACATCACCATCTTTC
SMED30013884	TAATGGTTCCTCAGAGAAGG	TCTTTAGATGATGCTGACCC
SMED30014140	AACTTATCCAGGAGGAAAGG	TCTGGGGTTGAGTGTATCTC
SMED30014221	CCAAAATCCGTTCTTGC	AATCTACAGGATTGTTCCCC
SMED30014416	AGCGAAATCTTGAAGCG	CCTGTCTGACATGATACTTCC
SMED30014642	TAGCGGGTCAAAGGTTAAAG	TCTCCTGGTGGTATCATTTC
SMED30015574	GACTGGATAATCCTGCAAAG	CAGTAGGGTTTCTGTTAGCG
SMED30015584	CGGAAAGTCTTGGAGTAGTG	GCTAAGTTTGACGTGGTTTC
SMED30016052	GAAAAAGTCCACTGGATGAG	ACTGCCAGGTGAAATAAGG
SMED30016082	GATTATCGACGACTCAATGC	TAACCATCCCTTCTCTATGG
SMED30016189	GTATCCCCAATTCCTAAACC	AGGTTTTCCTCGACAAAGTC

SMED30016661	CTTGGAAGTTAGCAGTGACC	TACTAGCTGCTCGATCTTCC
SMED30016674	AACTGATTGGACAGAGTTGC	TTCTGTTTCCATGGTAGAGG
SMED30016720	GGATTTACGAAGTGAGATCG	TCACATCTATTGTCACTGGG
SMED30017525	GCAGGAGAACTACCAGTCAC	CTATCTGCTCCCACATTTTC
SMED30017790	CAACCTAAATATGGGTCAGC	CGCAAACAATGTCTAGTGAC
SMED30018550	CAGGGACTGATGAAAAACTC	CTTGGACAGTATCGAAGCTC
SMED30018972	TTCCGATGATGAAGAGAGTC	CCAACCAATACTTTACCGAG
SMED30019258	GAAGCCACTTTTATACAGCG	GACAAAGGTTTCTCAGTTGG
SMED30019819	AACCTCTCATCATTCCACAG	AATCGATCTGTCACTTGGAG
SMED30019979	TGAGAGAATCAACGAGGAAC	GACTAACTTCGTCGTATCGG
SMED30020349	GAGATTTTATGGGGCCTAAC	ATAACAAGCCAGACTATCGG
SMED30020899	TCAAGTTAACGGAAGCTGAC	CATCTCTTCCTCTCTGAACG
SMED30021002	GGTGGCACACATCTACCTAC	GGATCGACATTCTATATGCC
SMED30021695	TTTACCTGCTCAAGAGCTTC	TGGATTCTCTCTAAAGCGTC
SMED30021715	GCACCATCTATCGTCCTAAC	CTTGTCTTCTTGGTGCTTTC
SMED30022144	GAATCGAAAGTACCGCATAC	GGACTCTATACGCAATGTCC
SMED30022307	AGTCTGGGAAATTAGAACCC	ATGCTGCTTCCAGAGTATTG
SMED30022317	CACACACACACATACACACG	CAACGAATACTGGAGAAACC
SMED30024800	AAGTTGTTGTGTCCCTCTTG	CTGTGCATAACCCTGTATCC
SMED30026604	GGAGAGTGCGAGAGTGATAC	CGTCGGGAATAACTGACTAC
SMED30027315	GTTCGGTATAGTCGTTTTCG	CTCACACTCAACTTAAGCCC
SMED30027324	ATCTTGCTGCATTGACAGAC	TTACCCTATGACGCGTAAAC
SMED30027376	CTGTCGAAATCCAATCTAGC	GAAGAGATACGTGAAGCAGC
SMED30028012	AACGCAATTGGAAGGTC	TGGCAGATTTGATGTCG
SMED30028153	AGTTATCAGGAGATTGAGCG	GTATCCCGTTTTGTTACTGC
SMED30028290	GCATTAGTCAGAAATACGGG	GAAAATACTCGCTTACTCGC
SMED30028456	GCTTCAATGCACCAATG	GATTGTGAAGACTGCTGTTG
SMED30028816	AAGCAGCCAATCAGAAGTC	ATTTGACGCTCGACTATCAC
SMED30028872	GGTACTGATGAAGAAGTCGG	ATTCTGGCATGAGATCTGTC
SMED30029112	ACAGGTTTTTGACAGGTGAC	ATAGGTCGACTTTGCTGAAG
SMED30029281	TGCATGTCAGAACTCAGAAC	TACACCAACACGACTGAGAC
SMED30029358	CTCCAATATTAAGGTTCGCC	CTCGATGGACAGAATATCAC
SMED30029492	GCTACGGTTAGTCGATTGAG	AACCCTGGACGTTGTATATG
SMED30029820	GTCAAGGGAACAGATAATGC	AGACCTACACACTGGACAGC
SMED30029909	TGAACGGGTACAACTCTCTC	GGGTTATGTGTTTGACGTTC
SMED30030319	ACAGTAAATGGTCATCCGAG	CGTTCAGCCTCTTCTCTAAG
SMED30031165	AAAAGCCCTACGAAGATACC	AACAACTCTGCATAACCCAC
SMED30031605	GGCTCTGTGTGGTATATTCTG	TAGTTGCCTTCTTCGCTATC
SMED30031722	TTCCGATGATGAAGAGAGTC	CCAACCAATACTTTACCGAG
SMED30031927	CTCCTATCACTGGCAAAGAC	GTTGTCCATAATCGTCATCC
SMED30032103	CATTAAGTATTCCACCTGGG	TACGACTTAGCCCCAGTTAC
SMED30032156	GTTGGGCAACTTACGAGTAG	CATGAGCCTATAAACCAACC
SMED30032832	GGCGAGAAAAGACTTATGTG	CTTCCAGATCTCTTGCATTC
SMED30032906	GAATGGTAGTTCTAGTGCGG	GGAAATCTTTGTCAGTGGAG
SMED30033093	GAGGATCTGATTGAAGAAGC	ATCTTGGATGACCGACTTG
SMED30033411	AATCAGGTGAGATCACAAGG	ATGGTGAGACTGTTCTTTGG
SMED30033423	GCAGTTGGTTCTTTTCTGAG	ATGCCTTCTGATTCAGTCAC
SMED30033689	GGGATCTCCTATTAACACCG	CCTTCTCACTGAATTTGGAC

SMED30033718	GAGTCACTTTTAATCGCTCC	GCTTTTTCAGCTTCTACGAG
SMED30034130	GAGACTCATCTTGAAGCAGG	GTAGTATCGGTGAAGATGCC
SMED30034249	TTGTCAGTACAAACCTGACG	GCTTGACACTCTCCTTTGAC
SMED30035617	TCCATTATTACCACTCCAGG	GAGCAACTTGGTTCGATTAC
SMED30000740	ACTCAATGACCAAGATACCG	TTTCAAGGTCCGTACATAGC
SMED30002243	CAATAACTTGAGAGCGGAAC	TCTCATCTAATCATCTCCGC
SMED30003118	CCAGCTCTAAATCGAAACC	GCAAATCTTCGCTAGCATTG
SMED30003738	GTCGCGTTTGTTTTACTAGC	GCTCATTGAATCTCTGTTCC
SMED30004065	ACTGCCATCAATTTACCGTC	GATCGTTGGTAGTGAAGAGG
SMED30004092	CTTTGTCGGTTATGGAAAGC	GTTCGATTGGTAGAGTGAGTG
SMED30005143	CATCTTAGCGATTCTCATGG	ACCCTTCCACACATATAAGC
SMED30005191	CACAAAGACAACAACAGCAG	TCTAACTAGCAAATGGGCTG
SMED30005345	TTGGAGGTCCGAATATAGAC	CTAGATCAGCTTTGGGTTTC
SMED30005462	TCTTCGACGTTACATTGCTC	CAATCTTTCGACTTGAGAGG
SMED30006268	GACAGTGGATTTCACGATTC	ATTCAGACTCGTTGTTCCAG
SMED30008239	GATGATCAGAGCTAATTGCC	CAATCAGTATAGCAGCCACC
SMED30008241	GGCTCTAGAAGCATCAAATG	CAGTTTCGATGACACTTTCC
SMED30008761	CTTGGTTTAAAGAGGCACAC	ATCCGACACTGAGACTATGG
SMED30008810	TGATTCTGACTTTAGCTGGG	ATTGCTAGACTGAGATTCGG
SMED30009007	TGAGATCCATGACGAACATC	AAAGAGCCCTCTATCGATTC
SMED30009121	TCAATCTACATGGATCTGCC	CAACGTCTCCCTTTGATTTC
SMED30009793	CTTAATTACGGTTCCAGACG	CTTTATCGGACAGAGACTCG
SMED30010180	CACAGCACAATCAACAACTC	CAATAGACCGATTGAAGAGG
SMED30011521	GCCCATTATCAGTTGATGTC	AAAACGACTACCACAACGAC
SMED30011842	TACGATGTCTGTGTTAACGG	CAAGTATTTCCTTCTGCGTG
SMED30012985	GAAAGTCAAGGTGACGAAAG	CATGTCAGATTCTTCTTCGG
SMED30013747	CGTAAATAAAGAGGTGGAGG	GATAAACTTTCTTGGGAGCC
SMED30014567	GAATTGTTACCAGAAGTCCG	GAAACATTAAGAGTGCGACC
SMED30014642	TAGCGGGTCAAAGGTTAAAG	GGTTTAGGCTTTGGTTGTG
SMED30015382	TGGCTTCACTGATTAGCAAC	GATCAAGGCCATTGGG
SMED30015978	TCTTCTAACCGACCCTACAC	TTTCCAGAGCTAGGAATGTG
SMED30016305	TTTAGATAGCAAGGGGGAAC	GATGACAATGAGGCTGTTG
SMED30017389	AACAGTGACATTCCTTCGAC	GTTACGGAAACAAACAGCTC
SMED30018339	TCAGTATTGGGATAGAAGGC	GAATGAGCAATCTTCTCGAC
SMED30018487	ATTCTACAATGCTGTCCACC	ATGATGAGGTTACTGGGTTG
SMED30018615	TTACAGGGATAACATCAGGC	GTCTTTCATAAACTGTCCCG
SMED30019025	CTAATAAGACGGTGGTCTCG	GCTGATGCCTCTTCTAACAC
SMED30020559	CAACACTTGGTCTCCAAATC	AGCACTCTGAAGGATACAGC
SMED30020862	AAAACCCCTATAGAGTTGGC	GTATCCTGGAGATTTTCGG
SMED30021277	CACTGAAAACGGTTCAAAGG	ATCTTGTGCATCTCGTCAAC
SMED30021613	AAGTTGGTGTGATGGAAGAG	CCGAACAATGAGGAGTTAAG
SMED30022344	AGATTACCGCACAAGATGTC	CGTTTGTCGACTTTCTTCTC
SMED30022370	TTAGCTATTTCGCCTCTGTC	GAAGGCAATAATGTCTCTGC
SMED30024211	CCACTCGAGAGTAGAACTGG	TCTAACATCAAGGGTTGGTC
SMED30025393	AGTACACGGTCCATTTCAAC	GGCCAAGATAGAACACAGAC
SMED30027074	CGAGCTTGAGTCAGAAAAAC	TCATTTACTCCACCCTGTTC
SMED30027368	ACTGGATTAGTGCCATTCAC	CTTCTCACGAATACCCTTTG
SMED30028069	GGTGCAAAGACAAACATACC	GGCTTATCGACTTTCCTTTC

SMED30028306	CTAGGATAAAAAGCACAGCG	CGTAAGGCGACTACTAAATG
SMED30029112	ACAGGTTTTTGACAGGTGAC	GTCTGACAGGAAATCTGAGC
SMED30030336	GTGGTGATCTACTTGATTCG	ATGACAACAAACCTGACTCC
SMED30030586	GTCGGTAGATTTGAGAATGG	CGACATAAAGAGGTAATGGG
SMED30030663	GATCTGATCGATGAAGCAAC	CATTATGCATCCTGACTGAC
SMED30031335	TCACGGGGGTAAATATACAG	GACTGGCTTTAATTGCCTC
SMED30031426	CAGAAAGCATGACCCTATTG	CATTCAGCGGTTACCTTTAG
SMED30031822	AACTCCAGTTCCAATGTCAG	GATTTCTACTGCTGTGGCTC
SMED30031828	TTGCATCGCAGCAAAC	AAAACTCTCCTTGTGAGTCG
SMED30032382	CTTCACTTATTCACTTCGGC	GTTTGATAGCAGGAACTTGG
SMED30032538	ATCGGTGGTGAAAGAGTTC	GTAACCAACGGTGTTTTCTC
SMED30033093	CGGGGTTCAATGTGAAGTAG	ATCTTGGATGACCGACTTG
SMED30033303	GTTGGCCTATACGATGTCTC	GACAAAGCAATAGTTCCTGG
SMED30033351	AACCAATCTCAGTTGAGTGC	GAGTACAAAAGATCCGACTG
SMED30033411	TCTCCAGTCCTACAACAACC	GAGACTGTTCTTTGGTTTGG
SMED30010749	TATTTACCACCGGTTGACTC	ATGAAGTGCTTCCTGAAGAG
SMED30020061	GAATTGAATACACCCGAGG	ATAGATTCATCACCCGTCAG
SMED30025100	GACTCAAGTCGATGAGAAGC	CCACGGGACATATGTTTATC
SMED30031794	GATGAAGAAAGCATACGAGC	GTGGCATAGGATTGAAGTTG
SMED30015014	GTACTTCAAAAGTGGGAACG	CTTCTGATGGGTCATTGTG
SMED30035226	CTCAGATCAGGGATTTTCTG	GATTGAGAATGATCTGGTGG
SMED30011754	AGAAACTCCATCGACTCCTC	GTGACAGGGAATCAAAACTC
SMED30032631	GTCTGCACTTGCACAATTAG	AATATGACTACGGATGTGGG
SMED30034228	TGTACGAGATGGAAACGAAG	CTTTCTCTTTCTATCCGGC
SMED30003887	GAAGAACCAGAAAAGCCAAG	ACCATTCAATTCCTGGG
SMED30034505	TTACACGTGTGCCTTGTTAG	CCAACTAAGTTTTCGTCCAG
SMED30023819	CTTCGGAACAACTGAAACTC	CACTTTATTCTATGGAGGCG
SMED30031862	TTAGCTTTAGGGGACAGTTC	CCTTTTTAGAGTGCTTACGG
SMED30018383	CTGAAACAAGTACAGAACGG	CAGTAAACGGAGGGTAAATG
SMED30013338	ACACAGAAGCAGCCTTAGAC	GATTTAACTGAGCGACAACC
SMED30030245	ATTGCTGGCAGTAGAGAATG	GCTGTCCTTCTCGATTATTG
SMED30029873	GCCATGTGTAGGGAAAATAG	GAAGATTGCTGTCGTCATAG
SMED30018122	AAAGAGCTAGCACGTTTGAC	GAATTCCCAGGAAATCTAGG
SMED30028898	GGCACAAAGTAGACTATCCG	CAAAAGGTAAGCCAAAGTCC
SMED30017865	TCGAACGGGATCATAGATAG	GAGGTTCAACTTTCACTTCG
SMED30009482	GCGTCAGGAGTTATTTGAAC	AGGGTGTCACTGAAATATGG
SMED30014937	ATCGCCTAATTCAGACAGTG	CTTTCCAGTTTCTTAGGTGC
SMED30014407	CAGGACGAGAATGAAAACTC	TACACACATGCATATCACCC
SMED30026337	CGAAATACTACCGAAACCTG	CCTTTCAAACTCCTTCAGTG
SMED30020022	TAACCATGGAATTGGGC	CCCTCTAGCAAAATTCTCG
SMED30006656	TATGACTTGTGTGGACCTTG	TCTAGGAAACAAGCCGATAG
SMED30000458	GTGAGACATGCAAACAGTTG	GACTTCGGCATTGTAGTTTC
SMED30009973	AGAGTTGAGCAACGTCATTC	AACACAGGATCCAGTAGCAG
SMED30003975	GGAGAACCTAAAGACTTAGCC	ACTGCTTCTTCGTCAGAAAG
SMED30029509	TAGAACCGGGAATGTAGATG	TCTCCGAATCATTACCTCTG
SMED30001601	ATTCGATACGACCTCAACAG	GAAATTGGCACTACAGAAGG
SMED30011885	CTTGCTGATTTACCATCTCC	TTCTACAGTTTTCCACGCTC
SMED30033237	TCAGTTGTGTTACCGAGTTG	AGATCCATGTGAATACTGGC

SMED30032477	AGTATGAGCAAGGTAAAGCG	GGAACTGTTGAAGTAATGCC
SMED30027170	CTCAAGAGTGGCAATTTCTC	TCAATCACCTCTTGGATAGG
SMED30019046	CACCGGATATAGAAAACAGC	ATATTGTGAGCCTTGGTCAG
SMED30024319	AAGATGACAGGGAATGGTG	ACGTTGGACACCAAAACTAC
SMED30020689	TAACAACTACGGCACACTTG	CTTCTTTTTCTGTTCTCCCC
SMED30021824	GCCAAACAAGAAAGACAGAC	ACTGTTTTCGATGTACCGTC
SMED30000740	ACTCAATGACCAAGATACCG	TTTCAAGGTCCGTACATAGC
SMED30023406	GACAGTGGTAAGCAAAGAGC	ATCTACGAACTCCACACTCG
SMED30002934	GCTCAATCAGGCTAATCATC	CAATAGATTCATCTAGGCGG
SMED30032675	GAAGTCGTTAGTACGGATGG	ATTGACTTGTGGAACTGGAG
SMED30015704	AATCAACTGCTACCTTCGTC	AAGGCTCCATATCTTCAAGG
SMED30031744	CGCGATGTCAGTTCTAAAG	CGCCTCTACATGCATTTTAC
SMED30019262	TTCTCAATGGAGTCATCCTC	GATTCGGTTCAAGATCAGAC
SMED30005904	CAGGAGAGGAAATCACTTTG	TGCTGTAGCGATGTATTGAG
SMED30004376	GCATATCACTTGCTCTGTCG	CAATATCGTTCAGATCCACC
SMED30035662	CGACTGTTTCCCTGTTTAAG	TGTGGTAGTCCTCCTCAATC
SMED30016301	ATCCAGTTTGGACTCTGATG	CTATTCCAGTTTCTTGGTCG
SMED30013043	GTATCATACGAATCGTTGGC	CTTTGGCATAGAAACTGCTC
SMED30013608	ATTCGAAGTCTGGATATGGG	CGTCTTCTATCACCACTTCTG
SMED30005237	GAGTTGGCCGATATTAACAG	GAGTACAGTTCTGAGCCGAC
SMED30004840	AGTCATTAGATCCGGTTGTG	CGATCATAGCACATTCACAG
SMED30025473	CCTGGAAGGATCAGAATTG	TGACACTATTTTCTGGTCCC
SMED30027645	GGGTTAATAGCAGCACAAAC	TGATACAGCACGTTGAGAAC
SMED30025205	TGGATTCCACAGGAGTTTAC	CTGAAGGGCTTGTATTATGG
SMED30035805	CTGACATTGTTGACAAGGAG	TACTCACCGGATTATCTTGG
SMED30002579	GATTGGGAAGACTTAAGCG	GTGCGCTGTTTCTTCATATC
SMED30015041	GACGGGTACTCAGTTCTTTG	CAATAGCCGAAAAGGTACAC
SMED30013810	GAACAATACCGAAACTCGTC	GAAGTGTTAGCAGTCGTTCC
SMED30030229	TCAATGACGACTGTTACTCG	GTAGTCAGACCTAAGCACCG
SMED30029242	TGTAACGCTTGTCAAGTCAG	AATCGACGAGGATATGTCAC
SMED30015354	CTCAACGTTAAGACCTCTGG	AGCTGATAATTTAGGGAGGC
SMED30021262	GACCGAAGAACAATTCTCAG	AGAAACACCACTTCAACCAC
SMED30011111	GCTGCAATAATAGGAACACC	TGTATATCCCCCTAGTGACG
SMED30016899	TGACTGCATGGAGTTATGC	ATTATTCCCAGCCAAGTTCG
SMED30018460	AATGCGAACAACAGAGAGAG	AATCTACCAGAATGAGCTGC
SMED30006256	GATTCGACGATCTTAACCTG	TCGCGAAGAATTGATCC
SMED30026172	TCCAATAGAGGAACTAAGCG	GTCATTAAGAATAGCCGGTG
SMED30010536	CAATCTATTGCCTCCTCATC	CAATGTTATGGGTGGGTAAG
SMED30033757	AACGCACTAGAGAGGAATTG	TCCATGATCTCTTCTCCATC
SMED30006454	AACCTGACTTATGAGCCAAC	TAATATCTCTCTCGGCTTGG
SMED30020410	CAGCAGTGATTACGTGATTG	GAACGCTTATAAGGCACTTG
SMED30028787	CTGAAGGATGATAATCGGAG	GTGAGCAAATGGAGATGG
SMED30001441	AGTCAAGCTTACTCTTTGCG	GTGCATAACAGTTCATCGTG
SMED30033789	CAGTCAGATCTTACCGCTTC	ATTGATAGATGACTGGCTGG
SMED30020090	TCCCGTAAACCACTCATATC	CTATATTGCGGTCTTTCGAC
SMED30006455	ATTGGGTGGTAGATGACAAG	AGCTAGCGAGAAACTGAATG
SMED30000184	AGTCCTTGACCGACATTTG	TTTCTCTGATCATCTGTCCC
SMED30035239	TGTCTGGGGATTATTACGAC	GTTGGAAACTTGGCTGTTAG

SMED30019431	TCATATTCCATGCCTACCTC	GGTTCTACGTCAAAAACGAC
SMED30015021	ATTGTACGAGGGTCATCTTG	AGATTTCCACAAGTGTCTGG
SMED30035968	TGGTTCCCTAATCACTCATC	TTCTGGTGAATCCTGATACC
SMED30013787	GTCACCAATCACAAGTTCAG	CGCCAATTATTCTGGTCAC
SMED30021726	ACAGGATGTGGTTACTTTGG	TCGTGCTTTACACACAACAC
SMED30008757	ACCAACATCAGCTCAAACTC	AAGAATCAGTCCACATCCAG
SMED30011204	GTGGAAAGTGAAAGAGAACG	GAATGCAATCAGAAGGTAGC
SMED30015427	GTGTGCTTTGGAGGATTTAG	CGGAGTAGAACTTGTTTTGG
SMED30003438	CTCGAATGTCTGAAAGAAGG	ATTCCGTCATAAGACTCGTG
SMED30024295	TGAATTTGACGTAGGTCCTC	ACTGTCGCACACATACACAC
SMED30007480	CTGAACGTAGAGGTCGAATC	AATTCTTCCTCGTCTTCTCC
SMED30025830	ACTACTCAAGCCGCTACAAG	ACCTCCACAATAATCTGACG
SMED30035923	AAGTGGCTTGAAACTGAGAG	CAGAATCTCTTAGACACGGG
SMED30026524	CTGGACAAGCTATGAGTCTG	ATGAGGCTCTATGGACTTCG
SMED30033971	TAACGTCATGTCTGCTCAAC	CCACCACTTTAACAGATTCC
SMED30032793	ATTTCTACCTGTGATGCCAC	CAAGAGCTTCTGTCCATTTC
SMED30008334	ACAACAGTTTCTCCAACAGC	TGGAGACTGTTACCATAGGC
SMED30020220	CTTACAACAGGCAAAACTCC	GTAACTGCCACTATTGCTCC
SMED30014565	TCTGCGAGGAGTATTCAAAC	GTGGCTTGATTCCTTGATAC
SMED30001824	AATCTGCTGGTGAAACAGAC	CATTATATAACCCGCCGATG
SMED30034824	ACATCAAGTACGACACTTCG	GACCACGACATATGATTTGC
SMED30010071	CTTGAAGCAGGGTAGAACAC	GTCTCTCGGATTGACTTCAG
SMED30026323	ACATTTGGACTAGCGAACTC	ATTCCGTTCCCTTTAGGTAG
SMED30013706	GGTTGACGGTAAAGAAAGTG	ATATTTGTCACCTCGACAGG
SMED30015660	TATCGAAGAGAATTGCGACG	CAACTTGGTGGTACCCTTC
SMED30015382	TGGCTTCACTGATTAGCAAC	GATCAAGGCCATTGGG
SMED30021874	TATGTGTTGAGCTGACAACG	ATCTCACATATGGGACCAAG
SMED30028535	AGAGTTTGCTAGCCAAGAAC	CAAGTCTTCCACGTTTATCC
SMED30017636	GGCTGTATGAGAAAATCTGC	TCCTCGTCATCTGGAATATC
SMED30032870	ACCCGTCTGTTATGGTTATC	TACCAGAACAACAAGAACCC
SMED30011669	GACGGCAACTGTATAAAAGG	GAGAGAGATGAAGTGGATGC
SMED30034787	AGGTCGAGGTGAAAAAGAAG	TGACTGCTATCGTCATTGAG
SMED30012902	GAAAACCCTTCATCAGTCAC	AATCAGTAAACGCACCAGAC
SMED30010405	ACTTATCGCTCAGGTGTACG	TGTCCTAAAGTATCCGCTTG
SMED30004590	GTGAATCACCTAGAGATGCC	GCCCTGATTTGTAGACTTTC
SMED30035101	CTGAACAAGTTGTGCTTGTG	TAAGCAACATCTTAGCGGTC
SMED30018599	CTGCTTCTGTTACGCAATG	GACATCAAATGAGCACGAG
SMED30018802	GAGCTCAGTGGACAGAATG	GATGTTGACCTCCTTTTGTG
SMED30010872	AGCCTACACAATTGATGCTC	GCTCTGGAAGTTGAAGTTTG
SMED30012786	TCAGTTCCTCCAACAGATTC	TCATCGAATAGGAAGAGAGC
SMED30022077	AGTACTCTCTCCGTTACTGTG	ACACAGACACCATAAGGCTC
SMED30008169	TGAAGGTCTGGATCTGTTTC	AACTTGTGGAGCATTCTGAC
SMED30001834	GTATAAAAGGTGAAGCCTGG	GTTACCATAGGCAGCTTGAG
SMED30013882	GATGCACATAGTGAACACAC	TTCTTTGAGAGTCAACGGAG
SMED30010581	TAGCCAGATTCCATATGAGC	CCGATATAGGCAACAATGAG
SMED30029019	GGCTACCAATGAACAACTTC	TAATTGAGTTCTCCGTCTCC
SMED30019771	CGGAAATGCTAACCATACTG	ACCACACTGTAATTTCCTGG
SMED30026612	CTCAGAAGATTCAAAGGCAC	GCTCAACCCTGTATTTCTTG

SMED30027542	TGTTATCGTCCACTGACAAG	TAACTAGCCACACCTCTTGG
SMED30024538	AATCGTAGCGTCTAGCAATG	ACAGCGAATTCAGAGTCATC
SMED30014731	GATAGCATACATCTGACGACC	CGGAGCCTTGTGATAGAG
SMED30002072	CTGGTTCTACTTACGGATCG	CTCTTCTTTGTAATGGGTCG
SMED30018173	CTCTACAACAGAAGAACGGG	TACGCAATGAACACTGG
SMED30019292	GACTAAAAGACCGTTGTTGC	TAGCAACACGTGGAATGAC
SMED30019993	TATTAGGCCAGTCATCTTGG	ATTAACTACCCCCTTCTTGC
SMED30002822	GAATCCGGGGAATTCAATAG	GCGTTACAAAGAGGACAAAC
SMED30003113	GTACATTGGATGTGTCCACC	GTAATATAACTGCCGATGCC
SMED30016902	ATCACCACTAACCAAACCAG	GACTCATCAACAGAAAACCC
SMED30023146	GTGTACAGCTCTTGCTAAAC	GCCAAAAGTCAACAACACAG
SMED30032199	TGCTCAACGACAACTGTTAC	CAGTCCTGTTGCACTTTTAG
SMED30021589	TGTAGTGGGGTAAAATGTCC	GTATTTGCCCATTGCTAGAG
SMED30031844	TAGATGGGATCAAAGGTCAG	CTCCAGATATTGCACAACAG
SMED30000749	ACTATCCCTCCTCAGCTTTC	ATCGGGAATCTCCTCTATTC
SMED30010749	TATTTACCACCGGTTGACTC	ATGAAGTGCTTCCTGAAGAG
SMED30023111	TTGGGAACAACTTGCTAGAC	TAGACTCCAATGGAACATCC
SMED30001237	TGTCAAAGGATATACCGGAG	TACGCGTGATACATGCTG
SMED30006763	TGGTTCTCTTTCTCCAACC	AGAGGAGGGAAGAATTTCAG
SMED30025100	GACTCAAGTCGATGAGAAGC	CCACGGGACATATGTTTATC
SMED30027478	CTCTTCCAAGTCCAATTGTC	GCTCATTTAGTGAAACCTCC
SMED30012229	CTCAGTTGTCCTGAATCTCC	CTTTTTCTACCGGCTGTTC
SMED30029546	CGAGTCCCAAATAATAGCAC	TGAATAGGGAGTTGGTCTTG
SMED30017762	GAAGTGCGTCGAGAAGTTAC	GTCTTTTAAACTGACCGCAG
SMED30009873	AACTGAACCTTCAAGTCACG	CTGCCAGATTCTCTCTCATC
SMED30029668	ACAGGCCTAATGTACCACAG	ACACAGAGGAAGACCATTTG
SMED30000158	AGGAAGTGATGGAGTTGATG	CTCGTTTCCAAACCTCATAC
SMED30009782	GGTCCACAATATATGCTTCC	TATGAGCAGCTAGCAGACAG
SMED30025672	CCACAAGTTCCAGATCAAAC	ACCTCCTCTTCTGGATTTTC
SMED30028223	GAACAAATACACCCCTCATC	TTCATAAGTAGCCCTTGGTG
SMED30034903	AGAGAAGCAGTTCGTAATGG	AGCTTATACGAGCATCAACC
SMED30010991	TATCGGACCTCTTTTCAGTG	AGAATTGGACGTTACAGTCG
SMED30032001	TCTTAGGGTGCTCGTACTTC	ATCATGAGAGACAGCATTCC
SMED30015955	CTTCGTGAAGAACTGGAGAG	TCTGAGGGTATACCGAATTG
SMED30026425	ATGGACACAAAGGTGGATAC	TACAGGTAAATCAGCCAAGC
SMED30019249	ATCTTTCTCCTCCTTCCATC	CCATTGGTGGGATATCAAG
SMED30024850	GATCTTGATGATGGCTGC	TCGATAGAGATTCGACTTGC
SMED30016922	AACAACAACTCCACCATCTC	ATATATGCGTCTTCCCCAC
SMED30027818	ACTGGAGCACTCCAAGAAC	TTAGTTTCCTGTGTGTGGTG
SMED30030007	GAACGAGATAGAGATGACGC	TCTCTGCCTTCTAGAGTTCG
SMED30035592	ACAGATGAGAGGACCATGAG	CAGAGCAATCATCACAACAC
SMED30000746	TGATTCAGATCGGACTTCTC	TATCGCAAGTCTTCAAGCAG
SMED30019318	AGACCGCAGAATATTGAGAC	GTGACAAAAAGTCTTCTGGC
SMED30029006	TCCTCCTGCGTATAATCAAC	TGCGTAACTCATAGAGCTTG
SMED30011512	CACGGATCAGGTAAAGCTAC	CACTGTTTTGATCAGCAGAC
SMED30019305	TTCAGTTTAGGCGTTCTCTC	GATTCGGAGACGAGTAATTG
SMED30001479	GCATGCTTAAGATTCCTCAC	GCTTTACCACCTTCATCTTG
SMED30011431	TTTTGGTAAGTCACAGACCC	GCTCCAGTAGCATAATGACC

SMED30013692	TCGATTTCTAGACGAACCG	GTAGCATCACCACTTTCCAC
SMED30033366	GCAATCTAGAGATCAAACGG	CAAACAGAGTAAGGACCAGC
SMED30025181	ATGTCGGTACCTTCAAATGC	TCGGTCCTATTATGCCATC
SMED30017802	CTTATCACACAATGGGTTGC	CTGAGCTATTCTGATTGCTG
SMED30014360	CAACCAGAATGGGTTTAGAG	ATCTGGATGGGTGACATTAG
SMED30000184	AGTCCTTGACCGACATTTG	TTTCTCTGATCATCTGTCCC
SMED30017127	ACGGTCCTATACAACAGTGG	GAACATCGTTACAAGCTTCC
SMED30012136	AGATTATCTGGGAAGCAGTG	ATAGCCCATATAGAGGGACC
SMED30013840	ACAGGCGAGTCATGATATTC	ATTGTCTTCCTGGAGTGTTG
SMED30009188	TCTACTTGAAGCGTGTGATG	CTATTTTAGCATGCTGTGCC
SMED30005253	TATATGGAACCACTCCCAAG	GAAATCGGTACGTGAAGAAG
SMED30010842	AAGAGCACACAGAGAAGCTC	GAGCCATATTCTTCCAACAG
SMED30027228	TAAGGCCTGGAAGTCATATC	AACAGGAACGGTACAGACAG
SMED30012757	CCTGTTATCAAGGCAATACC	CGCGAGTATCTAAAAGGTTC
SMED30003024	CATGTTAGCAACGAGATAGC	AGTGACTGTGTAATGGCCTG
SMED30000015	GTTAGAAAATTCCGGAGACG	CTATTCAGGTCGTTTCCTTG
SMED30000485	CAAGTTGCTCAATGACAGAG	GTTACTCGAACTGCTGAACC
SMED30000830	GCTTAGTTATCTCACCACGG	TCCATTACTCCCACTCTTTG
SMED30003125	ACCATGCAAGTATGAGTTCC	GAGATACAAAACCAGCTTGC
SMED30003389	CTCTAATGGATCCGAAACTG	CAACAAGAAATCTCGGTCAG
SMED30005935	TCAACAGAGACCTGAAATGC	CTGTCATTCAACGGCTTTAC
SMED30010650	TGAATGACACCTAGATTCCC	AGCTCGTTCAACTTTAGCAG
SMED30011553	TGTATCCCAACCGTATCTTC	TGAAGTCGACCAACTATTCC
SMED30012510	GGTTCTATTCATTCAGGCAG	GTTCCATTGTAGAGACAGGG
SMED30012845	AGTCAATGATGGCGTATCTC	TTTCTCATGGTGCTCATAGG
SMED30014114	GGAGTCAATGCCTGTCTTAG	GAAGATTCTGTTTGGAGCTG
SMED30014280	GAGCCAACAATAGAAGATGC	CTCAATAGAAGCATCGAAGG
SMED30014326	AGAGATCTTCCTATCGACCC	GCACTTGTAAGGACGGATAC
SMED30022030	CAGGAATTCATGAGTCGTTC	GAGAACATACATTGCACCG
SMED30025907	CAAATCTCTAACCAGGCAAG	CACTTATTGTTCCAAGGCTC
SMED30026019	CAGCATGAAACTGCACTAAC	TAAAAGGAAGATGACGAGGG
SMED30026745	CATCTAAAGAAGTCGTGCAG	AACACTCGGAATTCTGTGAC
SMED30028733	ATCAATCACACTTCCAGACC	ACACTCATGTCTTCGGATTC
SMED30029241	GTATGTGGAGCCAAATCTTC	ACATCATTATCCCACAGAGC
SMED30029780	CAGGAATTCATGAGTCGTTC	TTGTCTAATATGCCTGAGCC
SMED30029786	AAACCCCGGTTACTTCTATC	GACTGTGATCTGCTTGTGAG
SMED30031351	AGCAACTACAACAGCAACAG	AGTTGAAGGATGATGTGAGG
SMED30032395	TGGGTATCCATTCTTACCAC	AAGGCTGGTGTATGAAACTG
SMED30032592	CAACAGGTGTGGTCATTTC	CTCTTCGTTCTTTGTAACCG
SMED30000346	CTGATTTGGAGTCAAACGTG	ATCGGGTCCTTGTAATCTG
SMED30000786	GATCTCAAGACGCAGAAATC	TTATCTACTAATGCCGGAGG
SMED30001207	GTTGCAAAGATAGCCTTGAG	CCATTGTCACTTTTCCTAGC
SMED30001802	TTTTAGTAACCTCGCTGGG	GCTTCATGAATGACAGTCG
SMED30002761	CGTCCTAGTTTGCTTAATCG	TTGGACTTATTAGACTCGGG
SMED30003001	GTACTCGGATCAACGTATGG	TATATCCGTCGTCTGGATTC
SMED30003101	CGAATCTGTCTTTCGATCTC	CTGTCGAGAAGGTTAACTCG
SMED30008131	CCAAGCAAGAATAGATGGAC	CTCGTTGTAAATGGGTTGTC
SMED30009430	ATTCTAGCAGCTGACGAAAG	GAAAGATCACGATTGTACGC

SMED30010773	TGCCTATATTGCTCTCAGTG	CCGCAAACTTGTTAAGG
SMED30011041	GACTTTCTACGAGTCCATGC	CAATCGATGAGTCTGTTGTG
SMED30013740	CCCTTACTCCTATATTGCCC	ACTATCTGTCGATGAACACG
SMED30014356	CAATGTGGAGTGATTTGCC	AACAGCTCTTCTGCTTCTTG
SMED30015340	GTAACTTGTGCAAGGAAAGG	ACAGTCAGATACATACCGAGG
SMED30016575	ACGATTGAATCTCTCACAGG	CGTCGATGCAACACAAC
SMED30016788	TCCAATGTCCCAGTCTATTC	ATACTTCGATGGTCATGCTC
SMED30021511	GAACTTCATGGGGTTCTTG	GCACATACAGACAAATAGGG
SMED30021694	TTCTGAATGGAGTCATCCTC	TCGCACTTCACAGTTGTTAC
SMED30026965	TAAAGCTGAAGAGGATGGAG	GTCTATATTGACAATGGCCC
SMED30028789	TAGCAATGTGTCTTCTGCTG	CAGTTAGCACTGGAGCATTC
SMED30030504	GATGCAGGTTTCGTCAAC	CTGCCACATTTTTACAGACC
SMED30030829	CTACTAAGATCGAAAAGCCG	GCTCTTCTTCATTGTTGGC
SMED30032163	AAATTACTACTCGGCGACTG	GTTTTACATGGGAGTGGATG
SMED30035670	ACCTTGTAAATCAGGCTGC	CATACTGACAATTGTGTGCC
SMED30000179	TACCTGGGTTAACAGTGGAC	GGTAGATCTTCGTTGAAAGG
SMED30000821	AATGTACAGTTCTTCCGACC	TGCTGGTCACAGATTGATAG
SMED30001853	TATATGTAATGGGGTGGAGC	CAAACAGAACGACTCCAAAC
SMED30004187	GGACTATTGCTGATTGTTCC	CACATCTTGATCTGATGCC
SMED30005698	CATACGTTAACGCACATACC	GGAGACCTTGTACTCACTGG
SMED30005819	CAATCTATCTCTCGATTGCC	GTAGATCATTGCTTTCCGAG
SMED30008243	TCTAGATAAGGTGGAGGACG	CCAATCAACTCAATGCAAGG
SMED30010219	GGAAACCTGTGATTCTAACG	TCAGCAGTCAACTGAAACAC
SMED30011233	AAGAGGGATCCTCATTTGTC	GTTGGTGCTTCAGTGACTTC
SMED30011604	AATCGTGGTTAGTGCAGTTC	CAAGCTAGTAATCGGTGGTC
SMED30012149	TCGTCAGATAATGGTAACCC	GCAGATATTCGAGAGTTTGG
SMED30012996	GACATAACATGTGCCAACG	ATAATGACAGCAAGTACCCG
SMED30014180	CTTCACATTTTGCGGTG	ACGTGATCTCTTGGTGATTC
SMED30014623	GGAATTGTGAGAGTTCTTCG	ACGTATCCATGTAGACCGAC
SMED30014872	TGAGCTCTACATTTGTGTCG	CCATTCTTCCATGCATCTC
SMED30015111	CTTTCAACTGGTCTCCAAAG	GGATCGACGAGATACTTCTG
SMED30016091	TTGCTGAACCTCTATCTTCC	GATATGGGAGACAGAACGAG
SMED30020599	GTAAATGAGGCCCCAGAG	GTGATGGATTCCACATTCTC
SMED30022734	CTTCCGAAGAACACTATGC	GTACATGGGGAATCATGAAG
SMED30023146	GTGTACAGCTCTTGCTAAAC	GCCAAAAGTCAACAACACAG
SMED30025116	GTAATATGGTCCAAAGCACG	GTTGTTAACATTGGGTGGAG
SMED30026369	ATACGTTTTATCCTCCTCCG	CACTCTTTAAATCCACCAGG
SMED30031335	TCACGGGGGTAAATATACAG	GACTGGCTTTAATTGCCTC
SMED30031995	GGATTTACTGTTGGATCAGC	GCTACAGTGGAATGGAAAAG
SMED30003024	CATGTTAGCAACGAGATAGC	AGTGACTGTGTAATGGCCTG
SMED30004903	TCTAGTGGTGGATTTTCTGC	GAAGGAGATAATGTTGCGAG
SMED30007103	GTATATTTGAAGGCAGGCAG	TCAGAGATTCATCAGGTTCC
SMED30009541	TGTTGCTGTATCATCCGTAG	TCCTAGTTTGTCGAGATTGG
SMED30011041	GACTTTCTACGAGTCCATGC	CAATCGATGAGTCTGTTGTG
SMED30012874	GTTACAGACCTTATGCTGCC	GATCGTAGCGAAAATCACTC
SMED30012974	GGTTCAACGAAGTTCTATGC	TCTCAATGATTCAGGAGCAG
SMED30014403	ACACTCCTAACATTTCCACC	ATTGTGCAACACCTAGAAGC
SMED30015813	GGCTACAATGTTAGTGGCAG	TTGCAGTGAGACTTTGTACG

SMED30016795	TAAAAGCAGCCTCAGAAGAC	CCAGCAGAATGAACTCTACC
SMED30018978	CTTCAAATCAACCTCGCTAC	CTCATCGGTAAGGTTTTCTG
SMED30019535	GTGGTTATCCTCAAAACGAG	AATTATTCTCGTGGACTCCC
SMED30019657	ATTCGTGCCTTAGCTCATAG	CGTGGTTATAGCCAAAAGAC
SMED30023727	TGCATCGGGAGAGTTATG	TGTGTCTCTTGAATGCTGTG
SMED30024839	ACTCTTGCTTATGAAGTGCC	GAGTCGCCTTGTCAAGTTC
SMED30025787	CACCACAGCTACATTGACAG	GCTTGATCTATGGCATCTTC
SMED30025809	GTTGGTTATGGAACATCTGG	ACCAGTAACAGGCTCAAAAC
SMED30025886	CTAGACTTTGGCTATCGTGG	TTTGTGTTGTACCTTCCTCC
SMED30026457	GCTCATTTATTGAGACCTGC	CAGATTCCTATTCGACTTGC
SMED30027474	TAGATTGCTTCGTAACCCC	CTAGAATCTGCATTTACGCC
SMED30031875	CACCAGATTCGAAAAGTCTC	GGTCACTTAAGCGTTTTGG
SMED30032382	CTTCACTTATTCACTTCGGC	GTTTGATAGCAGGAACTTGG
SMED30034555	AAGTCCATAAATGAGCTCCC	ATACTGGTTGATGATCGGAG
SMED30035902	GCAGTTATCAGAAGCACAAG	AACATCTCAAGTAGCGACAG

Appendix 1

Epidermal marker

During this project, we routinely investigated whether any of the conserved epidermal markers could also be used to study planarian epidermis. Since the planarian transcriptome encoded several proteins with sequence similarity to vertebrate Ezrin, an ERM (Ezrin, Radixin, Moesin) family protein associated with the apical cortical cytoskeleton of a variety of epithelia tissues (Berryman et al., 1993; Bretscher et al., 2002), we sought to determine its localization in planarian tissues. Surprisingly, the staining pattern of anti-Ezrin antibody (CPTC-Ezrin-1, The Developmental Studies Hybridoma Bank) was not enriched in the apical cortex, but labeled all epidermal cell nuclei along the animal body and pharynx (Appendix 1. A, B). Occasionally we observed Ezrin-positive nuclei in sub-epidermal cells just underneath the basal membrane (Appendix 1, C), raising the possibility that this epitope expression could also mark late epidermal lineage progenitors as they undergo transition into epidermal layer. Nevertheless, the identity of a planarian epidermal-specific epitope could not be successfully determined by genetic or proteomic approaches. No reduction of this epitope was observed after RNAi knockdown of an ERM family homologs. It could also not be successfully immuno-precipitated from tissue lysates or be identified by proteomic approaches.

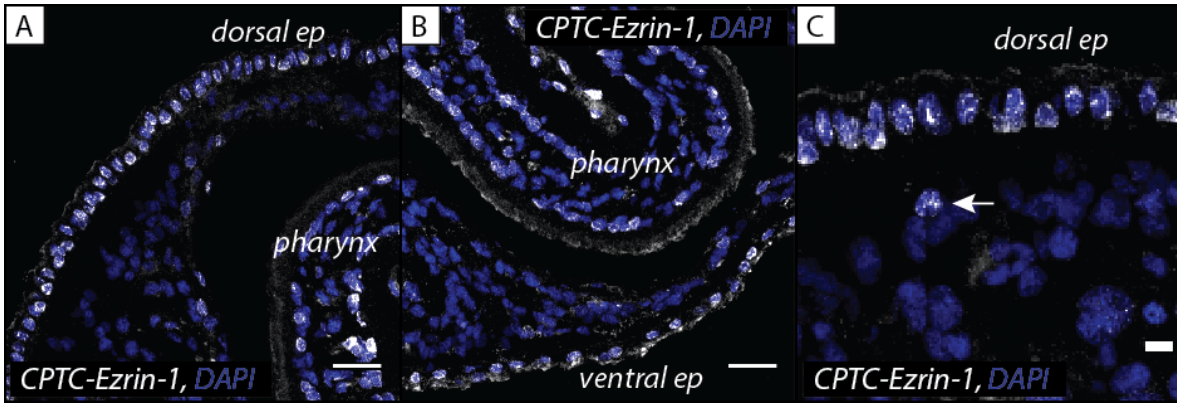

Appendix 1. CPTC-Ezrin-1 antibody specifically recognizes epidermal nuclei. Transverse section through dorsal (A and C) and ventral (B) epidermis. Occasionally the antibody also labelled sub-epidermal cells (C, arrow). Scale bar 20 µm in A and B, 5 µm in C.

Appendix 2

Post-transcriptional wound response marker

ERK signaling activation is conserved in wound response in various epithelia tissues (Cummins et al., 2003; Dieckgraefe and Weems, 1999; DuBuc et al., 2014; Li et al., 2013; Wang et al., 2009). ERK involvement in planarian epidermal wound response has not been investigated, however, it's role in mesenchymal wound response has already been suggested. Previous studies proposed that ERK activation in wound mesenchyme is responsible for blastemal cell differentiation and anterior fate specification in *D. japonica* (Tasaki et al., 2011). Some of the typical ERK pathway targets (*egr, jun, fos*) have also been found among the earliest wound response genes in *S. mediterranea* (Wenemoser et al., 2012). To investigate if this pathway is also implicated in epidermal wound response, we tested whether a commercial antibody raised against phosphorylated from of vertebrate ERK (#4370, Cell Signaling Technologies) would label the *S. mediterranea* wound epithelia or not. Unlike the previously reported ERK activation pattern in *D. japonica* (Tasaki et al., 2011), this commercial antibody specifically labeled wound epithelia (after poke and decapitation) and, in rare occasions, discrete cells patched along the intact epidermis (Appendix 2, A-D). This post-translational wound response was evident as early as 5 minutes after wound induction and it plateaued by 30min after the injury (Appendix 2, E). When the wound closure is completed at 60-90min, the signal started to gradually decrease, however this marker remained enriched in wound epithelia even 24hrs after injury (Appendix 2, C). This post-translational wound response marker was sensitive to pharmacological perturbation of the ERK pathway. Exposure to ERK inhibitors trametinib, selumetinib, vemurafenib and U0126 (but not sorafenib**)** reduced its signal, however none of these obviously perturbed wound closure. Subsequently we attempted to determine the identity of this wound marker. However, despite our efforts, a planarian epitope could not be successfully enriched by immuno-precipitation nor its identity could be successfully determined by RNAi knock-down screen of an array of MAPK-like proteins.

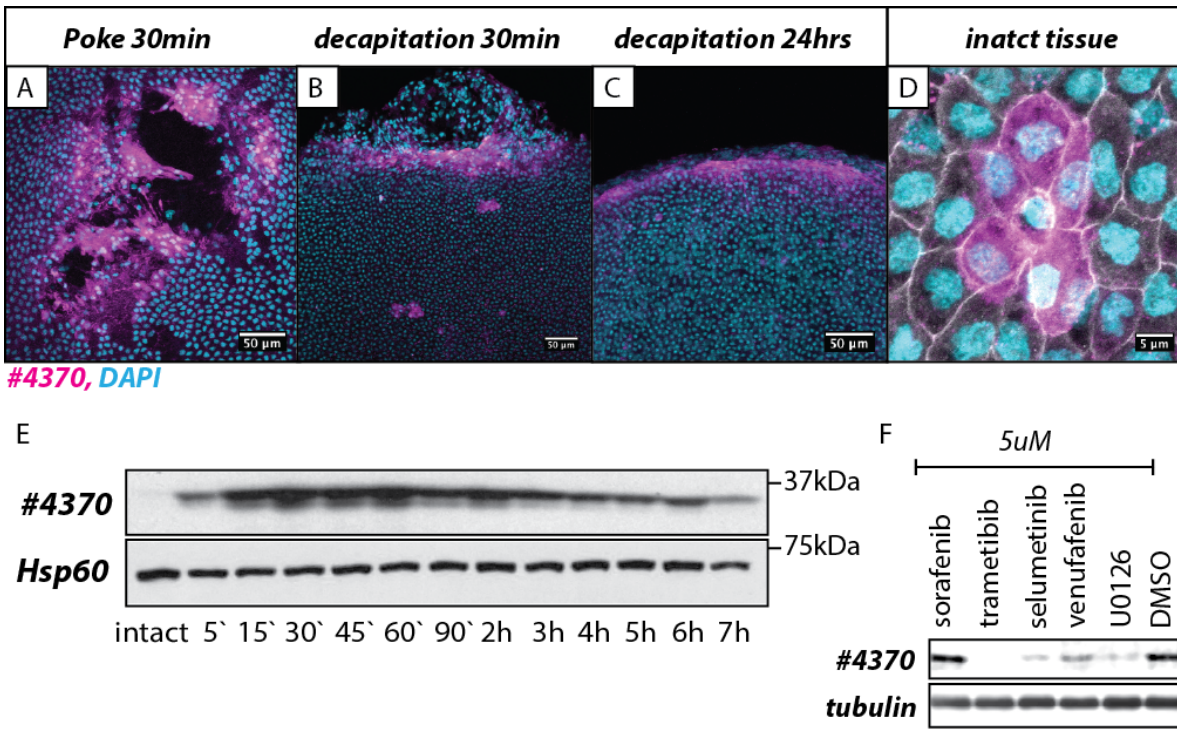

Appendix 2. Post-translational epidermal wound response marker in *S. mediterranea.* #4370 antibody labels (magenta) wound epithelia after poke (A) or (B and C) tissue loss (30min and 24hr after decapitation). (D) Occasionally it also labels cells in intact epidermis (cell boundaries labeled with Concanavalin A). (E) Time-course of post-translational wound response activation in decapitated animals. (F) Wound response marker can be reduced by ERK pathway inhibitors (30min after decapitation).

Appendix 3

Rhabdite characterization

Rhabdites, large rod-shaped intracellular vesicles, are abundant throughout the planarian epidermis, nevertheless neither their biology nor function is well understood. In *S. mediterranea*, up to eight prominent rhabdites can be found in virtually every cell of the dorsal (Appendix 3, A, B and C) and ventral epidermis (Appendix 3, D). The size of individual rhabdite can extend to almost the entire height of the cell, reaching around 10 µm in size in columnar dorsal epithelia. Although rhabdites are primarily found in epidermis, occasionally, these organelles can be also seen in sub-epidermal mesenchyme (Hori, 1978; Morita and Best, 1974; Skaer, 1961) (Appendix 3, C and D). Rhabdite presence is a marker for epidermal differentiation, these vesicles are present in the epidermal progenitors as they enter epidermal layer during intact epidermal maintenance and regeneration (Hori, 1978). During wound response, massive rhabdite content release is present along the wound edge epidermis (Appendix 3, F). Upon secretion, the bi-lipid rhabdite membrane (Appendix 3, E) fuse with the apical plasma membrane of the cell (Appendix 3, F') and the meshwork of released rhabdite content expands over the animal surface. Since rhabdite exocytosis is part of planarian wound response we sought to explore its potential role in planarian wound closure by pilot morphometric and proteomic analysis.

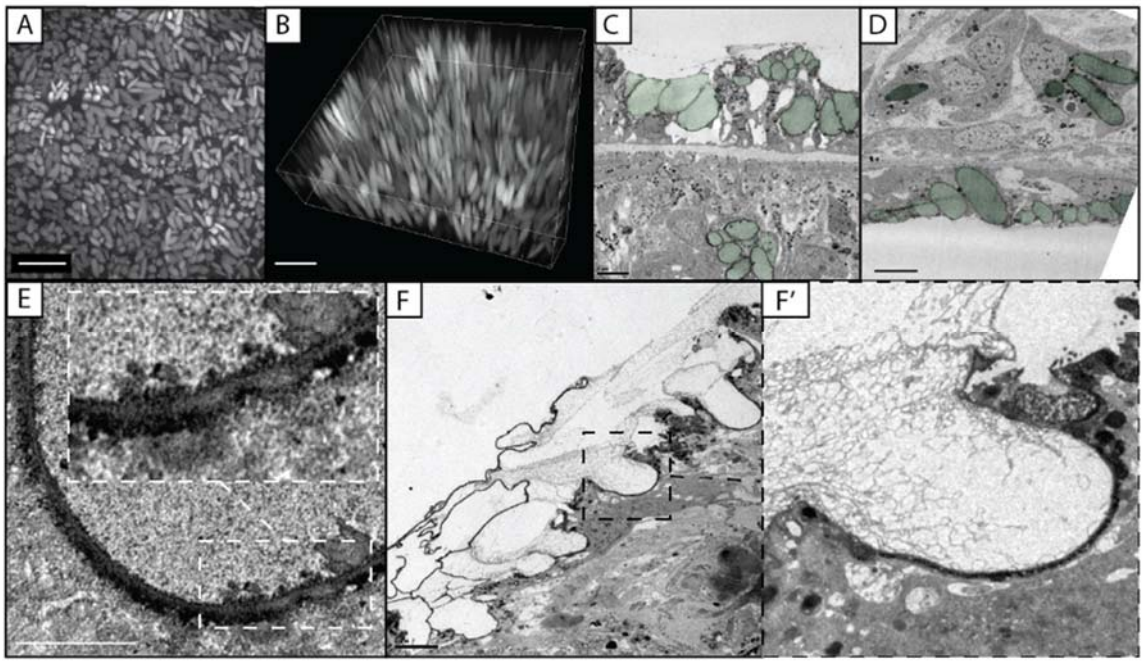

Appendix 3. Rhabdite characterization.
(A) Rhabdites are abundant throughout the *S. mediterranea* epidermis (dorsal epidermis, live tissue labeling with Cell Trace dye). (B) 3D reconstruction of labeled rhabdites (Cell Trace). (C-D) Rhabdites are occasionally seen in sub-epidermis (light green, cross-section thru dorsal and ventral tissue). (E) Rhabdites are covered by bi-lipid membrane. (F) Rhabdites material is released form wound edge epidermis, upon release rhabdite membrane fuse with apical membrane of the cell (F'). Scale bar is 20 μm in A and B, 5 μm in C-F.

To estimate the potential rhabdite exocytosis contribution to re-epithelialization we assessed whether rhabdite membrane incorporation into the epidermal plasma membrane would significantly increase the wound epithelia surface. The live labeling of epidermal cells (Cell Tracker), epidermal nuclei (Draq5) and rhabdites (Cell Trace) were used for this quantification. First, epidermal cells were labeled with Cell Tracker dye and the average basal surface (134.13um^2) as well as height of epidermal cell (20 μm) was measured. It was assumed that epidermal cells have a cylindrical shape and thus these measurements were used to calculate average epidermal cell surface (1090.03um^2). Secondly, we imaged Cell Trace labeled rhabdite compartment and to measure its surface by Imaris (Bitplane) software. The rhabdite surface area was divided by the number of nuclei (Draq5 labeling) to estimate rhabdite membrane surface per cell (1196.38 um^2). We calculated (Equation 1) that the intracellular rhabdite membrane surface was approximately equal to the average surface of an epidermal cell (rhabdite/cell surface=1.09). This observation suggests that wound edge epidermis could potentially double its surface by incorporating rhabdite membrane into its plasma membrane. Further studies are necessary to test whether

rhabdite exocytosis is a novel strategy to rapidly increase wound epithelial surface in post-mitotic epidermis.

Equation 1. Intracellular rhabdite membrane surface is roughly equal to the surface of epidermal cell.

$$Avr.rhabdite\ membrane\ surface\ within\ cell\ \left(\frac{rhabdite\ surface\ per\ area}{nuclei\ number\ per\ area}\right)$$
$$\approx Avr.cell\ surface\ (2\times avr.basal\ surafce + 2\pi\sqrt{\frac{avr.basal\ surafce}{\pi}}\times ep.height)$$

To further understand rhabdite biology and function, we performed a proteomic analysis of rhabdite content. During the development of animal immobilization methodologies, it was noted that high salt treatment (1M NaCl) elicits a massive release of rod like structures (Appendix 4, A and A'). Since the animals remained intact throughout the treatment it was reasoned that these particles (Appendix 4, B and C) were released from the epidermal tissue. Due to their obvious morphological resemblance and abundance it was reasoned that these rod-shaped structures likely represent rhabdites. These particles were then subjected to protein isolation and proteomic analysis. First, the complexity of isolated protein samples was assessed by SDS-PAGE electrophoresis and protein staining, which demonstrated that our samples were enriched with small proteins of around 12 kDa in size (Appendix 4, D). Protein isolates were then analyzed by mass-spectrometry and the most abundant proteins were identified (Table 5; unique spectra >20 and NSAF>0.01, NSAF protein abundance metrics described at Equation 2). The resulting list of detected proteins contained a few with sequence similarity to the proteomes of other organisms. These proteins included Vittellogenin, a vertebrate proto-protein which is cleaved to form smaller yolk associated proteins (Finn, 2007), proteolytic protein Neurotrypsin, a cysteine-rich secretory GLIPR1-like protein, as well as Alpha-1-macroglobulin-like protein. The remaining proteins had no obvious homologues in other species, thus their function could not be predicted. Nevertheless, some of the structural features were common among these proteins. Most of these proteins were small and/or contained predicted signal peptide sequence at their N-terminus.

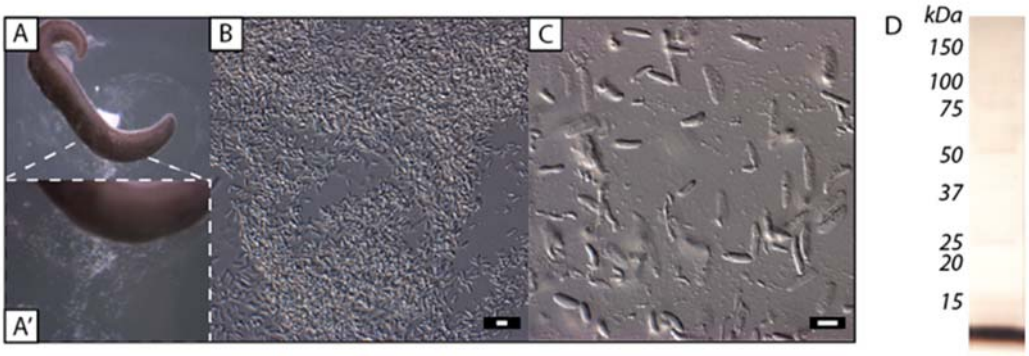

Appendix 4. Rhabdite material isolation.
(A and A') In response to high salt, rhabdites are released form epidermis. (B and C) Isolated rhabdite particles. (D) Small peptides are enriched in rhabdite particles. 10 μm scale bar.

The expression of a cohort of identified protein genes were localized by *in situ* hybridization. Identified expression pattern felt into several categories: discrete sub-epidermal expression, broad expression in mesenchyme, and gut (Appendix 5, expression patterns number corresponds to the protein abundance in the sample). Most small proteins (SmedAsxl_20140918_007295c, SmedAsxl_20140918_050218c, SmedAsxl_20140918_010747p and SmedAsxl_20140918_005256c) were expressed in discrete sub-epidermal cells and resembled the expression pattern of late epidermal lineage progenitor marker *agat* (Eisenhoffer et al., 2008; Tu et al., 2015). SmedAsxl_20140918_005955c protein transcript had broad expression pattern throughout the mesenchyme, Alpha-1-macroglobulin was expressed in neoblast marker like pattern and in the photoreceptors. SmedAsxl_20140918_004683c and SmedAsxl_20140918_030655p protein coding transcripts were expressed in the gut.

Table 7. The list of most abundant proteins in rhabdite isolate.
Unique spectra >20 and NSAF>0.01. NSAF, Normalized Spectral Abundance Factor; Spectra, spectral counts for peptides shared between protein isoforms;

	Protein ID	*homology*	*NSAF*	*Peptide*	*Spectra*	*U_ spectra*	*kDa*	*Sig.P*
1	SmedAsxl_20140918_007295c	NA	0.0872	20	125	125	18	
2	SmedAsxl_20140918_050484p	NA	0.0648	4	36	36	7	
3	SRG12_comp24533_c0_seq1_133	NA	0.0489	5	60	58	15	+
4	SmedAsxl_20140918_049708p	Vitellogenin	0.0373	191	1277	1277	420	
5	SmedAsxl_20140918_025510p	NA	0.0352	13	92	92	32	
6	SmedAsxl_20140918_019728c	Neurotrypsin	0.0336	40	363	359	132	+
7	SmedAsxl_20140918_050218c	NA	0.0300	3	39	39	16	
8	SmedAsxl_20140918_010747p	NA	0.0286	4	59	59	25	
9	SmedAsxl_20140918_015645c	NA	0.0267	6	38	38	17	
10	SmedAsxl_20140918_005955c	NA	0.0252	4	32	32	16	+
11	SmedAsxl_20140918_011102c	NA	0.0244	1	21	21	11	
12	SmedAsxl_20140918_010460c	NA	0.0241	15	180	180	92	+
13	SmedAsxl_20140918_004683c	NA	0.0238	13	94	94	49	+
14	SmedAsxl_20140918_005256c	NA	0.0213	4	26	26	15	+
15	SmedAsxl_20140918_030655p	Alpha-1-macroglobulin	0.0169	48	301	153	208	
16	SRG12_comp28634_c1_seq1_32	NA	0.0147	2	23	23	19	+
17	SmedAsxl_20140918_012403p	GLIPR1-like protein 1	0.0124	10	27	27	27	+
18	SmedAsxl_20140918_043941c	NA	0.0123	11	31	31	31	+

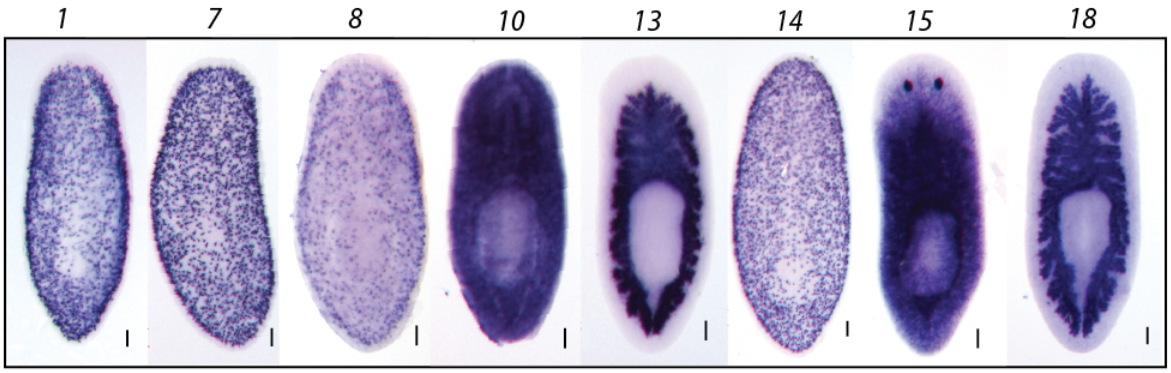

Appendix 5. Expression patters of a cohort of most abundant proteins in a rhabdite isolate. Number represents proteins abundance in the Table 5. the 100 µm scale bar.

Subsequent work is still necessary to validate rhabdite isolation and analysis protocols. Since no rhabdite markers are currently available, the validation of these protocols will require purified protein specific antibody generation. Moreover, it is likely that mass-spectrometry analysis protocols should be optimized. Although small (<12kDa) proteins are enriched in isolates (Appendix 4, D), it is not well reflected in the mass-spectrometry data (Table 6). Intriguingly, small peptides are also found in intracellular vesicles in hydra (Takaku et al., 2013) and their secretion mediates a wide range of functions including cell differentiation, axis establishment, and muscle contraction (Fujisawa and Hayakawa, 2012) Therefore, once established, rhabdite proteomic analysis methodologies will provide molecular characterization of this organelle and allow investigate whether peptides have any analogues in planaria.

References

Baek, S.H., Kwon, Y.C., Lee, H., and Choe, K.M. (2010). Rho-family small GTPases are required for cell polarization and directional sensing in Drosophila wound healing. Biochem Biophys Res Commun *394*, 488-492.

Báguna, J., Salo, E., and Auladell, C. (1989). Regeneration and pattern formation in planarians. III. Evidence that neoblasts are totipotent stem cells and the source of blastema cells. Development *107*, 77-86.

Baylis, H.A., Furuichi, T., Yoshikawa, F., Mikoshiba, K., and Sattelle, D.B. (1999). Inositol 1,4,5-trisphosphate receptors are strongly expressed in the nervous system, pharynx, intestine, gonad and excretory cell of Caenorhabditis elegans and are encoded by a single gene (itr-1). J Mol Biol *294*, 467-476.

Beck, C.W., Christen, B., Barker, D., and Slack, J.M.W. (2006). Temporal requirement for bone morphogenetic proteins in regeneration of the tail and limb of Xenopus tadpoles. Mechanisms of Development *123*, 674-688.

Bement, W.M., Mandato, C.A., and Kirsch, M.N. (1999). Wound-induced assembly and closure of an actomyosin purse string in Xenopus oocytes. Curr Biol *9*, 579-587.

Bement, W.M., Yu, H.-Y.E., Burkel, B.M., Vaughan, E.M., and Clark, A.G. (2007). Rehabilitation and the single cell. Current Opinion in Cell Biology *19*, 95-100.

Ben-Yakar, A., Chronis, N., and Lu, H. (2009). Microfluidics for the analysis of behavior, nerve regeneration, and neural cell biology in C. elegans. Current opinion in neurobiology *19*, 561-567.

Benink, H.A., and Bement, W.M. (2005). Concentric zones of active RhoA and Cdc42 around single cell wounds. J Cell Biol *168*, 429-439.

Bereiter-Hahn, J., Matoltsy, A.G., and Richards, K.S. (1984). Biology of the Integument: Invertebrates (Springer-Verlag).

Berryman, M., Franck, Z., and Bretscher, A. (1993). Ezrin is concentrated in the apical microvilli of a wide variety of epithelial cells whereas moesin is found primarily in endothelial cells. J Cell Sci *105 (Pt 4)*, 1025-1043.

Bibb, C., and Campbell, R.D. (1973). Tissue healing and septate desmosome formation in hydra. Tissue and Cell *5*, 23-35.

Bretscher, A., Edwards, K., and Fehon, R.G. (2002). ERM proteins and merlin: integrators at the cell cortex. Nat Rev Mol Cell Biol *3*, 586-599.

Bretscher, M.S. (1983). Distribution of receptors for transferrin and low density lipoprotein on the surface of giant HeLa cells. Proc Natl Acad Sci U S A *80*, 454-458.

Bretscher, M.S. (2008). Exocytosis provides the membrane for protrusion, at least in migrating fibroblasts. Nature Reviews Molecular Cell Biology *9*, 916-916.

Brockes, J.P., and Kumar, A. (2008). Comparative Aspects of Animal Regeneration. Annual Review of Cell and Developmental Biology *24*, 525-549.

Caira, J.N., and Littlewood, D.T.J. (2001). Caira: Worms, platyhelminthes - Google Scholar (Encyclopedia of biodiversity).

Carlson, B.M. (1974). Morphogenetic interactions between rotated skin cuffs and underlying stump tissues in regenerating axolotl forelimbs. Developmental Biology *39*, 263-285.

Carraway, C.A.C., and Carraway, K.L. (2007). Sequestration and segregation of receptor kinases in epithelial cells: implications for ErbB2 oncogenesis. Science's STKE : signal transduction knowledge environment *2007*, re3.

Carvalho, L., Jacinto, A., and Matova, N. (2014). The Toll/NF-kappaB signaling pathway is required for epidermal wound repair in Drosophila. Proc Natl Acad Sci U S A *111*, E5373-5382.

Cebria, F., and Newmark, P. (2005). Planarian homologs of netrin and netrin receptor are required for proper regeneration of the central nervous system and the maintenance of nervous system architecture. Development *132*, 3691-3703.

Chandebois, R. (1980a). The dynamics of wound closure and its role in the programming of planarian regeneration. II—Distalization. Development.

Chandebois, R. (1980b). The dynamics of wound closure and its role in the programming of planarian regeneration. II - Distalization. Development, Growth & Differentiation *22*, 693-704.

Chevallet, M., Luche, S., and Rabilloud, T. (2006). Silver staining of proteins in polyacrylamide gels. Nat Protoc *1*, 1852-1858.

Christou, P., McCabe, D.E., and Swain, W.F. (1988). Stable Transformation of Soybean Callus by DNA-Coated Gold Particles. Plant Physiol *87*, 671-674.

Clark, A.G., Miller, A.L., Vaughan, E., Yu, H.-Y.E., Penkert, R., and Bement, W.M. (2009). Integration of single and multicellular wound responses. Curr Biol *19*, 1389-1395.

Clark, R. (2013). The molecular and cellular biology of wound repair (Springer Science & Business Media).

Cordeiro, J.V., and Jacinto, A. (2013). The role of transcription-independent damage signals in the initiation of epithelial wound healing. Nature Reviews Molecular Cell Biology *14*, 249-262.

Cummings, S.G., and Bode, H.R. (1984). Head regeneration and polarity reversal inHydra attenuata can occur in the absence of DNA synthesis. Wilhelm Roux's archives of developmental biology *194*, 79-86.

Cummins, A.B., Palmer, C., Mossman, B.T., and Taatjes, D.J. (2003). Persistent localization of activated extracellular signal-regulated kinases (ERK1/2) is epithelial cell-specific in an inhalation model of asbestosis. Am J Pathol *162*, 713-720.

Danjo, Y., and Gipson, I.K. (1998). Actin 'purse string' filaments are anchored by E-cadherin-mediated adherens junctions at the leading edge of the epithelial wound, providing coordinated cell movement. J Cell Sci *111 (Pt 22)*, 3323-3332.

David, C.N., Ozbek, S., Adamczyk, P., Meier, S., Pauly, B., Chapman, J., Hwang, J.S., Gojobori, T., and Holstein, T.W. (2008). Evolution of complex structures: minicollagens shape the cnidarian nematocyst. Trends Genet *24*, 431-438.

Deng, M., Chen, W.L., Takatori, A., Peng, Z., Zhang, L., Mongan, M., Parthasarathy, R., Sartor, M., Miller, M., Yang, J., Su, B., Kao, W.W., and Xia, Y. (2006). A role for the mitogen-activated protein kinase kinase kinase 1 in epithelial wound healing. Mol Biol Cell *17*, 3446-3455.

Desmouliere, A., Geinoz, A., Gabbiani, F., and Gabbiani, G. (1993). Transforming growth factor-beta 1 induces alpha-smooth muscle actin expression in granulation tissue myofibroblasts and in quiescent and growing cultured fibroblasts. J Cell Biol *122*, 103-111.

Dieckgraefe, B.K., and Weems, D.M. (1999). Epithelial injury induces egr-1 and fos expression by a pathway involving protein kinase C and ERK. Am J Physiol *276*, G322-330.

Donaldson, D.J., and Dunlap, M.K. (1981). Epidermal cell migration during attempted closure of skin wounds in the adult newt: observations based on cytochalasin treatment and scanning electron microscopy. J Exp Zool *217*, 33-43.

Dovi, J.V., He, L.K., and DiPietro, L.A. (2003). Accelerated wound closure in neutrophil-depleted mice. J Leukoc Biol *73*, 448-455.

DuBuc, T.Q., Traylor-Knowles, N., and Martindale, M.Q. (2014). Initiating a regenerative response; cellular and molecular features of wound healing in the cnidarian Nematostella vectensis. BMC biology *12*, 24.

Eisenhoffer, G.T., Kang, H., and Alvarado, A.S. (2008). Molecular analysis of stem cells and their descendants during cell turnover and regeneration in the planarian Schmidtea mediterranea. Cell Stem Cell *3*, 327-339.

Endo, T., Bryant, S.V., and Gardiner, D.M. (2004). A stepwise model system for limb regeneration. Developmental Biology *270*, 135-145.

Felix, D.A., and Aboobaker, A.A. (2010). The TALE class homeobox gene Smed-prep defines the anterior compartment for head regeneration. PLoS Genet *6*, e1000915.

Finn, R.N. (2007). Vertebrate yolk complexes and the functional implications of phosvitins and other subdomains in vitellogenins. Biol Reprod *76*, 926-935.

Florens, L., and Washburn, M.P. (2006). Proteomic analysis by multidimensional protein identification technology. Methods Mol Biol *328*, 159-175.

Fujisawa, T., and Hayakawa, E. (2012). Peptide signaling in Hydra. Int J Dev Biol *56*, 543-550.

Galko, M.J., and Krasnow, M.A. (2004). Cellular and genetic analysis of wound healing in Drosophila larvae. PLoS Biology *2*, E239.

Gan, W.B., Grutzendler, J., Wong, W.T., Wong, R.O., and Lichtman, J.W. (2000). Multicolor "DiOlistic" labeling of the nervous system using lipophilic dye combinations. Neuron *27*, 219-225.

Garlick, J.A., and Taichman, L.B. (1994). Fate of human keratinocytes during reepithelialization in an organotypic culture model. Lab Invest *70*, 916-924.

Gates, J., Mahaffey, J.P., Rogers, S.L., Emerson, M., Rogers, E.M., Sottile, S.L., Van Vactor, D., Gertler, F.B., and Peifer, M. (2007). Enabled plays key roles in embryonic epithelial morphogenesis in Drosophila. Development *134*, 2027-2039.

Gavino, M.A., and Reddien, P.W. (2011). A Bmp/Admp regulatory circuit controls maintenance and regeneration of dorsal-ventral polarity in planarians. Curr Biol *21*, 294-299.

Ghannad-Rezaie, M., Wang, X., Mishra, B., Collins, C., and Chronis, N. (2012). Microfluidic chips for in vivo imaging of cellular responses to neural injury in Drosophila larvae. PLoS ONE *7*, e29869.

Gierer, A., Berking, S., Bode, H., David, C.N., Flick, K., Hansmann, G., Schaller, H., and Trenkner, E. (1972). Regeneration of hydra from reaggregated cells. Nature New Biology *239*, 98-101.

Gilbert, S.F. (2014). Developmental Biology (Sinauer).

Godell, C.M., Smyers, M.E., Eddleman, C.S., Ballinger, M.L., Fishman, H.M., and Bittner, G.D. (1997). Calpain activity promotes the sealing of severed giant axons. Proc Natl Acad Sci U S A *94*, 4751-4756.

Golson, M.L., and Kaestner, K.H. (2016). Fox transcription factors: from development to disease. Development *143*, 4558-4570.

Goss, R.J. (1956). Regenerative Inhibition Following Limb Amputation and Immediate Insertion into the Body Cavity. Anat Rec *126*, 15-27.

Grinnell, F. (1992). Wound repair, keratinocyte activation and integrin modulation. Journal of Cell Science *101 (Pt 1)*, 1-5.

Grinnell, F. (1994). Fibroblasts, myofibroblasts, and wound contraction. J Cell Biol *124*, 401-404.

Grondahl-Hansen, J., Lund, L.R., Ralfkiaer, E., Ottevanger, V., and Dano, K. (1988). Urokinase- and tissue-type plasminogen activators in keratinocytes during wound reepithelialization in vivo. J Invest Dermatol *90*, 790-795.

Guedelhoefer, O.C.t., and Sánchez Alvarado, A. (2012). Amputation induces stem cell mobilization to sites of injury during planarian regeneration. Development *139*, 3510-3520.

Gurley, K., Rink, J., and Sánchez Alvarado, A. (2008). Beta-catenin defines head versus tail identity during planarian regeneration and homeostasis. Science *319*, 323-327.

Hama, H., Kurokawa, H., Kawano, H., Ando, R., Shimogori, T., Noda, H., Fukami, K., Sakaue-Sawano, A., and Miyawaki, A. (2011). Scale: a chemical approach for fluorescence imaging and reconstruction of transparent mouse brain. Nature neuroscience *14*, 1481-1488.

Harrison, F.W.W., and Jane, A. (1991). Placozoa, Porifera, Cnidaria and Ctenophora.

Haugland, R.P., Gregory, J., Spence, M.T.Z., and Johnson, I.D. (2002). Handbook of fluorescent probes and research products (Molecular Probes).

Hershey, C.L., and Fisher, D.E. (2004). Mitf and Tfe3: members of a b-HLH-ZIP transcription factor family essential for osteoclast development and function. Bone *34*, 689-696.

Hertzano, R., Montcouquiol, M., Rashi-Elkeles, S., Elkon, R., Yücel, R., Frankel, W.N., Rechavi, G., Möröy, T., Friedman, T.B., and Kelley, M.W. (2004). Transcription profiling of inner ears from Pou4f3ddl/ddl identifies Gfi1 as a target of the Pou4f3 deafness gene. Human molecular genetics *13*, 2143-2153.

Hicklin, J., and Wolpert, L. (1973). Positional information and pattern regulation in hydra: the effect of gamma-radiation. J Embryol Exp Morphol *30*, 741-752.

Hori, I. (1978). Possible role of rhabdite-forming cells in cellular succession of the planarian epidermis. Journal of electron microscopy *27*, 611-621.

Hori, I. (1979). Regeneration of the epidermis and basement membrane of the planarian Dugesia japonica after total-body X irradiation. Radiation Research *77*, 521-533.

Hori, I. (1989). Observations on planarian epithelization after wounding. J Submicrosc Cytol Pathol *21*, 307-315.

Hulme, S.E., Shevkoplyas, S.S., Apfeld, J., Fontana, W., and Whitesides, G.M. (2007). A microfabricated array of clamps for immobilizing and imaging C. elegans. Lab on a Chip *7*, 1515-1523.

Hyman, L. (1951). The Invertebrates: Platyhelminthes and Rhynchocoela The acoelomate bilateia, Vol II.

Illingworth, C.M. (1974). Trapped fingers and amputated finger tips in children. J Pediatr Surg *9*, 853-858.

Ito, M., Liu, Y., Yang, Z., Nguyen, J., Liang, F., Morris, R.J., and Cotsarelis, G. (2005). Stem cells in the hair follicle bulge contribute to wound repair but not to homeostasis of the epidermis. Nature medicine *11*, 1351-1354.

Iype, T., Taylor, D.G., Ziesmann, S.M., Garmey, J.C., Watada, H., and Mirmira, R.G. (2004). The transcriptional repressor Nkx6.1 also functions as a deoxyribonucleic acid context-dependent transcriptional activator during pancreatic beta-cell differentiation: evidence for feedback activation of the nkx6.1 gene by Nkx6.1. Mol Endocrinol *18*, 1363-1375.

Jedd, G., and Chua, N.H. (2000). A new self-assembled peroxisomal vesicle required for efficient resealing of the plasma membrane. Nat Cell Biol *2*, 226-231.

Jendretzki, A., Wittland, J., Wilk, S., Straede, A., and Heinisch, J.J. (2011). How do I begin? Sensing extracellular stress to maintain yeast cell wall integrity. European Journal of Cell Biology *90*, 740-744.

Kato, K., Orii, H., Watanabe, K., and Agata, K. (2001). Dorsal and ventral positional cues required for the onset of planarian regeneration may reside in differentiated cells. Developmental Biology *233*, 109-121.

Kawakami, Y., Rodriguez Esteban, C., Raya, M., Kawakami, H., Martí, M., Dubova, I., and Izpisúa Belmonte, J.C. (2006). Wnt/beta-catenin signaling regulates vertebrate limb regeneration. Genes & Development *20*, 3232-3237.

King, R.S., and Newmark, P.A. (2013). In situ hybridization protocol for enhanced detection of gene expression in the planarian Schmidtea mediterranea. BMC developmental biology *13*, 1.

Kiortsis, V., Moraitou, M., Kiortsis, V., and Trampusch, H. (1965). Factors of regeneraiton in Spirographis spallanzanii.

Knust, E., and Bossinger, O. (2002). Composition and formation of intercellular junctions in epithelial cells. Science *298*, 1955-1959.

Kono, K., Saeki, Y., Yoshida, S., Tanaka, K., and Pellman, D. (2012). Proteasomal degradation resolves competition between cell polarization and cellular wound healing. Cell *150*, 151-164.

Kragl, M., Knapp, D., Nacu, E., Khattak, S., Maden, M., Epperlein, H.-H., and Tanaka, E.M. (2009). Cells keep a memory of their tissue origin during axolotl limb regeneration. Nature *460*, 60-65.

Krämer, H. (2000). The ups and downs of life in an epithelium. The Journal of cell biology *151*, F15-F18.

Krawczyk, W.S. (1971). A pattern of epidermal cell migration during wound healing. J Cell Biol *49*, 247-263.

Kumar, A., Godwin, J.W., Gates, P.B., Garza-Garcia, A.A., and Brockes, J.P. (2007). Molecular basis for the nerve dependence of limb regeneration in an adult vertebrate. Science *318*, 772-777.

Kwon, Y.C., Baek, S.H., Lee, H., and Choe, K.M. (2010). Nonmuscle myosin II localization is regulated by JNK during Drosophila larval wound healing. Biochem Biophys Res Commun *393*, 656-661.

Lacy, E.R., and Ito, S. (1984). Rapid epithelial restitution of the rat gastric mucosa after ethanol injury. Laboratory investigation; a journal of technical methods and pathology *51*, 573-583.

Langton, A.K., Herrick, S.E., and Headon, D.J. (2008). An extended epidermal response heals cutaneous wounds in the absence of a hair follicle stem cell contribution. J Invest Dermatol *128*, 1311-1318.

Lee, Y., Hami, D., De Val, S., Kagermeier-Schenk, B., Wills, A.A., Black, B.L., Weidinger, G., and Poss, K.D. (2009). Maintenance of blastemal proliferation by functionally diverse epidermis in regenerating zebrafish fins. Developmental Biology *331*, 270-280.

Lesch, C., Jo, J., Wu, Y., Fish, G.S., and Galko, M.J. (2010). A targeted UAS-RNAi screen in Drosophila larvae identifies wound closure genes regulating distinct cellular processes. Genetics *186*, 943-957.

Levin, D.E. (2011). Regulation of cell wall biogenesis in Saccharomyces cerevisiae: the cell wall integrity signaling pathway. Genetics *189*, 1145-1175.

Levy, V., Lindon, C., Zheng, Y., Harfe, B.D., and Morgan, B.A. (2007). Epidermal stem cells arise from the hair follicle after wounding. FASEB J *21*, 1358-1366.

Lewbart, G.A. (2011). Invertebrate Medicine (John Wiley & Sons).

Li, J., Zhang, S., Soto, X., Woolner, S., and Amaya, E. (2013). Erk and PI3K temporally coordinate different modes of actin-based motility during embryonic wound healing. Journal of Cell Science.

Lin, G., and Slack, J.M. (2008). Requirement for Wnt and FGF signaling in Xenopus tadpole tail regeneration. Dev Biol *316*, 323-335.

Lin, Y.C., Grigoriev, N.G., and Spencer, A.N. (2000). Wound healing in jellyfish striated muscle involves rapid switching between two modes of cell motility and a change in the source of regulatory calcium. Developmental Biology *225*, 87-100.

Liu, Z.-Q., Mahmood, T., and Yang, P.-C. (2014). Western blot: technique, theory and trouble shooting. North American journal of medical sciences *6*, 160.

Losick, V.P., Fox, D.T., and Spradling, A.C. (2013). Polyploidization and Cell Fusion Contribute to Wound Healing in the Adult Drosophila Epithelium. Current Biology *23*, 2224-2232.

Macrae, E. (1967). The fine structure of sensory receptor processes in the auricular epithelium of the planarian, Dugesia tigrina. Z Zellforsch Mikrosk Anat *82*, 479-494.

Mandato, C.A., and Bement, W.M. (2001). Contraction and polymerization cooperate to assemble and close actomyosin rings around Xenopus oocyte wounds. J Cell Biol *154*, 785-797.

Martin, G.G. (1978). A new function of rhabdites: Mucus production for ciliary gliding. Zoomorphologie *91*, 235-248.

Martin, P. (1997). Wound healing--aiming for perfect skin regeneration. Science *276*, 75-81.

Martin, P., and Parkhurst, S.M. (2004). Parallels between tissue repair and embryo morphogenesis. Development *131*, 3021-3034.

Mescher, A.L. (1976). Effects on adult newt limb regeneration of partial and complete skin flaps over the amputation surface. Journal of Experimental Zoology *195*, 117-127.

Millard, T.H., and Martin, P. (2008). Dynamic analysis of filopodial interactions during the zippering phase of Drosophila dorsal closure. Development *135*, 621-626.

Molina, M., Salo, E., and Cebria, F. (2007). The BMP pathway is essential for re-specification and maintenance of the dorsoventral axis in regenerating and intact planarians. Developmental Biology *311*, 79-94.

Moore, K.J. (1995). Insight into the microphthalmia gene. Trends in Genetics *11*, 442-448.

Morita, M., and Best, J.B. (1974). Electron microscopic studies of planarian regeneration. II. Changes in epidermis during regeneration. The Journal of Experimental Zoology *187*, 345-373.

Nacu, E., and Tanaka, E.M. (2011). Limb regeneration: a new development? Annual Review of Cell and Developmental.

Newmark, P., and Sánchez Alvarado, A. (2000). Bromodeoxyuridine specifically labels the regenerative stem cells of planarians. Developmental Biology *220*, 142-153.

Nye, H.L.D., Cameron, J.A., Chernoff, E.A.G., and Stocum, D.L. (2003). Regeneration of the urodele limb: a review. Developmental Dynamics *226*, 280-294.

O'Brien, J., and Lummis, S.C. (2004). Biolistic and diolistic transfection: using the gene gun to deliver DNA and lipophilic dyes into mammalian cells. Methods *33*, 121-125.

O'Brien, J.A., and Lummis, S.C. (2007). Diolistics: incorporating fluorescent dyes into biological samples using a gene gun. Trends Biotechnol *25*, 530-534.

O'Brien, J.A., and Lummis, S.C.R. (2006). Diolistic labeling of neuronal cultures and intact tissue using a hand-held gene gun. Nature Protocols *1*, 1517-1521.

Odland, G., and Ross, R. (1968). Human wound repair. I. Epidermal regeneration. J Cell Biol *39*, 135-151.

Orii, H., and Watanabe, K. (2007). Bone morphogenetic protein is required for dorso-ventral patterning in the planarian Dugesia japonica. Development, Growth & Differentiation *49*, 345-349.

Paladini, R.D., Takahashi, K., Bravo, N.S., and Coulombe, P.A. (1996). Onset of re-epithelialization after skin injury correlates with a reorganization of keratin filaments in wound edge keratinocytes: defining a potential role for keratin 16. J Cell Biol *132*, 381-397.

Pascolini, R., Gargiulo, A.M., Spreca, A., and Orlacchio, A. (1979). Studies on the cytochemical localization of adenylate-cyclase activity in Dugesia lugubris s.I. Experientia *35*, 1315-1317.

Pascolini, R., Lorvik, S., and Camatini, M. (1988a). Cell migration during wound healing of Dugesia lugubris sl (Fortschr Zool).

Pascolini, R., Lorvik, S., Maci, R., and Camatini, M. (1988b). Immunoelectron microscopic localization of actin in migrating cells during planarian wound healing. Tissue and Cell *20*, 157-163.

Pascolini, R., Tei, S., Vagnetti, D., and Bondi, C. (1984). Epidermal cell migration during wound healing in Dugesia lugubris. Observations based on scanning electron microscopy and treatment with cytochalasin. Cell Tissue Res *236*, 345-349.

Pearson, B., Eisenhoffer, G., Gurley, K., Rink, J., Miller, D., and Sánchez Alvarado, A. (2009). Formaldehyde-based whole-mount in situ hybridization method for planarians. Developmental Dynamics *238*, 443-450.

Pedersen, K. (1959). Some features of the fine structure and histochemistry of planarian subepidermal gland cells. Z Zellf *50*, 121-142.

Pedersen, K.J. (1976). Scanning Electron Microscopical Observations on Epidermal Wound Healing in the Planarian Dugesia tigrina. Wilhelm Roux's Archives *179*, 251-273.

Person, R.E., Li, F.-Q., Duan, Z., Benson, K.F., Wechsler, J., Papadaki, H.A., Eliopoulos, G., Kaufman, C., Bertolone, S.J., and Nakamoto, B. (2003). Mutations in proto-oncogene GFI1 cause human neutropenia and target ELA2. Nature genetics *34*, 308-312.

Poleo, G., Brown, C., Laforest, L., and Akimenko, M. (2001). Cell proliferation and movement during early fin regeneration in zebrafish. Developmental Dynamics *221*, 380-390.

Poss, K., Keating, M., and Nechiporuk, A. (2003). Tales of regeneration in zebrafish. Developmental Dynamics *226*, 202-210.

Poss, K., Shen, J., Nechiporuk, A., McMahon, G., Thisse, B., Thisse, C., and Keating, M. (2000a). Roles for Fgf signaling during zebrafish fin regeneration. Developmental Biology *222*, 347-358.

Poss, K.D., Shen, J., and Keating, M.T. (2000b). Induction of lef1 during zebrafish fin regeneration. Developmental dynamics *219*, 282-286.

Praitis, V. (2006). Creation of transgenic lines using microparticle bombardment methods. C elegans: Methods and Applications, 93-107.

Quint, E., Smith, A., Avaron, F., Laforest, L., Miles, J., Gaffield, W., and Akimenko, M.-A. (2002). Bone patterning is altered in the regenerating zebrafish caudal fin after ectopic expression of sonic hedgehog and bmp2b or exposure to cyclopamine. Proceedings of the National Academy of Sciences *99*, 8713-8718.

Radice, G.P. (1980). The spreading of epithelial cells during wound closure in Xenopus larvae. Developmental Biology *76*, 26-46.

Rawlins, E.L., Okubo, T., Xue, Y., Brass, D.M., Auten, R.L., Hasegawa, H., Wang, F., and Hogan, B.L. (2009). The role of Scgb1a1+ Clara cells in the long-term maintenance and repair of lung airway, but not alveolar, epithelium. Cell Stem Cell *4*, 525-534.

Razzell, W., Evans, I.R., Martin, P., and Wood, W. (2013). Calcium flashes orchestrate the wound inflammatory response through DUOX activation and hydrogen peroxide release. Curr Biol *23*, 424-429.

Reddien, P., Bermange, A., Kicza, A., and Sánchez Alvarado, A. (2007). BMP signaling regulates the dorsal planarian midline and is needed for asymmetric regeneration. Development *134*, 4043-4051.

Reddien, P., and Sánchez Alvarado, A. (2004). Fundamentals of planarian regeneration. Annual Review of Cell and Developmental Biology *20*, 725-757.

Reddien, P.W., Bermange, A.L., Murfitt, K.J., Jennings, J.R., and Sánchez Alvarado, A. (2005). Identification of genes needed for regeneration, stem cell function, and tissue homeostasis by systematic gene perturbation in planaria. Developmental Cell *8*, 635-649.

Rees, W.D.W. (1988). Advances in peptic ulcer pathogenesis (Kluwer Academic Publishers).

Ridley, A.J., Schwartz, M.A., Burridge, K., Firtel, R.A., Ginsberg, M.H., Borisy, G., Parsons, J.T., and Horwitz, A.R. (2003). Cell migration: integrating signals from front to back. Science *302*, 1704-1709.

Riento, K., and Ridley, A.J. (2003). Rocks: multifunctional kinases in cell behaviour. Nat Rev Mol Cell Biol *4*, 446-456.

Rink, J.C., Gurley, K.A., Elliott, S.A., and Sánchez Alvarado, A. (2009). Planarian Hh signaling regulates regeneration polarity and links Hh pathway evolution to cilia. Science *326*, 1406-1410.

Rinkevich, Y., Lindau, P., Ueno, H., Longaker, M.T., and Weissman, I.L. (2011). Germ-layer and lineage-restricted stem/progenitors regenerate the mouse digit tip. Nature *476*, 409-413.

Rittie, L., Sachs, D.L., Orringer, J.S., Voorhees, J.J., and Fisher, G.J. (2013). Eccrine sweat glands are major contributors to reepithelialization of human wounds. Am J Pathol *182*, 163-171.

Rodriguez, O.C., Schaefer, A.W., Mandato, C.A., Forscher, P., Bement, W.M., and Waterman-Storer, C.M. (2003). Conserved microtubule-actin interactions in cell movement and morphogenesis. Nat Cell Biol *5*, 599-609.

Ross, L.G., and Ross, B. (2009). Anaesthetic and Sedative Techniques for Aquatic Animals (John Wiley & Sons).

Russo, J.M., Florian, P., Shen, L., Graham, W.V., Tretiakova, M.S., Gitter, A.H., Mrsny, R.J., and Turner, J.R. (2005). Distinct temporal-spatial roles for rho kinase and myosin light chain kinase in epithelial purse-string wound closure. Gastroenterology *128*, 987-1001.

Sambrook, J., and Russell, D.W. (2006). DNA transfection by biolistics. CSH Protoc *2006*.

Sander, M., Paydar, S., Ericson, J., Briscoe, J., Berber, E., German, M., Jessell, T.M., and Rubenstein, J.L. (2000). Ventral neural patterning by Nkx homeobox genes: Nkx6.1 controls somatic motor neuron and ventral interneuron fates. Genes Dev *14*, 2134-2139.

Sandoval-Guzman, T., Wang, H., Khattak, S., Schuez, M., Roensch, K., Nacu, E., Tazaki, A., Joven, A., Tanaka, E.M., and Simon, A. (2014). Fundamental differences in dedifferentiation and stem cell recruitment during skeletal muscle regeneration in two salamander species. Cell Stem Cell *14*, 174-187.

Satoh, A., Graham, G.M.C., Bryant, S.V., and Gardiner, D.M. (2008). Neurotrophic regulation of epidermal dedifferentiation during wound healing and limb regeneration in the axolotl (Ambystoma mexicanum). Developmental Biology *319*, 321-335.

Schapire, A.L., Voigt, B., Jasik, J., Rosado, A., Lopez-Cobollo, R., Menzel, D., Salinas, J., Mancuso, S., Valpuesta, V., Baluska, F., and Botella, M.A. (2008). Arabidopsis synaptotagmin 1 is required for the maintenance of plasma membrane integrity and cell viability. Plant Cell *20*, 3374-3388.

Schnapp, E., Kragl, M., Rubin, L., and Tanaka, E.M. (2005). Hedgehog signaling controls dorsoventral patterning, blastema cell proliferation and cartilage induction during axolotl tail regeneration. Development *132*, 3243-3253.

Schneider, C.A., Rasband, W.S., and Eliceiri, K.W. (2012). NIH Image to ImageJ: 25 years of image analysis. Nat methods *9*, 671-675.

Shimizu, H., Zhang, X., Zhang, J., Leontovich, A., Fei, K., Yan, L., and Sarras, M.P., Jr. (2002). Epithelial morphogenesis in hydra requires de novo expression of extracellular matrix components and matrix metalloproteinases. Development *129*, 1521-1532.

Singer, A.J., and Clark, R.A. (1999). Cutaneous wound healing. The New England journal of medicine *341*, 738-746.

Skaer, R.J. (1961). Some Aspects of the Cytology of Polycelis nigra. Journal of Cell Science *s3-102*, 295-317.

Skaer, R.J. (1965). The origin and continuous replacement of epidermal cells in the planarian Polycelis tenuis (Iijima). Development *13*, 129-139.

Smith, A., Avaron, F., Guay, D., Padhi, B., and Akimenko, M. (2006). Inhibition of BMP signaling during zebrafish fin regeneration disrupts fin growth and scleroblast differentiation and function. Developmental biology *299*, 438-454.

Smith, S., Kenyon, J., Kelley, P., Hoover, D., and Comer, B. (1997). Tietz syndrome (hypopigmentation/deafness) caused by mutation of MITF. Paper presented at: American Journal of Human Genetics (UNIV CHICAGO PRESS 5801 S ELLIS AVENUE, CHICAGO, IL 60637 USA).

Sonnemann, K.J., and Bement, W.M. (2011). Wound repair: toward understanding and integration of single-cell and multicellular wound responses. Annual Review of Cell and Developmental Biology *27*, 237-263.

Spiegelman, M., and Dudley, P.L. (1973). Morphological Stages of Regeneration in the Planarian Dugesia tigrina: A Light and Electron Microscopic Study. The Journal of Moorphology *139*, 155-184.

Steinhardt, R.A., Bi, G., and Alderton, J.M. (1994). Cell membrane resealing by a vesicular mechanism similar to neurotransmitter release. Science *263*, 390-393.

Stenn, K.S., and Depalma, L. (1988). Re-epithelialization. In The molecular and cellular biology of wound repair (Springer), pp. 321-335.

Stevenson, C.G., and Beane, W.S. (2010). A low percent ethanol method for immobilizing planarians. PLoS One *5*, e15310.

Stoick-Cooper, C.L., Weidinger, G., Riehle, K.J., Hubbert, C., Major, M.B., Fausto, N., and Moon, R.T. (2007). Distinct Wnt signaling pathways have opposing roles in appendage regeneration. Development *134*, 479-489.

Sugiura, T., Wang, H., Barsacchi, R., Simon, A., and Tanaka, E.M. (2016). MARCKS-like protein is an initiating molecule in axolotl appendage regeneration. Nature.

Szpaderska, A.M., Zuckerman, J.D., and DiPietro, L.A. (2003). Differential injury responses in oral mucosal and cutaneous wounds. J Dent Res *82*, 621-626.

Szubinska, B. (1971). "New membrane" formation in Amoeba proteus upon injury of individual cells. Electron microscope observations. J Cell Biol *49*, 747-772.

Takaku, Y., Shimizu, H., Takahashi, T., and Fujisawa, T. (2013). Subcellular localization of the epitheliopeptide, Hym-301, in Hydra. Cell Tissue Res *351*, 419-424.

Tasaki, J., Shibata, N., Nishimura, O., Itomi, K., Tabata, Y., Son, F., Suzuki, N., Araki, R., Abe, M., Agata, K., and Umesono, Y. (2011). ERK signaling controls blastema cell differentiation during planarian regeneration. Development *138*, 2417-2427.

Tassava, R.A., and Garling, D.J. (1979). Regenerative responses in larval axolotl limbs with skin grafts over the amputation surface. J Exp Zool *208*, 97-110.

Tata, P.R., Mou, H., Pardo-Saganta, A., Zhao, R., Prabhu, M., Law, B.M., Vinarsky, V., Cho, J.L., Breton, S., Sahay, A., Medoff, B.D., and Rajagopal, J. (2013). Dedifferentiation of committed epithelial cells into stem cells in vivo. Nature *503*, 218-223.

Taylor, G., Lehrer, M.S., Jensen, P.J., Sun, T.T., and Lavker, R.M. (2000). Involvement of follicular stem cells in forming not only the follicle but also the epidermis. Cell *102*, 451-461.

Technau, U., Cramer von Laue, C., Rentzsch, F., Luft, S., Hobmayer, B., Bode, H.R., and Holstein, T.W. (2000). Parameters of self-organization in Hydra aggregates. Proc Natl Acad Sci U S A *97*, 12127-12131.

Technau, U., and Steele, R.E. (2011). Evolutionary crossroads in developmental biology: Cnidaria. Development *138*, 1447-1458.

Terasaki, M., and Jaffe, L.A. (2004). Labeling of cell membranes and compartments for live cell fluorescence microscopy. Methods Cell Biol *74*, 469-489.

Terasaki, M., Miyake, K., and McNeil, P.L. (1997). Large plasma membrane disruptions are rapidly resealed by Ca2+-dependent vesicle-vesicle fusion events. J Cell Biol *139*, 63-74.

Thompson, C.R., and Bretscher, M.S. (2002). Cell polarity and locomotion, as well as endocytosis, depend on NSF. Development *129*, 4185-4192.

Thornton, C.S. (1960). Influence of an eccentric epidermal cap on limb regeneration in Amblystoma larvae. Developmental Biology *2*, 551-569.

Tu, K.C., Cheng, L.-C., T K Vu, H., Lange, J.J., McKinney, S.A., Seidel, C.W., and Sánchez Alvarado, A. (2015). Egr-5 is a post-mitotic regulator of planarian epidermal differentiation. eLife *4*, e10501.

Tyler, S. (2003). Epithelium--The Primary Building Block for Metazoan Complexity. Integrative and Comparative Biology *43*, 55-63.

van Es, J.H., Sato, T., van de Wetering, M., Lyubimova, A., Nee, A.N., Gregorieff, A., Sasaki, N., Zeinstra, L., van den Born, M., Korving, J., Martens, A.C., Barker, N., van Oudenaarden, A., and Clevers, H. (2012). Dll1+ secretory progenitor cells revert to stem cells upon crypt damage. Nat Cell Biol *14*, 1099-1104.

Van Lommel, A.T. (2003). From cells to organs: a histology textbook and atlas (Springer Science & Business Media).

van Wolfswinkel, J.C., Wagner, D.E., and Reddien, P.W. (2014). Single-cell analysis reveals functionally distinct classes within the planarian stem cell compartment. Cell Stem Cell *15*, 326-339.

Vermeer, P.D., Einwalter, L.A., Moninger, T.O., Rokhlina, T., Kern, J.A., Zabner, J., and Welsh, M.J. (2003). Segregation of receptor and ligand regulates activation of epithelial growth factor receptor. Nature *422*, 322-326.

Vermeer, P.D., Panko, L., Welsh, M.J., and Zabner, J. (2006). erbB1 functions as a sensor of airway epithelial integrity by regulation of protein phosphatase 2A activity. J Biol Chem *281*, 1725-1730.

Vij, S., Rink, J.C., Ho, H.K., Babu, D., Eitel, M., Narasimhan, V., Tiku, V., Westbrook, J., Schierwater, B., and Roy, S. (2012). Evolutionarily ancient association of the FoxJ1 transcription factor with the motile ciliogenic program. PLoS Genet *8*, e1003019.

Vu, H.T.-K., Rink, J.C., McKinney, S.A., McClain, M., Lakshmanaperumal, N., Alexander, R., and Alvarado, A.S. (2015). Stem cells and fluid flow drive cyst formation in an invertebrate excretory organ. Elife *4*, e07405.

Wagner, D.E., Ho, J.J., and Reddien, P.W. (2012). Genetic regulators of a pluripotent adult stem cell system in planarians identified by RNAi and clonal analysis. Cell Stem Cell *10*, 299-311.

Wang, S., Tsarouhas, V., Xylourgidis, N., Sabri, N., Tiklova, K., Nautiyal, N., Gallio, M., and Samakovlis, C. (2009). The tyrosine kinase Stitcher activates Grainy head and epidermal wound healing in Drosophila. Nat Cell Biol *11*, 890-895.

Wang, Y., Antunes, M., Anderson, A.E., Kadrmas, J.L., Jacinto, A., and Galko, M.J. (2015). Integrin Adhesions Suppress Syncytium Formation in the Drosophila Larval Epidermis. Curr Biol *25*, 2215-2227.

Watanabe, A., Takeda, K., Ploplis, B., and Tachibana, M. (1998). Epistatic relationship between Waardenburg syndrome genes MITF and PAX3. Nature genetics *18*, 283-286.

Welch, M.D., and Mullins, R.D. (2002). Cellular control of actin nucleation. Annu Rev Cell Dev Biol *18*, 247-288.

Wenemoser, D., Lapan, S.W., Wilkinson, A.W., Bell, G.W., and Reddien, P.W. (2012). A molecular wound response program associated with regeneration initiation in planarians. Genes & Development *26*, 988-1002.

West, G., Heard, D., and Caulkett, N. (2014). Zoo Animal and Wildlife Immobilization and Anesthesia (John Wiley & Sons).

Whitehead, G., Makino, S., Lien, C., and Keating, M. (2005). fgf20 Is Essential for Initiating Zebrafish Fin Regeneration. Science *310*, 1957-1960.

Wood, W., Jacinto, A., Grose, R., Woolner, S., Gale, J., Wilson, C., and Martin, P. (2002). Wound healing recapitulates morphogenesis in Drosophila embryos. Nature Cell Biology *4*, 907-912.

Woodley, D.T. (1988). Reepithelialization. In The molecular and cellular biology of wound repair (Springer), pp. 339-354.

Wu, Y., Brock, A.R., Wang, Y., Fujitani, K., Ueda, R., and Galko, M.J. (2009). A Blood-Borne PDGF/VEGF-like Ligand Initiates Wound-Induced Epidermal Cell Migration in Drosophila Larvae. Current Biology *19*, 1473-1477.

Xu, S., and Chisholm, A.D. (2011). A Gαq-Ca^{2+} signaling pathway promotes actin-mediated epidermal wound closure in C. elegans. Curr Biol *21*, 1960-1967.

Yokoyama, H., Ide, H., and Tamura, K. (2001). FGF-10 stimulates limb regeneration ability in Xenopus laevis. Developmental Biology *233*, 72-79.

Yokoyama, H., Ogino, H., and Stoick-Cooper, C.L. (2007). Wnt/β-catenin signaling has an essential role in the initiation of limb regeneration. Developmental ….

Yokoyama, H., Yonei-Tamura, S., Endo, T., Izpisúa-Belmonte, J.C., Tamura, K., and Ide, H. (2000). Mesenchyme with fgf-10 expression is responsible for regenerative capacity in Xenopus limb buds. Developmental Biology *219*, 18-29.

Zani, B.G., and Edelman, E.R. (2010). Cellular bridges: Routes for intercellular communication and cell migration. Communicative & integrative biology *3*, 215-220.

Zani, B.G., Indolfi, L., and Edelman, E.R. (2010). Tubular bridges for bronchial epithelial cell migration and communication. PLoS ONE *5*, e8930.

Zhu, H. (2016). Forkhead box transcription factors in embryonic heart development and congenital heart disease. Life sciences *144*, 194-201.